THESIS FOR THE DEGREE OF DOCTOR OF PHILOSOPHY

Photon Upconversion through Triplet-Triplet Annihilation

Towards Higher Efficiency and Solid State Applications

DAMIR DŽEBO

Department of Chemistry and Chemical Engineering
CHALMERS UNIVERSITY OF TECHNOLOGY

Göteborg, Sweden 2016

Photon Upconversion through Triplet-Triplet Annihilation:
Towards Higher Efficiency and Solid State Applications
DAMIR DŽEBO
ISBN 978-91-7597-420-0

Doktorsavhandlingar vid Chalmers tekniska högskola
Ny serie nr. 4101
ISSN 0346-718X
Department of Chemistry and Chemical Engineering
Division of Chemistry and Biochemistry - Physical Chemistry
Chalmers University of Technology
SE-412 96 Göteborg
Sweden
Telephone: +46 (0)31-772 1000

Cover:
Front: Photograph by author of two melt sealed sample tubes exhibiting Photon Upconversion through Triplet-Triplet Annihilation and only the Sensitizer emission from left to right, respectively. Process is driven by excitation with green laser from left to right.

Back: Photograph by Peter Sandin

Chalmers Reproservice
Göteborg, Sweden 2016

Photon Upconversion through Triplet-Triplet Annihilation:
Towards Higher Efficiency and Solid State Applications
Thesis for the degree of Doctor of Philosophy
DAMIR DŽEBO
Department of Chemistry and Chemical Engineering
Division of Chemistry and Biochemistry - Physical Chemistry
Chalmers University of Technology

Abstract

The sun is the only renewable energy source that can accommodate humanity's energy needs today and in the foreseeable future. The sunlight reaching the planet's surface is filtrated through the atmosphere, reducing its UV-light intensity in the 300-400 nm range, which indeed can be harmful to life as we know it in too large doses. However, many useful photoreactions require in practice such high-energy UV-photons, like the catalytic splitting of water to oxygen and hydrogen gas or molecular in-bond energy storage through isomerization to produce heat when reverting to the initial state. The efficiency of these applications could be improved with efficient conversion of low-energy visible to high-energy UV-light.

One way to achieve this type of photon upconversion (UC) is through the process called Triplet-Triplet Annihilation (TTA) relying on the interaction between two molecules; a sensitizer and an annihilator. The sensitizer absorbs low energy visible photons as input and transfers that energy through Triplet Energy Transfer (TET) to an annihilator. Two triplet-excited annihilators can thereafter perform TTA, merging the energy equivalents of the two low-energy photons to produce one high-energy photon as output.

This Thesis is focused on improving the known bimolecular UC system in fluid environment and approaching the ultimate goal of high efficiency UC in solid materials. In the fluid system I demonstrate the employment of thiol- and thioether-based compounds as scavengers for singlet excited oxygen with positive effect on UC efficiency and stability. In an attempt to aid future design and optimization of upconversion system components the anthracene is 9,10-substituted with electron withdrawing or donating groups while its TTA-UC function is evaluated revealing that substitution at *para*-positions leads to least perturbation of its spectroscopic properties. The ultimate goal is to achieve supramolecular TTA-UC systems capable of efficient *intra*-molecular TET and TTA processes and unhindered emission of the upconverted photons. As a first step, we focus on the *intra*-molecular TTA process with oligomers and dendrimers of 9,10-diphenyl anthracene (DPA) which display positive effects on UC efficiency in solid matrix. In the second step the focus is on the *intra*-molecular TET process where the sensitizer-annihilator complexes are explored through Lewis base-acid coupling with orthogonal transition moments for minimum excited state short circuit effect. Additionally, kinetic simulations of the TTA-UC processes are conducted to aid understanding and optimization. Finally, one TTA-UC system is also applied to chemical in-bond energy storage.

Keywords: photon upconversion, triplet-triplet annihilation, energy transfer, excited state, anti-stokes, spectroscopy, delayed fluorescence, fluorescence anisotropy, photophysics, photochemistry, solar energy conversion, anthracene, oligomers, dendrimers, porphyrins

To my son,
Adrian Edin Džebo

List of Publications

This thesis is based on the following publications and manuscripts, referred to in the text as:

Paper I
Damir Dzebo, Kasper Moth-Poulsen, and Bo Albinsson.
Robust Triplet-Triplet Annihilation Upconversion by Efficient Oxygen Scavenging.
(Manuscript in preparation)

Paper II
Karl Börjesson, Damir Dzebo, Bo albinsson and Kasper Moth-Poulsen.
Photon upconversion facilitated molecular solar energy storage.
J Mater Chem A **2013**, 1 (30), 8521-8524.

Paper III
Victor Gray, Damir Dzebo, Angelica Lundin, Jonathan Alborzpour, Maria Abrahamsson, Bo Albinsson, and Kasper Moth-Poulsen.
Photophysical characterization of the 9,10-disubstituted anthracene chromophore and its applications in triplet-triplet annihilation photon upconversion.
J Mater Chem C **2015**, 3 (42), 11111-11121

Paper IV
Karl Börjesson, Mélina Gilbert, Damir Dzebo, Bo Albinsson, and Kasper Moth-Poulsen.
Conjugated anthracene dendrimers with monomer-like fluorescence.
RCS Adv. **2014**, 4 (38), 19846-19850.

Paper V
Damir Dzebo, Karl Börjesson, Victor Gray, Kasper Moth-Poulsen, and Bo Albinsson.
Intramolecular Triplet-Triplet Annihilation in 9,10-diphenyl anthracene oligomers and dendrimers.
(Manuscript, submitted to *J. Phys. Chem. C*)

Paper VI
Victor Gray, Karl Börjesson, Damir Dzebo, Maria Abrahamsson, Bo Albinsson, and Kasper Moth-Poulsen.
Porphyrin-Anthracene Complexes: Potential in Triplet-Triplet Annihilation Upconversion.
J Phys Chem C **2016**, (Accepted)

Paper VII
Victor Gray, Damir Dzebo, Maria Abrahamsson, Bo Albinsson, and Kasper Moth-Poulsen.
Triplet-triplet annihilation photon-upconversion: towards solar energy applications.
Phys Chem Chem Phys **2014**, 16 (22), 10345-10352.

Contribution Report

Paper I. Suggested the project. Designed and performed the experiments. Analyzed and interpreted the data. Wrote the paper.

Paper II. Performed some of the experiments and wrote a minor part of the paper. Made the illustrations.

Paper III. Contributed in the design of the experiments. Took part in analysis and interpretation of the data.

Paper IV. Contributed in designing and performing the measurements and data analysis. Wrote part of the paper.

Paper V. Developed the employed experimental procedures. Designed and performed the experiments. Simulated, analyzed and interpreted the data. Did most of the mathematical work. Wrote the paper.

Paper VI. Designed and performed initial experiments. Contributed in further experimental design and interpretation of the final data. Wrote part of the paper.

Paper VII. Wrote part of the paper and derived some of the mathematical statements.

The organic synthesis work covered in the publications included in this thesis was performed by colleagues and co-authors.

Contents

List of Abbreviations and Symbols

Abbreviations

DFT	Density functional theory 36, 38
ES	excited state 13, 25, 43
FRET	Förster resonance energy transfer x, xi, 4, 6, 8, 14, 35, 44, 53–57, 60, 65
GS	ground state 13, 25, 43
IC	internal conversion 13, 14, 18, 44
ISC	inter system crossing 5, 13–16, 18, 19
PV	photovoltaics 2, 3
SI	supporting information 19, 20, 33, 40
TET	*inter*-molecular triplet energy transfer x, 5, 8, 9, 15–20, 30, 33, 35, 46, 47, 54, 56, 57, 60
TET1	first sequential *inter*-molecular triplet energy transfer ix, x, 47, 49
TET2	second sequential *inter*-molecular triplet energy transfer to the same molecule as TET1 x, 47, 49
***intra*TET**	*intra*-molecular triplet energy transfer 4, 51, 55, 56, 59, 60, 64, 65
TTA	triplet-triplet annihilation x, 2–9, 15–20, 30–36, 39, 40, 45–47, 49–51, 53, 55–60, 64, 65
TTA1	*inter*-molecular triplet-triplet annihilation x, 3, 4, 45, 47, 49, 50
TTA2	*intra*-molecular triplet-triplet annihilation x, 3, 4, 45, 47, 49–51, 59, 60, 64, 65
TTAS	triplet-triplet annihilation of the sensitizer x, 20, 49, 57
UC	photon upconversion xi, 2–9, 15–20, 30–36, 38–40, 45–47, 49–51, 53–60, 64, 65
UES	upconversion energy shift 4, 56, 58, 65
VR	vibrational relaxation 13–15, 18

Molecules and chemicals

2-MTHF	2-methyltetrahydrofuran 42, 44
A	annihilator 2–4, 15–17, 30, 31, 35, 48, 50, 57, 58
$^{\mathbf{1}}$**A***	singlet excited annihilator 16, 18
$^{\mathbf{1}}$**A**	singlet ground state annihilator 15, 16, 18, 19, 47
$^{\mathbf{3}}$**A***	triplet excited annihilator 16, 18, 19, 21, 30, 47
$^{\mathbf{3}}$**A****	doubly excited triplet annihilator 47
BME	2-mercaptoethanol 30, 32, 33
DBS	Dibenzyl sulfide 30, 33
DMS	Dimethyl sulfide 30, 31, 33, 36
DPA	9,10-diphenylanthracene x, 3, 4, 6–8, 31–34, 36–38, 40–42, 44–48, 50, 51, 53–55, 58, 59, 64, 65
DPropS	Dipropyl sulfide 30, 33, 36
FvRu$_2$	fulvalene diruthenium 33–35, 64

G1	1st generation DPA dendrimer 3, 40–46, 48–50, 59, 64, 65
G2	2nd generation DPA dendrimer 3, 40–42, 44–46, 48–50, 59, 64, 65
O_2	molecular oxygen x, 3–5, 15, 19, 30–33, 35, 36, 64
$^1O_2$*	singlet excited O_2 19, 31, 35, 64
$^3O_2$	triplet ground state O_2 19, 31
Oligo	DPA oligomer 3, 45–48, 50, 59, 64, 65
PdOEP	palladium(II)–octaethylporphyrin 7, 31–34, 45, 46, 58, 59
Ph_nAnPyr	pyridine–substituted DPA connected with a phenyl bridge of modulated length 4, 51, 53–55
PMMA	poly(methyl methacrylate) 4, 45–47, 49, 50, 59
PtOEP	platinum(II)–octaethylporphyrin 38–40, 54, 59
S	sensitizer 2–4, 15, 16, 30, 31, 35, 48, 50, 57
^1S	singlet ground state sensitizer 15, 16, 20
^3S*	triplet excited sensitizer 15, 19, 30
ZnOEP	zinc(II)–octaethylporphyrin 4, 40, 51, 53–55, 59, 65

Roman symbols

Abs	absorbance 24, 25, 39
E	energy 12, 13, 16, 18
I_0	initial unquenched intensity 16, 20, 24, 25
I_{th}^{ideal}	ideal excitation intensity threshold 20, 49
I_{th}	excitation intensity threshold 4, 19, 49, 56, 60, 65
I	intensity 16, 20, 21, 24–27
K_B	binding constant 53, 54
R_0	characteristic FRET distance corresponding to 50% energy transfer efficiency 14, 55
S_0	singlet ground state 13
S_1	first singlet excited state 13, 14, 16
S_2	second singlet excited state 13
T_1	first triplet excited state 14–16, 40
T_2	second triplet excited state 14
c	speed of light 12
f	frequency 12, 13
h	Planck's constant 12, 13
k_{TET1}	TET1 rate constant 48–50
k_{TET2}	TET2 rate constant 48–50
k_{TET}	TET rate constant 16, 17, 19, 38, 39, 54
k_{TTA1}	TTA1 rate constant 20, 48–50
k_{TTA2}	TTA2 rate constant 48
k_{TTAS}	TTAS rate constant 48–50
k_{TTA}	TTA rate constant 18–21, 39, 40, 49
k_T	triplet excited state rate constant 19–21
k_f	radiative rate constant 40, 41
r_0	fundamental anisotropy 27, 44

r_{max}	maximum anisotropy 27, 42
t	time 21
T	temperature 44
Q	arbitary quencher 16

Greek symbols

Φ_f	fluorescence quantum yield 16, 18, 19, 38–41, 46, 48, 51, 53, 59
Φ_{TET}	triplet energy transfer efficiency 16–19
Φ_{TTA}	triplet-triplet annihilaton quantum yield 18, 19, 21
Φ_{UC}	UC fluorescence quantum yield 4–8, 15, 16, 18–20, 31–33, 36, 38–40, 53, 54, 56, 60
α	absorption cross section 20, 24
η_{TTA}	triplet-triplet annihilaton efficiency 18, 19
η_{FRET}	FRET efficiency 14, 55, 56
λ	wavelength 12
ω	relative absorption/emission transition dipole angle 27, 42
τ_0	unquenched excited state lifetime 16, 17, 55
τ_{PS}	phosphorescence lifetime of the sensitizer 48
τ_T	triplet excited state lifetime 20, 21, 38–40, 46, 48–50
τ_f	fluorescence lifetime 38, 39, 41, 46, 48, 53
τ	excited state lifetime 16, 17
θ	rotational correlation time 44
ε	molar absorptivity 24, 25, 39

CHAPTER 1

Introduction

Obtaining clean, secure and sustainable energy world wide is one of the most important scientific tasks for humanity. The use of fossil fuels so far has given us much in terms of technological development but as our population increases together with our strive for further technological development so does the demand for energy, even more so with developing countries reaching higher living standards.[1–3] The total energy consumption for 2010 is estimated to 152 PWh and scenario projections indicate that it will rise to 193 - 244 PWh in the year 2050.[3] This increase in energy demand can be accommodated with fossil fuels in one form or another when also taking into account present energy reserves.[1,2] However such a "business-as-usual" scenario would be devastating to the environment, keeping in mind that the air pollution in 2015 was estimated to be the fourth greatest threat to human health after high blood pressure, dietary risks and smoking.[1,2,4]

It is however possible to avoid the expected negative effects on the environment and population health caused by our current lifestyle. A number of recommendations are given from international health and energy organizations as guidelines to a more sustainable future. These include to not invest only in the cheapest energy options thus stimulating the development of alternative energy sources that may not give profit in the immediate future, stimulate a consumer attitude-change in order to facilitate development and production of clean energy to possibly a higher cost, and support more basic research for both increasing efficiency of current- as well as opening possibilities for new energy sources.[3,4]

Solar energy indeed holds great promise in our search for an environmentally sustainable future. The estimates are that if only 0.1% of the sunlight reaching Earth can be converted to electricity with an efficiency of 10%, the generated electricity would be four times larger than the present electricity generating capacity.[5] While the efficiency is a key factor for solar photovoltaics (PV) technology another key factor, often referred to as a "game-changer" is the chemical storage of solar energy.[6–8]

All solar energy harvesting technologies depend in one way or another on the solar spectrum, the energy distribution of sunlight reaching the surface of our planet. However the most abundant light is often not of high enough energy to drive energetically useful reactions. It is here that the work presented in this Thesis comes into the picture.

The process of organic photon upconversion (UC) through triplet-triplet annihilation (TTA), which is the focus of this Thesis, is one of several technologies that can, in principle, convert low-energy photons to high-energy. Two of these are simultaneous two-photon absorption and second-harmonic generation. Unlike these technologies TTA–UC has the possibility to achieve this using low-intensity, incoherent and non-collimated low-energy light as input, much like the natural light from our sun.[9,10] In short it relies on two molecular species; a sensitizer (S) and an annihilator (A). The S has the ability to absorb low-energy photons and transfer the equivalent energy to A. If this occurs at least twice, two sensitized A can merge their low energy packages to form a photon of higher energy than the two individual low-energy photons used in the beginning of the process. This process will be covered in more detail later in Section 2.2.

As a technology that has the ability to manipulate the solar spectrum by absorbing photons somewhere in the spectrum and emitting them elsewhere with higher energy it certainly holds great promise for increasing the efficiencies of solar harvesting technologies that depend on the naturally less abundant high-energy photons in the solar spectrum.

For PVs UC is estimated to increase the efficiency to as much as 43% which is beyond the Shockley–Queisser limit of $\sim 30\%$ for a single junction solar cell.[11,12] The UC is also, if not more, useful in facilitating the creation of solar fuels.[13,14] One example is the splitting of water using WO_3 photocatalyst utilizing near-UV photons.[13] Another example is given in **Paper II** where we have facilitated the production of a molecular solar thermal fuel consisting of a fulvalene diruthenium compound, using TTA–UC and achieved an increase in conversion efficiency from its low- to high energy form.

In addition to applications, the focus of this Thesis is improvement of the TTA–UC process both in fluid and in solid environment with the end-goal to achieve high-efficiency UC in solid matrices. TTA–UC systems in fluid media have been shown by others to operate at high efficiencies given correct composition of the S and A components in combination with thorough removal of molecular oxygen (O_2).[13,15,16] This removal process often involves rigorous freeze–pump–thaw cycling followed by a secure sample sealing, preferably melt seal. In **Paper I** we show preliminary results of the possibility to utilize oxygen scavengers in the form of thiols and thioethers as sacrificial agents to scavenge molecular oxygen. The long-lived excited species involved in the TTA–UC process are very sensitive to the presence of O_2 which resides in its triplet ground state. The O_2 can efficiently quench the long-lived excited triplet states of both S and A while being excited to its own very reactive singlet excited state. This reactive O_2 species reacts readily with the scavengers and is therefore no longer active in the quenching of TTA–UC. Therefore, by preparing TTA–UC samples with sufficient amount of scavenger and closing them, the dissolved O_2 can be significantly reduced through simple excitation of the S in the sample. Preliminary results indicate that utilizing this method results in easily obtained high efficiencies above 10% with little effort.

The major part of the work presented in this Thesis is focused on the pursuit of high–efficiency TTA–UC in solid media. As a first step towards this goal, in **Paper III** we have examined the possibility of modifying the well studied TTA–UC annihilator 9,10-diphenylanthracene (DPA) (Figure 4.6) by modifying its substituents in the 9,10-positions. The results indicate that modification at the *para*-positions of the DPA 9,10-substituents leads to minimal distortion to the molecule's spectroscopic properties. In accordance with these findings and in pursuit of large supramolecular TTA–UC component structures suitable for usage in solid matrices, we synthesized in **Paper IV** a 1^{st} generation DPA dendrimer (G1) containing 3 DPA-units and a 2^{nd} generation DPA dendrimer (G2) containing 9 DPA-units (Figure 4.8). The synthesis of dendrimers in this manner yields no size-distribution of the molecules which is an asset in photophysical characterization while maintaining a high solubility due to the dendrimer structure. The results here indicate that it is possible to connect DPA-like monomers in dendrimer structures with covalent connections and maintain the absorption and emission characteristics of the monomer while still having fast exciton cross-walk within the supramolecular structures.

This is indeed an encouraging result in the pursuit of high–efficiency TTA–UC in solid matrix as the annihilator must have the capability to delocalize excitons within its molecular structure in order to perform *intra*-molecular triplet-triplet annihilation (TTA2) as opposed to *inter*-molecular triplet-triplet annihilation (TTA1) which occurs between individual annihilator molecules. In **Paper V** we put this hypothesis to the test using G1, G2 and also a linear DPA oligomer (Oligo) (Figure 4.11a) as supramolecular annihi-

lators. The study was conducted in Liquid (toluene) and Solid poly(methyl methacrylate) (PMMA) media in order to facilitate the differentiation between the diffusion dependent TTA1 and the *intra*-molecular diffusion independent TTA2 process. The results of this study indicate that connecting annihilator molecules in this manner has a positive effect on the TTA–UC efficiency in Solid media and there appears to be a correlation between the size of the supramolecular annihilators and the increase of TTA–UC efficiency, the larger the annihilator the better. The effects of TTA2 were not as prominent in the fluid media as diffusion–controlled processes dominate and annihilation occurs mainly through the TTA1–channel.

As a second step towards high–efficiency TTA–UC in solid media we explore in **Paper VI** the effects of attaching pyridine–substituted DPA connected with a phenyl bridge of modulated length (Ph_nAnPyr) to zinc(II)–octaethylporphyrin (ZnOEP) through a simple Lewis base-acid coupling between the pyridine-nitrogen and the ZnOEP metal core. The motivation for this kind of coordination binding was to maintain as close to orthogonal orientation as possible between the singlet-singlet transitions of the Ph_nAnPyr and ZnOEP. This strategy to miss–align the transition moments was an attempt to minimize the expected parasitic Förster resonance energy transfer (FRET) of the UC emission back to ZnOEP. However, the orientation between the two species' transition moments turned out to be quite far from orthogonal contributing to highly efficient FRET quenching of the UC excited singlet state. Insufficient binding between ZnOEP and Ph_nAnPyr made it difficult to prove wether or not *intra*-molecular triplet energy transfer (*intra*TET) can occur in the system. The obtained results will, however, be useful for the experimental design of future studies on *intra*TET which is essential for achieving fully supramolecular TTA–UC systems capable of high efficiency even in the presence of O_2.

Throughout all of the studies in this Thesis the kinetic aspects of the TTA–UC process have always been in focus to facilitate understanding and optimization. The kinetics has been modeled with sets of differential equations constituting our models which in many cases were fit to experimental data to estimate the magnitude of the rate constants involved in the process. In **Paper VII** however, aside from the outlook we also elaborate on the topic of the TTA–UC figures of merit like UC fluorescence quantum yield (Φ_{UC}) and excitation intensity threshold (I_{th}) and the necessity of determining Φ_{UC} at high enough excitation intensities. Furthermore, we also suggest a standardized method of reporting the upconversion energy shift (UES) of TTA–UC systems as this is also seen as a figure of merit, especially for new S and A molecules.

1.1 Outline and scope of this Thesis

Here in Chapter 1 a general motivation for the pursuit of solar energy technology improvements and optimization in association to TTA–UC has been given along with a brief overview of the original work constituting the foundation of this Thesis. Further, an overview will be given to introduce the reader to the field of organic TTA–UC and its current status in different approaches.

In Chapter 2 the fundamental theoretical aspects related to the the work in this Thesis will be presented. Also a more thorough overview of the TTA–UC process will be given

with emphasis on the intermediate photophysical and photochemical steps that are often encountered together with a kinetic description. The experimental methods employed throughout the studies will be described in Chapter 3. Hopefully these chapters will provide sufficient theoretical foundation to make the results of the work presented here more understandable. Readers well acquainted with the field of physical chemistry and TTA–UC may find the information in these chapters very familiar and might want to skip to the results in Chapter 4 directly.

The results of the original work in this Thesis will be summarized in Chapter 4, in two sections. Firstly, work conducted in the Fluid media will be summarized and consists of **Paper I** where preliminary results are presented on the usage of oxygen scavengers to easily and consistently remove dissolved O_2 giving reproducibly high Φ_{UC}. Additionally, the work in **Paper II** will be summarized where fluid TTA–UC in combination with microfluidics is used to facilitate the generation of solar thermal energy fuel. The second and more dominant section of the summary will focus on the pursuit of the supramolecular TTA–UC system which is covered in **Paper III**–**VII**.

1.2 Overview of the field

Photon upconversion via triplet-triplet annihilation (TTA–UC) is a process comprised of a sensitizer and an annihilator which results in the net increase of the supplied light frequency. It has its origin in the early 1960's when it was first introduced by Parker and Hatchard by employing only organic sensitizers and annihilators.[17–20] Through excitation of the sensitizer by light outside of the absorption band of the annihilator, the annihilator emission was still observed with non-linear excitation intensity dependence which was attributed to the bimolecular process of TTA–UC. The organic sensitizers used at the time were a limiting factor and little progress was made in the field for several decades.

During the last 14 years there has been an increased interest in the field as a consequence of the introduction of inorganic sensitizers with high inter system crossing (ISC) efficiency.[21–23] The development and optimization of TTA–UC systems in fluid solution with free diffusion of the sensitizer and annihilator has dominated throughout this time. In recent years however, significant progress has been made in alternative materials with a more focused goal of applying TTA–UC to various solar energy technologies.

A Jablonski diagram illustrating the relevant energy levels involved in the TTA–UC process is given together with the most fundamental theoretical background in Section 2.2. In the following subsections a somewhat categorized overview is given of the directions in which the TTA–UC field is evolving.

1.2.1 Fluid systems

The initial and major part of the development in the TTA–UC field includes the process in fluid solution. The reason for this is the ability to tune the crucial *inter*-molecular triplet energy transfer (TET) and triplet-triplet annihilation (TTA) steps to a degree with concentrations of the sensitizer and annihilator. Also, as the *inter*-molecular interactions in fluid solvents rely on the predictable rate of diffusion, the fluid environment serves as a good testing ground for new TTA–UC systems.[24,25]

The earliest TTA–UC system employing an inorganic sensitizer in fluid solvent was introduced by the Castellano group in 2004.[22] In this system a ruthenium complex covalently attached to an anthracene was used. The UC emission was observed but was low in intensity, which was attributed to non-radiative UC singlet excited state FRET-type quenching due to the proximity of the sensitizer and annihilator. As a confirmation of this negative quenching effect, the same system without covalent attachment was investigated under equivalent experimental conditions and displayed a ∼3-fold efficiency increase. The Castellano group later employed the same sensitizer with different annihilators to achieve higher efficiency, broad-band visible light generation and drive photochemical dimerization of anthracene in a freely diffusing sensitizer-anthracene setup.[21,26,27]

One important goal for the TTA–UC field is to expand the upconversion to reach across the visible spectrum to the red-IR region. Achieving this goal often involves the synthesis of new sensitizers and annihilators. The design of the sensitizer often involves flat porphyrin-like center with expansion of its conjugated framework.[28–37]

Different variations of sensitizers and annihilators are also designed to increase the UC fluorescence quantum yield (Φ_{UC}). In the case of the annihilator, often established structures are modified with electron donating or withdrawing groups. For the sensitizers the same ranges from modifications of established inorganic ones by replacing the heavy atoms or minute change to the surrounding structure to replacing them with entirely organic ones like C70-fullerenes and perylenebisimide derivatives.[38–48] Furthermore, TTA–UC systems employing several types of annihilators have been investigated and display an increase of TTA efficiency through hetero-TTA processes while producing spectrally wider UC emission.[15,16] As a result some of the highest obtained Φ_{UC} are found in fluid solution systems and the highest yet is 38%.[33,49–51]

The main goal often mentioned for the TTA–UC system is the application to solar energy. However, due to the need of (relatively) intense excitation light for the system to function at its maximum Φ_{UC} (see Chapter 2), an alternative route has been proposed where multiple sensitizers are used in the same TTA–UC system. This cocktail of sensitizers provides a wider spectral range to absorb a greater number of low energy photons than a single sensitizer would and thus compensate for lower excitation intensity.[52,53]

The majority of TTA–UC systems in fluid solution are dissolved in organic solvents. As an alternative, ionic liquids are also explored as potential fluid media for TTA–UC. The findings reveal that the composition of the ionic liquids can be used to modulate the rate of the inter-molecular processes.[54–56] Furthermore, the Kimizuka group developed a new ionic liquid based on a ionic derivative of the DPA annihilator which enhanced the triplet energy migration in the sample due to the formation of ionic chromophore networks.[57]

1.2.2 Soft systems

This subsection will cover soft systems which will include TTA–UC in gel and rubber-like materials and also systems in encapsulation, as well as solvent-free and self-organized systems. The general goal of these systems is to increase TTA–UC efficiency and to protect from oxygen quenching.

A good example of a bridge between soft and fluid systems is the solvent-free TTA–UC system devised by the Kimizuka group which consists of alkyl-substituted sensitizers and annihilators. The two TTA–UC components themselves constitute a liquid and due to direct contact between them the energy transfer is efficient and Φ_{UC} is reported to be as high as 14%.[58]

The usage of self-organized systems is also of interest to minimize the distance between the chromophores and increase the effective concentration. This way the sensitizer and annihilator are used more optimally while at the same time the energy transfer rates are increased due to the dense packing of the chromophores. Several examples exist and range from lipid bilayers[59–61] to using DNA as an assembly scaffold[62]. Associated to this is also encapsulation of the TTA–UC system into protective environments with the intent to be used in polar solvents like water which would increase the usability of TTA–UC in real life applications. This has been demonstrated using micelles and rigid polymers to form microcapsules.[63,64]

Going further into rigidity, gel media is a popular way to still maintain the low viscosity of a fluid combined with the stability and robustness of a solid. Since a gel contains microscopic solvent pockets in a polymeric matrix the sensitizer and annihilator can interact through diffusion while the system stays protected from molecular oxygen.[65–73] On the same path are the rubbery polymers which are flexible enough to make it possible for the sensitizer and annihilator to diffuse slowly through the material. Earliest versions of TTA–UC in rubbery polymer matrix were made by soaking the rubber in solvent containing the sensitizer and annihilator. This did typically not provide high enough concentrations inside the rubber resulting in low TTA–UC signal. The key concept is to utilize polymers with low glass transition temperature and to polymerize the rubber precursor while mixed with the sensitizer and annihilator. Utilizing this strategy the Castellano and Meinardi groups achieved impressive Φ_{UC} of $\sim$20%.[74,75]

1.2.3 Solid systems

TTA–UC in solid media is very appealing for applications for practical reasons. However, moving a system that is inherently dependent on diffusion in to a fully diffusion restrictive environment while maintaining a high Φ_{UC} is a challenge.

The first example of thin solid films doped with palladium(II)–octaethylporphyrin (PdOEP) as the sensitizer and a polyfluorene as the annihilator was presented by Baluschev already in 2003.[23] Since then the pursuit of TTA–UC in solid media through doping has been ongoing but the definitive restrictions on diffusion between the sensitizer and annihilator kept the Φ_{UC} down.[76–79] Better results were obtained when the polymer was melt-processed allowing for higher concentrations of annihilator in the polymer matrix but still compared to fluid and soft materials, the Φ_{UC} was low.[80,81] Deeper investigations revealed that the triplet exciton migration length was long and that it might be causing the low Φ_{UC} due to the increased probability of the exciton finding non-radiative decay sites.[82]

One way to circumvent the problems of triplet migration in solid matrices is to use nanoparticles. By soaking 16 nm polystyrene nanoparticles in a solution containing PdOEP and DPA the Meinardi group managed to load the sensitizer and annihilator in

an approximate ratio of 1:50. The nanoparticles were then coated with a surfactant to enclose the system and protect it from air and the obtained threshold value between the quadratic and linear UC excitation intensity dependence was found to be a few mW/cm^2 which is close to the solar irradiance.[83] Another approach made by the Morandeira group was to physisorb a TTA–UC system on the surface of nanocrystaline ZrO_2 with the aim to do the same on TiO_2 to draw photocurrent instead of TTA–UC emission. Initially low performance values were obtained due to non-optimal orientation of the annihilator on the ZrO_2.[84] This issue was addressed later through anchoring of the annihilator to the ZrO_2 surface increasing the Φ_{UC} 60-fold.[85,86] Further improvement was achieved when both the sensitizer and annihilator were anchored to the ZrO_2 and a 400% efficiency increase was obtained relative to the first physisorbed system.[87]

Much like the solvent-free soft material the metal-organic framework (MOF) can be viewed as a matrix-free solid in the sense that it is only composed of modified sensitizer and annihilator. The Kimizuka group devised a MOF crystalline system with good contact between the MOF-comprising material displaying fast and long triplet energy migration due to the long lived triplet excited states of the framework components. However, as a trade-off, the fluorescence quantum yield of the annihilator in the MOF was lowered. The maximum UC efficiency of ∼4% was reached with ultra low excitation intensity, well below that from the sun which makes it a promising TTA–UC technology for future solar applications. Optimization suggestions include usage of MOFs with higher fluorescence quantum yield, better alignment of the MOF π planes and larger pore size to fit the sensitizer inside the MOF nanospaces.[88] The fluorescence quantum yield trade-off was later addressed by applying a dye coating on the outside of the MOF which acts as a collector for the UC singlet excited state. Once the UC energy is collected it is emitted from the surface of the MOF instead of inside from the actual annihilator that performed the TTA–UC.[89]

A TTA–UC system that would be expected to function well in solid media is a fully supramolecular TTA–UC system capable of *intra*-molecular TET and TTA. This is still far from realization and work is being conducted towards that end. The first paper demonstrating TTA–UC in fluid system using an inorganic sensitizer by Castellano group uses a potential system for *intra*-molecular TET. However, due to the vicinity between the covalently attached sensitizer and annihilator the UC emission was quenched, probably due to FRET-type quenching. The *intra*-molecular TET could not be excluded though and the system was not tested in solid media.[22] Bergamini *et.al.* demonstrated a multichromophoric dendrimer for *intra*-molecular TTA–UC in rigid matrix. Four DPA molecules would be linked to a single $[Ru(bpy)_3]^{2+}$ as the sensitizer core. A TTA–UC signal was observed even at 77 K where diffusion and therefore also the bimolecular processes are inhibited, suggesting that there is, at least to some degree, a functional *intra*-molecular TTA–UC channel active. The same system did not perform as well compared to the comprising compounds without covalent connection at room temperature, suggesting that there is a significant quenching of the attached annihilators back to the sensitizer. This is also expected given the short distance between the two.[90] Similarly Boutin *et.al.* demonstrated DPA-functionalized polymers attached to sensitizers but with similar results as Bergamini.[79] Tilley *et.al.* demonstrated kinetic measurements and

simulations supporting a possible existence of *intra*-molecular TET and TTA that occurs at times shorter than the employed time-resolution.[91]

It is evident that there are numerous challenges to be overcome before the realization of a solid state TTA–UC system functioning at unit efficiency. One path towards this goal might be through the use of fully *intra*-molecular TTA–UC systems. However, as seen in this short summary of earlier work, the definitive proof of *intra*-molecular processes of this kind are very elusive.

CHAPTER 2

Theory

In this chapter I aim to provide a brief theoretical background which will hopefully aid in the understanding of the research presented in this Thesis. Firstly, the general fundamental concepts related to the presented work will be described in short. Secondly, more specific concepts related to molecular upconversion will be presented to further facilitate the understanding of the research presented in this Thesis.

2.1 Fundamentals

All the work presented in this Thesis is the result of light interacting with matter. This section will mainly focus on the light-matter interactions with emphasis on the possible results of such interactions and how it can be used to characterize molecular systems. The complete and thorough description of these concepts is beyond the scope of this Thesis, therefore the description will be kept at a basic level to the point of necessity for understanding the presented research results. For a moore thorough description of these topics the reader may consult the many excellent books on the subject.[92–95]

2.1.1 Light-matter interaction

Light can be described as an electromagnetic wave consisting of an electric and a magnetic field vector, both perpendicular to the propagation direction and to each other, as seen in Figure 2.1. The energy of the light is proportional to the frequency and inversely proportional to the wavelength according to

$$E = hf = \frac{hc}{\lambda} \tag{2.1}$$

where the parameters are energy (E), Planck's constant (h), frequency (f), speed of light (c) and wavelength (λ).

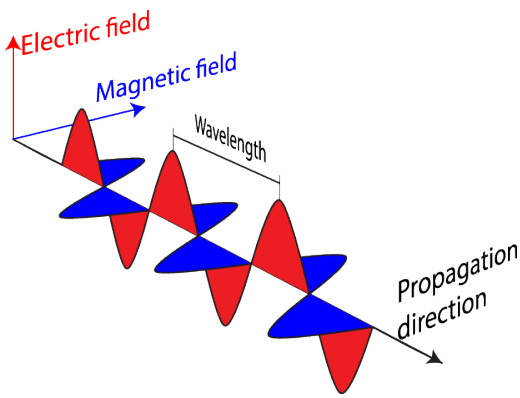

Figure 2.1: Illustration of light as an electromagnetic wave traveling in the propagation direction.

Light emitted from most light sources is depolarized in the sense that the electric field is randomly oriented. In the case where the electric field is oriented in one direction the

light is linearly polarized which can be very useful in investigations regarding orientation of molecular electronic transitions.

When light passes near a molecule the electric field of the light can induce changes in the electron cloud of the molecule if the *Bohr frequency condition* is satisfied, as given in equation (2.2)

$$\Delta E = E_{n+1} - E_n = hf \tag{2.2}$$

This condition states that if the energy of the light is equal to the energy gap (ΔE) between two electronic energy levels of the molecule, the molecule can absorb the light (photon) and in response promote one electron from a lower energy level (n) to the higher one ($n+1$). In this manner the molecule has been excited and may stay in that excited state (ES) for a time before relaxing back to the initial ground state (GS).

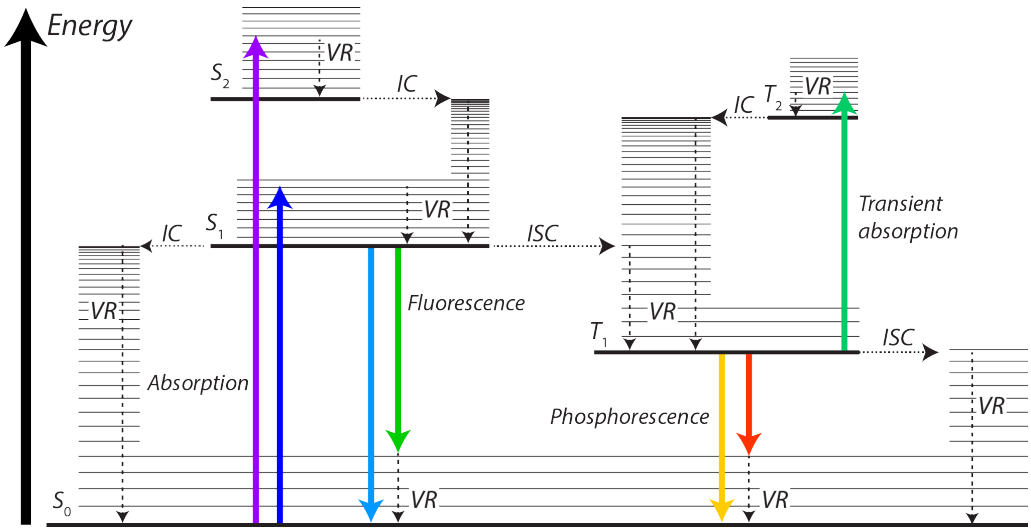

Figure 2.2: Jablonski diagram. The thick horizontal lines represent the electronic singlet (S_n) and triplet (T_n) levels while the thin horizontal lines represent vibrational levels. The acronyms are vibrational relaxation (VR), internal conversion (IC) and ISC.

The Jablonski diagram in Figure 2.2 illustrates the absorption process which usually occurs between states of the same spin multiplicity which in this case is singlet since all the electrons are paired. The excitation due to absorption occurs usually from the electronic singlet ground state (S_0) to a higher vibrational level of the first singlet excited state (S_1) or second singlet excited state (S_2). The reason for this is that the molecular geometry of the ground and excited states differ and so their electronic potential wells are often misaligned. Since the electronic transitions are much faster than the nuclear motion the transitions occur from the lowest vibrational level of the origin state to a higher vibrational level of the final state, and then relax through vibrational relaxation (VR) to the lowest vibrational level. This is often referred to as the *Franck–Condon principle*. Furthermore, excitations to higher excited states like S_2 often result in non-radiative

deactivation through internal conversion (IC) followed by VR down to the lowest excited state (*Kasha's rule*) from where radiative deactivation may occur.[96]

An electron in the excited state may also change its spin when the molecule undergoes inter system crossing (ISC). This process is however considered forbidden which is why the triplet (spin multiplicity is three) excited state is often long lived. The ISC efficiency can be increased with the presence of heavy atoms in the molecular structure due to increased *spin-orbit coupling*. It is also possible to facilitate absorption from one excited state to another as depicted in Figure 2.2 between the first triplet excited state (T_1) and second triplet excited state (T_2). However, this requires a continuous and sufficient supply of the T_1 state species which is usually obtained with intense excitation.

The lowest excited states can often display radiative deactivation down to the ground state. In the case of S_1 the deactivation is usually fast and is referred to as fluorescence. Since the depopulation of the T_1 is forbidden, its radiative deactivation usually produces long lived emission called phosphorescence.

Each transition between the electronic states can be described with a rate constant which reflects the probability of that transition occurring. With this in mind the definition of the quantum yield of a process i is defined as the fraction between the that processes' rate constant and all deactivation rate constants from that state as

$$\Phi_i = \frac{\#\ of\ i\ events}{\#\ of\ photons\ absorbed} = \frac{k_i}{\sum_j k_j} \tag{2.3}$$

where k_j includes k_i. Similarly the lifetime of a process i (τ_i) is determined by the rate constants describing the deactivation of that process as

$$\tau_i = \frac{1}{\sum_i k_i}. \tag{2.4}$$

2.1.2 Förster resonance energy transfer (FRET)

Förster resonance energy transfer (FRET) is a non-radiative energy transfer process from an excited molecule to one in the ground state. It can operate over relatively long distances and has a strong distance (r) dependence as seen in its definition of efficiency

$$\eta_{FRET} = \frac{{R_0}^6}{{R_0}^6 + r^6} = 1 - \frac{\tau_D}{\tau_{DA}} \tag{2.5}$$

where the parameters are the characteristic FRET distance corresponding to 50% energy transfer efficiency (R_0), *inter*-molecular distance (r), and the donor lifetime without and with acceptor (τ_D and τ_{DA}).

The R_0 is given by

$$R_0 = 0.211(\kappa^2 n^{-4} \Phi_D \int_0^\infty F_D(\lambda)\epsilon_A(\lambda)\lambda^4\ d\lambda)^{1/6} \tag{2.6}$$

where κ^2 is an orientation factor, n is the refractive index, Φ_D is the fluorescence quantum yield of the donor, $F_D(\lambda)$ is the are area-normalized donor fluorescence spectra, ϵ_A is the molar absorptivity of the acceptor, and λ is the wavelength.

2.2 Molecular upconversion

This section aims to cover the basic theory behind the TTA–UC process. After a mechanistic overview of the process some emphasis will be put on the vital interaction steps of TET and triplet-triplet annihilation (TTA). This is followed by an overview of the role of spin-statistics in this process and a theoretical view into the maximum UC fluorescence quantum yield (Φ_{UC}). Finally the process of triplet quenching by O_2 will be covered followed by some fundamental kinetic aspects of the TTA–UC process. For deeper coverage on the topic several excellent review articles exist.[10,12,97–100]

2.2.1 The mechanism of the TTA–UC process

Molecular upconversion is the process of upconverting photons in energy using molecules. The process, as depicted in its ideal form in Figure 2.3, relies on the presence of two types of molecules; a sensitizer and an annihilator.

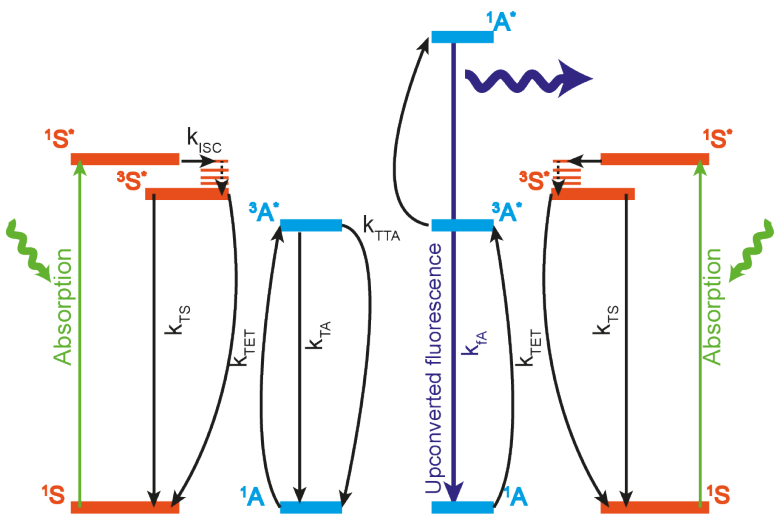

Figure 2.3: Schematic illustration of the TTA–UC process. The superscript numerals denote the spin multiplicity of the sensitizer (S) and annihilator (A) while the asterisk denotes an excited species. k is the rate constant of the processes *inter*-molecular triplet energy transfer (TET), triplet-triplet annihilation (TTA), triplet state decay of the S and A (TS and TA) and annihilator fluorescence (fA).

The sensitizer (S) is chosen such that it can absorb low energy light and through an efficient ISC followed by minor VR result in the triplet excited sensitizer (^{3}S*). An annihilator (A) is chosen such that its T_1 state is slightly lower in energy than the T_1 of the sensitizer. This is necessary in order for the *inter*-molecular triplet energy transfer (TET) process to occur in which the triplet excited sensitizer (^{3}S*) is returned to its ground state (^{1}S) while the singlet ground state annihilator (^{1}A) is sensitized to its excited

triplet state (^{3}A*). Another requirement for a well functioning annihilator is that that the energy of its first excited singlet state should be lower than twice the energy of the triplet excited state ($2E_{T_1} > E_{S_1}$). If this is true and a sufficiently high concentration of the ^{3}A* exists, the TTA process may occur where two ^{3}A* can merge the equivalence of their triplet excited state energies so that one can populate its singlet excited state (^{1}A*) while the other one returns to the ground state (^{1}A). Such event leads to the upconverted fluorescence from the ^{1}A* which is of shorter wavelength than the light used to excited ^{1}S in the first place. It is also very beneficial if the annihilator exhibits high fluorescence quantum yield (Φ_f) for two reasons. Firstly, it assures that most of the UC generated ^{1}A* emits light thus avoiding negative effects on Φ_{UC}. Secondly, a high Φ_f often means a very inefficient ISC channel. In extension this means that once the annihilator is sensitized to its triplet excited state it can stay there for a long time provided no external quenching mechanisms are applied. This is in turn highly beneficial since diffusion controlled TTA–UC systems rely on the collisions between triplet excited annihilators to produce UC emission.

2.2.2 Triplet Energy Transfer

The *inter*-molecular triplet energy transfer (TET) is the process of transferring the triplet excited state energy from the sensitizer (S) triplet state to the annihilator (A) triplet state. In the classic case of the diffusion controlled TTA–UC system this is expected to occur through collision mediated *inter*-molecular orbital overlap in accordance with the *Dexter mechanism.*[25,95,97,101,102]

The triplet energy transfer rate (k_{TET}) can be estimated using the Stern-Volmer relationship by following the quenching of the triplet sensitizer with increasing concentration of the quencher which in this case is the annihilator.[92,94] In the case of dynamic quenching, as TET normally is under diffusion conditions, the same result can be obtained by following either the change in steady-state emission or the change in triplet state lifetime of the sensitizer. In the case of static quenching only the steady-state emission of the triplet state reveals the quenching efficiency or the rate of quenching. In equation (2.7) the relation for dynamic quenching is displayed

$$\frac{I_0}{I} = \frac{\tau_0}{\tau} = 1 + k_{TET}\tau_0[Q] \tag{2.7}$$

where the parameters are emission intensity (I), initial unquenched intensity (I_0), unquenched excited state lifetime (τ_0), excited state lifetime (τ), TET rate constant (k_{TET}), and the concentration of an arbitary quencher (Q). Using the relation in eq. (2.7) the triplet energy transfer efficiency (Φ_{TET}) can be expressed as[92]

$$\begin{aligned} \Phi_{TET} &= 1 - \frac{I}{I_0} = 1 - \frac{\tau}{\tau_0} \\ &= 1 - \frac{1}{1 + k_{TET}\tau_0[Q]} \end{aligned} \tag{2.8}$$

One important optimization parameter to consider when assembling a TTA–UC system is to use appropriate sensitizer and annihilator concentrations. The sensitizer should be

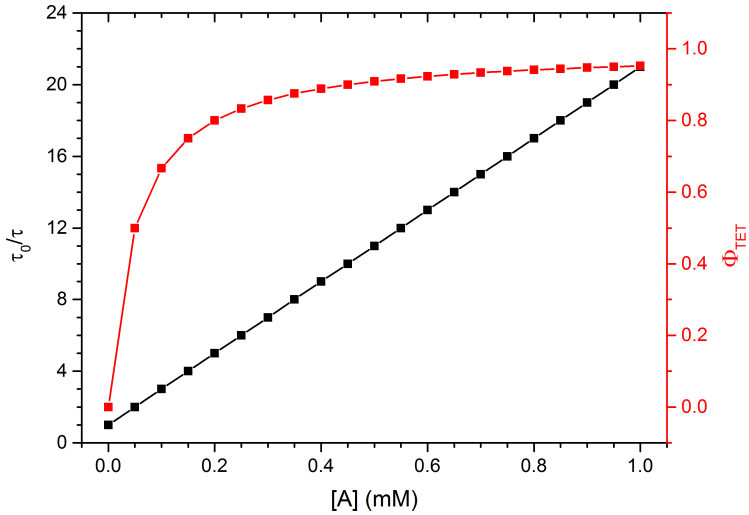

Figure 2.4: The quenching of a hypothetical sensitizer with the triplet lifetime of $\tau_0 = 20$ μs given as the ratio τ_0/τ (black) and the Φ_{TET} (red) vs the annihilator concentration ([A]) in mM. The quenching or TET rate is assumed to be diffusion controlled ($k_{TET} = 1 \times 10^9$ $M^{-1}s^{-1}$).

in high enough concentration to absorb the excitation light well but not too high to cause negative effects on the UC emission. The annihilator concentration should be set so that the triplet excited sensitizer is efficiently quenched. If we assume a diffusion controlled $k_{TET} = 1 \times 10^9$ $M^{-1}s^{-1}$ and a sensitizer lifetime of 20 μs, a sensitizer quenching efficiency of 90% is obtained already with 0.45 mM of annihilator, as seen in Figure 2.4. Normally a TTA–UC sensitizer displays a triplet excited state lifetime more than one order of magnitude longer than what is used in the example and often the employed annihilator (quencher) concentration is in the mM range. With this in mind it is clear that the TET process in a fairly well optimized TTA–UC system operates at near unity efficiency.

2.2.3 Triplet-Triplet Annihilation

The *inter*-molecular triplet-triplet annihilation (TTA) is the process through which two annihilators interact and combine their triplet excited state energies to form one higher singlet excited state on one of the annihilators which will radiate the UC photons. The same diffusion constraints apply to this process as to the TET together with one additional condition prior to the creation of a singlet excited state which radiates the UC photon. The combination of two triplet states does not always yield one excited singlet state and one singlet ground state.[10,97,103]

According to spin statistics the interaction between two triplet excited states of the same two molecules can result in 9 (3×3) possible encounter complex spin states which can be of singlet, triplet or quintet spin multiplicity, according to the rules for combining spin quantum numbers ($s_1 + s_2 = 2$, 1, 0 if $s_1 = s_2 = 1$).[104]

$$^3\mathrm{A}^* + {}^3\mathrm{A}^* \rightleftharpoons {}^1(AA)^* \longrightarrow {}^1\mathrm{A}^* + {}^1\mathrm{A} \tag{2.9}$$

$$^3\mathrm{A}^* + {}^3\mathrm{A}^* \rightleftharpoons {}^3(AA)^* \longrightarrow {}^3A^{2*} + {}^1\mathrm{A} \longrightarrow {}^3\mathrm{A}^* + {}^1\mathrm{A} \tag{2.10}$$

$$^3\mathrm{A}^* + {}^3\mathrm{A}^* \rightleftharpoons {}^5(AA)^* \longrightarrow {}^5A^* + {}^1\mathrm{A} \tag{2.11}$$

Normally, due to degeneracy of the encounter complex spin states, the probability of the spin state formation is weighted with their multiplicity. Thus the relative ratio is 1:3:5 for the formation of singlets, triplets and quintets out of the 9 possible encounter complex spin states. From this perspective the maximum triplet-triplet annihilaton efficiency (η_{TTA}) of forming the ^{1}A* (2.9) is $1/9 \approx 11\%$. It was thought for some time that this was the maximum η_{TTA} and would therefore set the limit on the Φ_{UC} to 5.5% (11%/2 due to maximum of 50%, see subsection 2.2.4).[41,105]

However, it has been observed that the TTA process can exceed this efficiency limitation.[106] This is attributed to the high energy of the annihilator quintet state ($E_{^5A^*}$) which exceeds the singlet excited state energy as well as twice the triplet excited state energy ($E_{^5A^*} > 2E_{^3\mathrm{A}^*} > E_{^1\mathrm{A}^*}$).[107] Therefore, the quintet state is energetically inaccessible by the energy combination of two triplet excited states, thus the path in (2.11) is considered inactive and any quintet encounter complex is forced to dissociate back to the initial triplet states.

Now with only two paths left for the annihilator triplets to be consumed through it is interesting to investigate the triplet encounter complex path (2.10). If this channel is open (i.e. $2E_{^3\mathrm{A}^*} > E_{^3A^{2*}}$), one $^3A^{2*}$ will be created which would return to ^{3}A* through IC and VR (Figure 2.2). This implies that for every two triplets consumed in the triplet channel (2.10), one is returned to participate again in TTA. With this in mind the new maximum η_{TTA} of forming ^{1}A* through (2.9) is $1/(1 + 3/2) = 40\%$.[108]

However, if the second triplet excited state is not accessible with the energy of the two initial triplet states (i.e. $2E_{^3\mathrm{A}^*} < E_{^3A^{2*}}$) as depicted in Figure 2.2, then the (2.10) channel is also inactive and the triplet encounter complex is forced to dissociate back to the two initial ^{3}A*. This would imply, assuming the singlet encounter complex does not dissociate for any reason, that the η_{TTA} could reach 100% in a fully optimal TTA–UC system and thus that the TTA rate constant (k_{TTA}) would be truly diffusion controlled.[97,103] This may not be entirely unrealistic since η_{TTA} as high as 60% have been reported, suggesting that the triplet channel can at be at least partially inactive.[49]

2.2.4 Maximum TTA–UC quantum yield

The TTA–UC quantum yield (Φ_{UC}) can be defined as

$$\Phi_{UC} = \Phi_{ISC} \times \Phi_{TET} \times \Phi_{TTA} \times \Phi_f \tag{2.12}$$

where the Φ_{ISC} is the triplet formation efficiency of the sensitizer, Φ_{TET} is the TET efficiency, Φ_{TTA} is the TTA quantum yield including the effects of spin-statistics and Φ_f is the fluorescence quantum yield of the annihilator. As Equation 2.12 contains the TTA quantum yield, the effect of 1 UC photon from 2 low energy photons is accounted for and hence the maximum UC quantum yield (Φ_{UC}) is 50%.

For an optimally prepared TTA–UC system the Φ_{TET} can be expressed as

$$\Phi_{TET} = \frac{k_{TET}[^1\mathrm{A}]}{k_{TET}[^1\mathrm{A}] + k_{TS}} \tag{2.13}$$

where ^{1}A is the ground state annihilator, k_{TET} is the TET rate constant (subsection 2.2.2), and k_{TS} is the rate of all first and pseudo-first order decay processes of the sensitizer triplet excited state. Likewise the triplet-triplet annihilaton quantum yield (Φ_{TTA}) can be expressed as

$$\Phi_{TTA} = \eta_{TTA}\frac{k_{TTA}[^3\mathrm{A}^*]}{2k_{TTA}[^3\mathrm{A}^*] + k_{TA}} \tag{2.14}$$

where η_{TTA} is the maximum allowed TTA efficiency due to spin-statistics, k_{TTA} is the TTA rate constant, k_{TA} is the rate of all first and pseudo-first order decay processes of the annihilator triplet excited state and ^{3}A* is the triplet excited annihilator. For derivations of equations (2.13) and (2.14), please refer to **Paper VII SI**.

As can be seen from equation (2.13) the Φ_{TET} increases towards unity as the rate $k_{TET}[^1\mathrm{A}]$ exceeds k_{TS}. As k_{TET} normally is diffusion controlled, the TET process can be optimized using high enough annihilator concentration ($[^1\mathrm{A}]$). Similarly the Φ_{TTA} increases towards 0.5, due to the factor 2 in the denominator, as the rate $k_{TTA}[^3\mathrm{A}^*]$ exceeds k_{TA} if $\eta_{TTA} = 1$. However, this yield depends on ^{3}A* concentration which in turn, through ^{3}S* via the TET process, depends on the excitation intensity if the intensity is below a certain threshold I_{th} (see subsection 2.2.6). Therefore, given an optimal TTA–UC system with high enough excitation intensity, and η_{TTA}, Φ_{ISC} and Φ_f at unity, the Φ_{UC} may reach its theoretical maximum of 50%.

2.2.5 Triplet quenching by O_2

Molecular oxygen resides in its triplet ground state ($^3\sum_g^-$), here referred to as $^3O_2$ and has a relatively low first excited singlet state ($^1\Delta_g$) at 0.98 eV, here referred to as $^1O_2$*. With such low excited state $^3O_2$ can quench most triplet excited species through a *Dexter mechanism* energy transfer and in the process raise to its first singlet excited state $^1O_2$*.[109] Additionally, it can also interact with other species and affect the electronic structure resulting in the enhancement of the ISC from triplet excited state to singlet ground state.[110–112]

The TTA–UC system relies heavily on long lived excited triplet states of its components and the efficiency hinges on the TET and TTA processes outcompeting any first or pseudo-first order excited state deactivations, including any unwanted triplet state quenching. Considering that $^3O_2$ has a diffusion and quenching rate which is approximately one order of magnitude above the same for sensitizers and annihilators in most fluids, it is a very efficient triplet excited state quencher.[94,109] This has a twofold negative impact on the system as a whole. Aside from lowering Φ_{UC}, it is sensitized to its reactive $^1O_2$* which may readily react with the available TTA–UC components contributing to degradation and permanently lowering the possible Φ_{UC}. Therefore, the O_2 content in the TTA–UC samples should be kept as low as possible, preferably at sub ppm levels.

2.2.6 Threshold intensity

The TTA–UC process is bimolecular and because of this it can, at low excitation intensities, display a quadratic UC emission dependence on excitation intensity. In this region the kinetics of TTA–UC is mainly governed by first order processes like the natural decay of the sensitizer and annihilator which constantly compete with the bimolecular TET and TTA processes. In this region the Φ_{UC} depends linearly on the excitation intensity.

As the excitation intensity increases so does the concentrations of the triplet excited sensitizer and the annihilator and with that the bimolecular processes start to work more efficiently. Further increase of the excitation intensity supply the bimolecular TET and TTA processes with enough triplet excited state species to saturate the efficiency of the processes. At this point Φ_{UC} is independent of excitation intensity, like a normal chromophore would be.

One such characteristic is the threshold between the linear and the quadratic region. For an ideally prepared TTA–UC system it is given as

$$I_{th}^{ideal} = \frac{{k_{TA}}^2}{2k_{TTA}} \tag{2.15}$$

as also described by others[25,113,114], where the parameters are triplet excited state rate constant for the annihilator (k_{TA}) and k_{TTA}.

The expression in equation (2.15) give the excitation intensity in the somewhat odd unit of concentration per time (M/s). While being a convenient expression which only depends on two annihilator-associated rate constants, it may be more useful to express it in terms of photon flux as

$$P_{th}^{ideal} = \frac{{k_{TA}}^2}{2k_{TTA1}\alpha\left[{}^1\mathrm{S}\right]} \tag{2.16}$$

where the parameters are absorption cross section (α) and singlet ground state sensitizer (^{1}S) concentration. For deeper discussion and derivation of these expressions refer to **Paper V** and its supporting information (SI).

2.2.7 Triplet lifetime with second order channels

Measuring a long triplet lifetime in diffusion allowed environment can be problematic as part of the recorded kinetic trace may represent bimolecular quenching interactions. Measurements of the sensitizer triplet lifetime are often perturbed by a competing triplet-triplet annihilation of the sensitizer (TTAS) process while for the annihilator it is the TTA process. As discussed earlier, these processes depend on the triplet excited state concentrations, thus it is recommended to record the data using different excitation intensities.

The triplet lifetime can be obtained through global fit of the equation (2.17) on the data with different excitation intensity. This expression takes into account the relative contribution of the second order channel and the trivial first order decay by

$$I(t) = I_0 \frac{1-\beta}{\exp(t/\tau_T) - \beta} \tag{2.17}$$

where the parameters are I, time (t), triplet excited state lifetime (τ_T) and a dimensionless parameter in the range 0 to 1 (β) describing the fraction of the initial decay that is governed by the second order channel ($\beta = 1$) compared to the first-order ($\beta = 0$).[108]

The parameter β is defined as

$$\beta = \frac{k_{TTA}[^3\mathrm{A}^*]}{k_{TTA}[^3\mathrm{A}^*] + k_{TA}} \tag{2.18}$$

which is very similar to the definition of Φ_{TTA} in equation (2.14).

CHAPTER 3

Methods

This chapter will briefly cover the most used experimental techniques in the research comprising this Thesis.

3.1 Absorption spectroscopy

Steady-state absorption spectroscopy records the average absorbance of the molecules in a sample as a function of wavelength. An overview of a typical experimental setup is given in Figure 3.1.

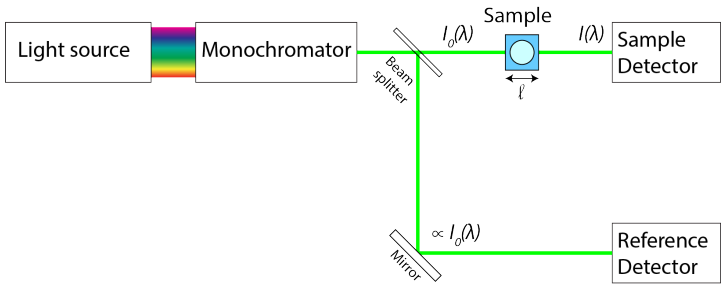

Figure 3.1: Simple schematic illustration of a typical setup inside an absorption spectrometer.

By relating the incident light intensity (I_0) and the transmitted (I), the absorbance (Abs) as a function of wavelength (λ) is obtained through

$$Abs(\lambda) = -\log\left(\frac{I(\lambda)}{I_0(\lambda)}\right). \tag{3.1}$$

The absorbance is related to the molecular concentration via *Lambert-Beer law* which states that

$$Abs(\lambda) = \varepsilon(\lambda) C l \tag{3.2}$$

where $\varepsilon(\lambda)$ is the molar absorptivity ($\mathrm{M}^{-1}\mathrm{cm}^{-1}$), l is the path length that light travels through the sample (cm) and C is the molecular concentration (M). Care must be taken to not use too high concentrations as this might cause aggregate formation, or simply too high absorbance where the linearity of the equation (3.2) is not valid.

Absorption is additive in the sense that the total absorption of n species is given by

$$Abs(\lambda) = l \sum_{i=1}^{n} \varepsilon_i(\lambda) C_i. \tag{3.3}$$

The ε is related to the absorption cross section (α) in cm^2 via

$$\alpha(\lambda) = \frac{2.303\varepsilon(\lambda)}{N_A} \tag{3.4}$$

where N_A is Avogadro's number. The absorption cross section is useful when calculating the excitation rate from excitation intensity, amongst other things.

3.1.1 Transient absorption spectroscopy

Transient absorption is performed with time-resolution to follow the kinetics of non-emissive excited states (Figure 2.2). The general setup is given in Figure 3.2.

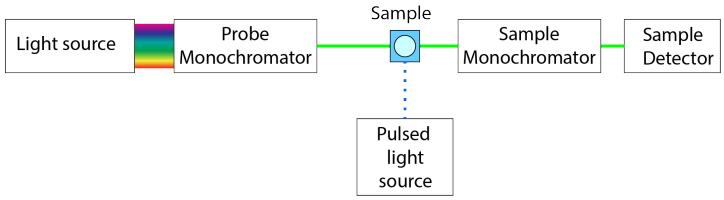

Figure 3.2: General setup for a transient absorption measurement. This setup resembles in particular nano-second transient absorption laser equipment setup.

Normally a probe beam is sent through the sample to the detector, giving the absorbance of the ground state. A pulsed light source (often a pulsed laser) is then used to provide enough excitation light for exciting a significant amount of molecules to their excited state. This is timed on the detection side and so upon excitation another measurement of absorbance is made. The difference ($\Delta Abs(\lambda)$) is calculated according to equation (3.5) and arises from the difference in concentration and molar absorptivity between the ground state (GS) and excited state (ES) ($\varepsilon_{GS} \neq \varepsilon_{ES}$).

$$\begin{aligned} \Delta Abs(\lambda) &= Abs_{ES}(\lambda) - Abs_{GS}(\lambda) \\ &= \log\left(\frac{I_0(\lambda)}{I_{ES}(\lambda)}\right) - \log\left(\frac{I_0(\lambda)}{I_{GS}(\lambda)}\right) = \log\left(\frac{I_{GS}(\lambda)}{I_{ES}(\lambda)}\right) \end{aligned} \tag{3.5}$$

Through variation of the time delay between the excitation pulse and the capture of the signal a time trace can be constructed which will reflect the kinetics of the excited state of interest.

3.2 Emission spectroscopy

The emission spectroscopy techniques in this section are limited to fluorescence and phosphorescence spectroscopy. Steady-state emission is normally measured perpendicular to the incident excitation light according to the schematic in Figure 3.3.

Fluorescence spectroscopy can be performed in two ways. The most common type of measurement is where the excitation wavelength is fixed and emission wavelength is scanned to give the emission spectra. This measurement reveals the spectral emission properties of the investigated compound. Alternatively, the excitation light is scanned over the absorption spectrum while the emission wavelength is fixed and the emission intensity is displayed as a function of excitation wavelength. This type of measurement produces excitation spectra which can be useful for investigating if the excitation over the absorption spectra leads to emission from the same excited state or species.

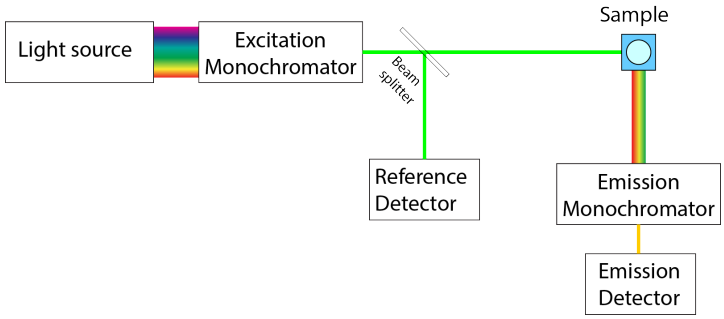

Figure 3.3: General setup for emission measurement. Excitation light can be modulated using the excitation monochromator. As steady-state measurements of this kind can take from seconds to minutes to perform, the excitation light intensity is monitored to account for any possible fluctuations. The emission monochromator selects the wavelength of the emitted light that will reach the emission detector.

3.2.1 Time-resolved emission spectroscopy

The experimental setup for time-resolved emission spectroscopy is very similar to that of the steady-state case (Figure 3.3). The main difference lies in the light source and emission detection. Normally a pulsed light source is used and the detection of the signal is timed with the excitation frequency. For kinetics on long time scale compared to the length of the excitation pulse, often direct capture of the emission signal can be made. If the kinetics time scale approach that of the excitation pulse, the signal may be differentiated from the instrument response of the excitation pulse using reconvolution analysis. This in especially useful for picosecond and slower kinetics where time correlated single photon counting (TCSPC) is often employed.

In TCSPC, a small fraction of photons are detected per excitation pulse as the electronics cannot detect and store all emitted photons in the correct time channels. It is important to keep the rate of emitted photons per excitation low to avoid counting two or more photons as one in the detection system which would result in faster kinetics than it actually is. Since the time scale is split up in discrete channels which are gradually filled for each photon count at that specific time, the obtained kinetic trace is represented in the form of a histogram of photons detected most frequently (in the beginning) to least often detected ones (in the end).

3.2.2 Fluorescence anisotropy

The fluorescence anisotropy measurement is a form of emission measurement that can reveal the rotational mobility of the emissive transition moments that are investigated. This mobility can be correlated to the size and shape of the molecular structure as well as the viscosity of the surrounding environment. The most common way of measuring fluorescence anisotropy is by applying alternating vertical and horizontal polarization of excitation and emission. This is commonly denoted in the first and second subscripts of the intensity (I) for excitation and emission, respectively. Thus, the fluorescence

anisotropy is defined as

$$r = \frac{I_{VV} - GI_{VH}}{I_{VV} + 2GI_{VH}} \tag{3.6}$$

where G is a correction factor for the possible polarization bias at the emission side of the equipment and is defined as

$$G = \frac{I_{HV}}{I_{HH}}. \tag{3.7}$$

For example a value of $G = 2$ would imply that the throughput of vertically polarized light on the emission detection side is twice as efficient compared to the same for the horizontally polarized light.

For a molecule, the orientational information in the form of anisotropy is only maintained if the molecule is prevented from moving or rotating, alternatively that it is doing so to a minor extent during its excited state lifetime. The degree of mobility can be expressed in the form of a relative absorption/emission transition dipole angle (ω). Knowing this angle will give the fundamental anisotropy (r_0) for a certain molecule as

$$r_0 = r_{max}\left(\frac{3cos^2\omega - 1}{2}\right) \tag{3.8}$$

where the maximum anisotropy (r_{max}) is $2/5$.[92,115]

In the case of polarized excitation sources, like lasers, it is expected that the emission can be biased to the polarization direction of the excitation light. Therefore it is important to have a "magic angle" of 54.7° between the polarization direction of the excitation source and the emission detection, since at this angle r_0 in equation (3.8) is zero.

CHAPTER 4

Summary of work

This chapter contains summarized content of the papers upon which this Thesis is based on together with comments and discussion of the results. It is my intention to present the work of this Thesis in the order of progression towards functional solid state TTA–UC system. Therefore, first work concerning TTA–UC in fluid media will be described. This will be followed by work concerning the pursuit of supramolecular TTA–UC system capable of UC in Solid media.

4.1 Optimization and application of the fluid system

In this section **Paper I** and **Paper II** are covered and describe general optimization of TTA–UC sample preparation avoiding tedious mechanical oxygen removal and also TTA–UC as a general independent add-on technology for increased efficiency of solar thermal fuel generation.

4.1.1 Making fluid TTA–UC more user friendly

Due to the reliance on diffusion in fluid TTA–UC systems based on *inter*–molecular energy transfer processes it is of high importance that the ^{3}S* and triplet excited annihilator (^{3}A*) are long lived to maximize the statistical probability of collision facilitated interaction necessary for the TET and TTA processes. Given these requirements, any presence of diffusive triplet quencher is bound to result in lowering of the TTA–UC efficiency as the quencher would have plenty of time to interact with the triplet excited TTA–UC components. Naturally O_2 is one such quencher with a rate of diffusion in the order of 1×10^{10} s^{-1} in toluene while larger molecules like S and A often diffuse one order of magnitude slower,[116] making O_2 a very efficient quencher.

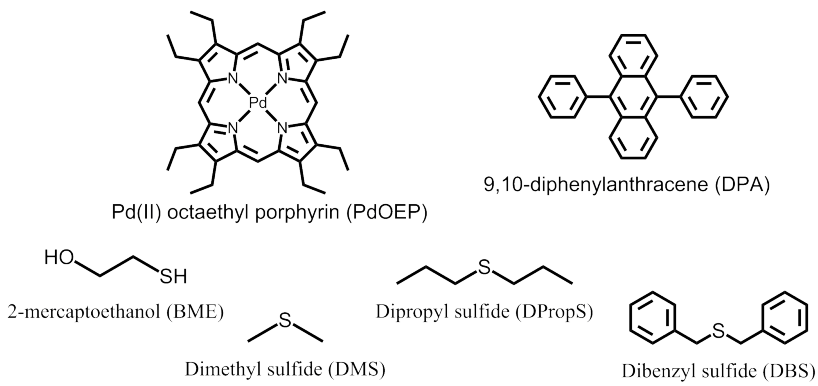

Figure 4.1: Structures and names of the molecules used in this study. The PdOEP and DPA are sensitizer and annihilator, respectively. The four scavengers used are 2-mercaptoethanol (BME), Dimethyl sulfide (DMS), Dipropyl sulfide (DPropS) and Dibenzyl sulfide (DBS).

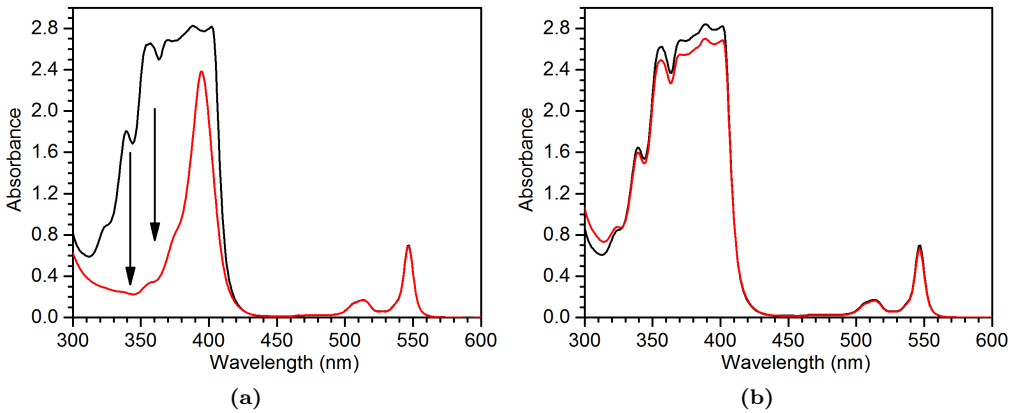

Figure 4.2: Absorption spectrum before (black) and after (red) irradiation at 532 nm of high concentration TTA–UC system without scavenger (a) and with 500 mM DMS as scavenger (b).

Preliminary results in **Paper I** demonstrate how deoxygenation can be performed using the TTA–UC system itself by adding an O_2 scavenger (Figure 4.1) to the sample containing PdOEP and DPA as S and A, respectively, in toluene. As the TTA–UC process proceeds more and more of the triplet ground state O_2 ($^3O_2$) is sensitized to the more reactive singlet excited O_2 ($^1O_2$*) which readily reacts with the scavenger yielding an oxidation product. A general schematic of this reaction is given in Figure 4.3a.

Thus, by exciting the sensitizer and attempting to drive the TTA–UC process the dissolved O_2 is gradually being depleted. As the depletion proceeds the Φ_{UC} increases and therefore the sensitization and production of the $^1O_2$* also increases until either of the two oxidation reactants are consumed.

The kinetics of this process is dependent on the excitation intensity, the TTA–UC component concentration and the concentration of the scavenger. The excitation intensity at 532 nm was set to a power density of 8 W/cm^2 ($\sim 2.2 \times 10^{19}$ photons/cm^2/s) and samples were irradiated for 30 minutes. At this high intensity the UC emission is expected to depend linearly on excitation intensity, once the quenching by O_2 is minimized (see Chapter 2). Under these premises two concentrations of the TTA–UC system were investigated. The high concentration TTA–UC system consisted of 16 μM PdOEP and 500 μM DPA, while the low concentration TTA–UC system consisted of 5 μM PdOEP and 100 μM DPA.

For the high concentration TTA–UC system (Figure 4.3b), a sample with no scavenger was investigated yielding no UC emission and high degradation of DPA as seen in Figure 4.2a. Using the scavenger DMS (Figure 4.1) at a concentration of 500 mM with the same TTA–UC system, an impressive Φ_{UC} of 12% is obtained after 7 minutes of irradiation as seen in Figure 4.3b. A minor decrease in Φ_{UC} is observed at the end of the irradiation process but no major indication of DPA degradation was observed, as seen in Figure 4.2b. Similar Φ_{UC} value is also obtained using 10 mM DMS but a more

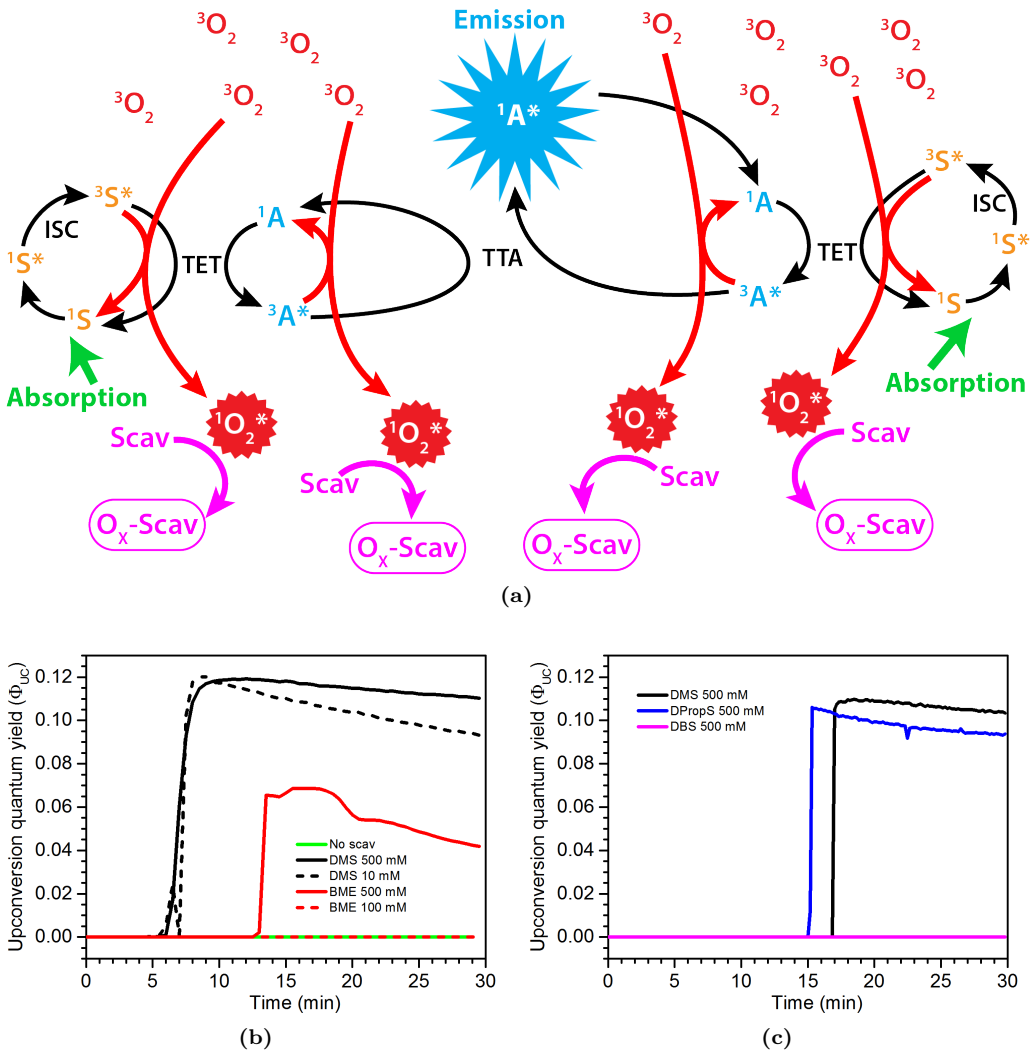

Figure 4.3: (a) Schematic description of the TTA–UC process in presence of O_2 and an oxygen scavenger (Scav). (b) Measured Φ_{UC} trace during continuous excitation with varying scavengers and without. The high concentration TTA–UC system consists of [PdOEP] = 16 μM and [DPA] = 500 μM. Displayed traces are for sample without scavenger and samples containing DMS and BME as scavengers. (c) Low concentration TTA–UC system consisting of [PdOEP] = 5 μM and [DPA] = 100 μM. Displayed are traces for samples containing DMS, DPropS and DBS.

significant decrease in UC intensity was observed towards the end of the irradiation. Upon investigating the scavenger BME (500mM) the onset of the UC emission appeared later in time (∼13 min) and reached a maximum Φ_{UC} of about 7%. Absorption measurement

revealed substantial degradation of DPA and almost complete degradation in the case of 100 mM BME which, in addition, did not produce any UC emission.

The late activation of the UC emission in the case of BME was attributed to poor scavenging. In the case of insufficient or inefficient scavenger, oxidation of the TTA–UC components starts to occur and as a consequence lowers the Φ_{UC}.[98,117] To explore this further, a low concentration TTA–UC system was prepared (*vide supra*) with about equal sensitizer to annihilator ratio as in the high concentration system, which is vital for an efficient *inter*-molecular triplet energy transfer (TET) process (see Chapter 2). In this setup (Figure 4.3c) 500 mM DMS was applied again and as expected the UC emission appeared later in time. Since the concentration ratio of sensitizer/annihilator was about the same as for the previous TTA–UC system, the obtained Φ_{UC} was also close to 12%. Another potential scavenger, DPropS (Figure 4.1), was investigated in the same system at 500 mM and UC emission appeared even sooner than with DMS, though with slightly lower Φ_{UC}. A more rapid lowering of Φ_{UC} was observed for the remainder of the irradiation process but without degradation of DPA. The final scavenger tested was DBS (Figure 4.1) at a concentration of 500 mM which did not give rise to any UC emission but no significant DPA degradation either. Instead new absorption bands appeared in the 300-350 nm region. For absorption measurements see **Paper I** SI.

In an attempt to quantify the O_2 concentration after scavenging, a sample containing 16 μM PdOEP and 500 mM DMS was prepared and irradiated for 30 minutes. The phosphorescence lifetime was determined to 112 μs which is far from the unquenched 770 μs.[118] Using this information along with the assumption that the bimolecular quenching rate for oxygen is $\sim 1 \times 10^{10}$ $M^{-1}s^{-1}$ and solving equation (2.7) for the quencher concentration, the obtained oxygen concentration is 0.76 μM. This can be compared to the estimated 1740 μM O_2 in toluene at atmospheric pressure and room temperature (see **Paper I**).

In short, oxygen scavengers were used to deplete O_2 from closed TTA–UC systems under continuous irradiation. DMS and DPropS appear to be the best scavengers tested. Lifetime measurements of PdOEP reveal almost complete oxygen depletion with DMS. These are preliminary results and more scavengers will be investigated with additional types of experiments.

4.1.2 Applying fluid TTA–UC to solar energy harvesting technology

As mentioned in Chapter 1 one big game-changer in terms of solar energy is the storage of solar energy. Today that is mainly done with batteries but in-chemical-bond storage is also a viable option.[8,119]

The solar thermal energy storage system fulvalene diruthenium ($FvRu_2$) has a lowest absorption band at around 400 nm with a tail stretching up to 450 nm.[119] Absorption of light in this region facilitates the photoisomerisation from its low-energy *cis* form to the high-energy *trans* form (Figure 4.4a) which does not absorb at all in the visible region, as indicated in Figure 4.4b.[120,121] Like in the previous section the employed TTA–UC system consists of PdOEP and DPA as the sensitizer and annihilator, respectively in toluene. The motivation of choosing this TTA–UC system was based on the good absorption and

triplet formation of the sensitizer and the matching emission spectrum of DPA with the *cis*-form of the $FvRu_2$.

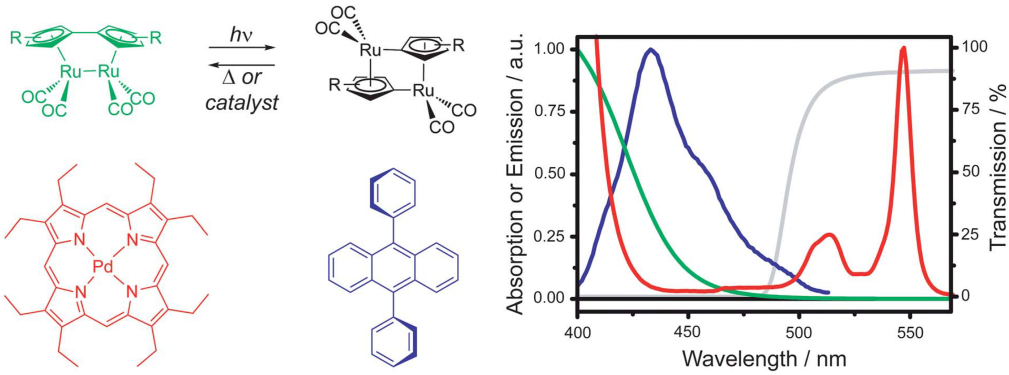

(a) **(b)**

Figure 4.4: (a) The $FvRu_2$ derivative (green/black, R = 1,1-dimethyltridecyl) is used as solar fuel with recycling capability. The TTA photon upconversion system consisting of PdOEP (red) and DPA (blue) as sensitizer and annihilator, respectively. (b) Normalized absorption spectra of $FvRu_2$ *cis*/*trans*-form (green/black) and PdOEP (red), fluorescence spectrum of DPA in the presence of PdOEP (blue), and transmission spectrum of the glass filter (grey).

A custom made microfluidic device was constructed to act as a flow reactor to enable continuous solar energy harvesting. As illustrated in Figure 4.5a the construction is based on stacking of two identical microfluidic chips and the channel in each chip has a total irradiation area of 400 mm^2 and a total volume of 25 µL. The solar fuel is pumped through the upper chip allowing it firstly to be exposed to the filtered light. Part of the light that passes through the solar fuel is absorbed by the TTA–UC system in the lower chip and upconverted. This UC-light is in the correct spectral region to drive photoisomerization of the solar fuel.

In Figure 4.5b photoisomerization efficiency from the low-energy *cis* to the high-energy *trans* form of the $FvRu_2$ is given as a function of retention time in the chip, with and without TTA–UC system beneath it. The dependence is close to linear and an enhancement of the solar fuel conversion due to the presence of TTA–UC is 130 % in this benchmark setup where conversion from direct excitation of the solar fuel is minimized using the glass filter.

4.1.3 Discussion and conclusions

The work summarized in Section 4.1 focuses mainly on the fluid based TTA–UC systems. The fluid based TTA–UC system constitutes the origin of the TTA–UC field itself as it was in solution that the phenomenon was firstly observed in the early 1960s.[17–20] Some of the most efficient TTA–UC have been produced in fluid environments[49,122] as the

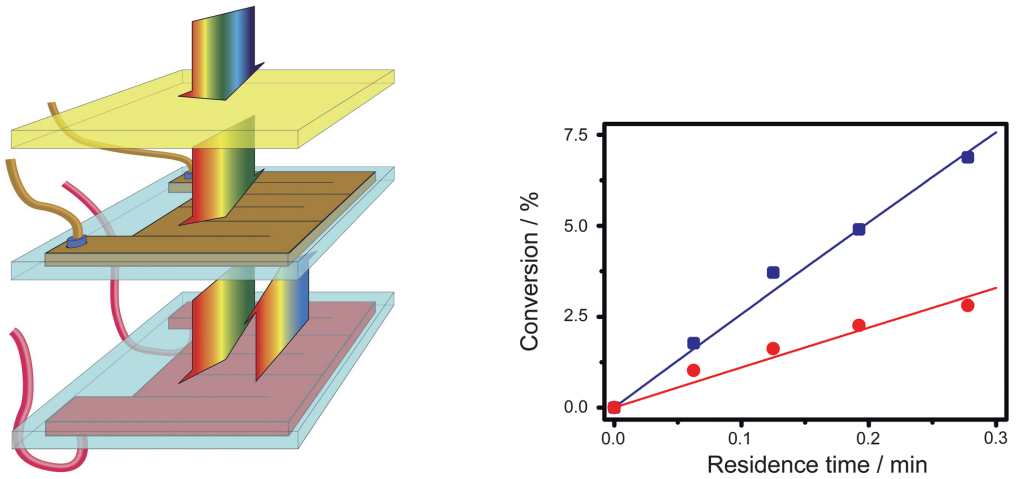

(a) **(b)**

Figure 4.5: (a) A schematic illustration of the microfluidic reactor. White light illuminates the system through a glass filter (cut-on wavelength = 495 nm). The filtered light illuminates the microfluidic glass chips. The solar fuel flows through the upper chip while TTA–UC fluid resides in the lower. (b) Conversion efficiency (%) of photoisomerized $FvRu_2$, with (blue squares) and without (red circles) the TTA–UC system, as a function of residence time in the microfluidic flow reactor.

diffusion is beneficial in the sense that once the TET process occurs the S and A can dissociate so that the parasitic FRET process (Chapter 2) cannot occur from the excited A back the sensitizer, S.

However, a long standing issue with fluid samples has been the preparation to avoid dissolved O_2 in the system. Numerous solutions to the problem have been suggested ranging from encapsulating the active molecules in microemulsion or nanocapsules[123,124], to applying protective non-O_2-permeable barrier around semifluid solvents[125], to mechanical gluing of sample cells[124], as well as the probably oldest and still very efficient melt-sealing of the sample cell. While these methods may be doable in a laboratory environment they pose problems for possible real-life applications due to being impractical. This can be efficiently circumvented by introducing an oxygen scavenger as a third species to the TTA–UC system.

The requirements for such a scavenger are several though. Firstly the scavenger must be spectroscopically inactive, at the very least spectroscopically incompatible with the S and A chromophores to not perturb the TTA–UC process. Furthermore, the scavenger should be selectively reactive with $^1O_2$* and should produce spectroscopically inactive products after oxidation. The scavenger should also ideally be commercially available to allow usage in large quantities.

Provided that these requirements are met the employment of scavengers to degas TTA–UC would be advantageous in several ways; i) allow for usage of TTA–UC in larger

quantities, ii) give efficient removal of O_2 since the complete TTA–UC process acts as O_2 sensitizer until it is depleted, iii) permanent depletion of O_2 due to irreversible reaction with the scavenger, iv) highly reproducible O_2 removal resulting in higher reproducibility of TTA–UC systems performance, v) high performance TTA–UC systems could be prepared in application-optimized sample containers.

In the preliminary stage of the oxygen scavenging study it is concluded that it is possible to utilize oxygen scavengers to deplete O_2 in closed TTA–UC samples through excitation of the TTA–UC system. The best scavengers out of those few tested seem to be the thioethers DMS and DPropS. DMS displays higher robustness over longer times while DPropS seems to be more efficient in the sense that the UC emission appears sooner during irradiation. Before this study is concluded more scavengers will be tested in different experiments. For example it will be interesting to find out how the scavenged samples compare to the mechanically deoxygenated ones both in terms of Φ_{UC} and long term robustness as well as if there is any gain in combining mechanical removal of O_2 with scavenging.

Concerning the solar thermal energy fuel it is demonstrated that it is possible to drive TTA–UC with non-coherent light which in turn is used to drive a solar energy harvesting reaction. This has been achieved by stacking solar energy harvesting technology on top of the TTA–UC device to supply the harvester with upconverted light produced by otherwise non-useful photons from the light source.

4.2 Towards supramolecular TTA-UC - design and evaluation

In this section **Papers III-VII** are covered and describe a stepwise pursuit towards supramolecular TTA–UC systems with the aim to have all the necessary energy transfer processes occurring *intra*-molecularly. This is of high interest as the *intra*-molecular energy transfer processes are expected to operate at rates far exceeding the rate of diffusion. In such case the rate at which an intra-molecular TTA–UC process operates would outcompete that of any *inter*-molecular quenching processes, thus circumventing the problematic quenching by O_2.

4.2.1 Probing modification possibilities of the DPA annihilator

As a first step towards supramolecular TTA–UC with complectly *intra*-molecular mechanisms capable of UC in diffusion free environments an investigation in to the extent of how much one can manipulate the structure of DPA while still maintaining its excellent spectroscopic properties is necessary. Knowing the answer to this question is crucial for the design of supramolecular annihilators with multiple covalently attached DPA units.

In **Paper III** eight modified versions of DPA were synthesized (Figure 4.6; **3-10**) containing either electron donating, electron withdrawing or both group types and their photophysical properties were investigated with support of Density functional theory (DFT) calculations. The absorption spectra for all compounds display strong similarity to DPA (**1**) with minor (< 10 nm) red shift (Table 4.1) which is in good agreement with the

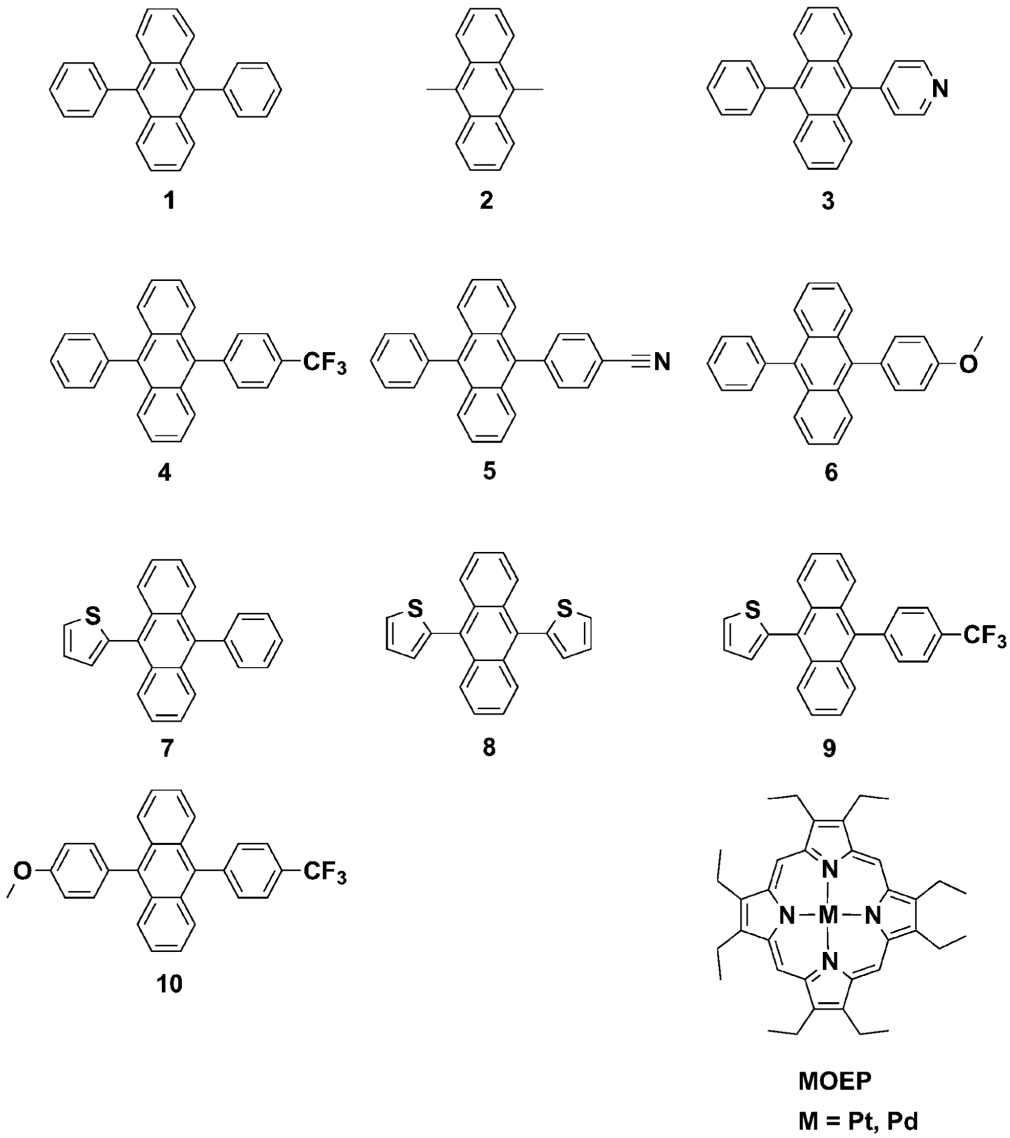

Figure 4.6: Structures of the 9,10-substituted anthracenes and octaethylporphyrins with palladium and platinum metal cores investigated in this study. Compound **1** is the well known DPA which is used as reference.

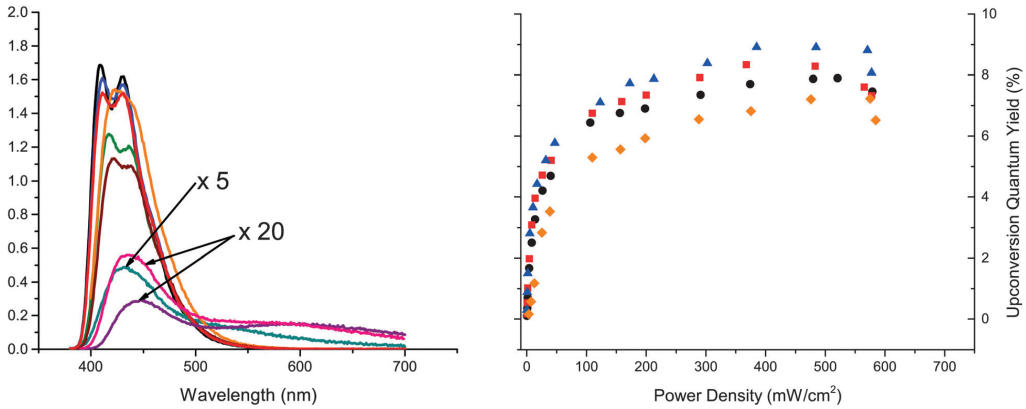

Figure 4.7: (a) Emission of the compounds **1**(▬), **3**(▬), **4**(▬), **5**(▬), **6**(▬), **7**(▬), **8**(▬), **9**(▬) and **10**(▬), (b) Φ_{UC} of chosen compounds **1**(●), **3**(■), **4**(▲), **5**(◆).

DFT. The phenyl-substituted compounds **3**–**6** and **10** have similar fluorescence spectra to that of DPA, **1** (Figure 4.7a), as well as similarly high fluorescence yields (Table 4.1). The same is not true for compounds containing thiophene as seen in Figure 4.7a and these compounds also display substantially lower Φ_f compared to DPA with **8** as the lowest at 2%. The emission spectra for these derivatives (**7**–**9**) display a long tail into the red reaching up to about 750 nm suggesting that the excitation is more delocalized due to the small thiophene substituent having more rotational freedom than the more sterically hindered phenyl substituent.[126] This easier rotation of the thiophene group is likely responsible for opening new non-radiative deactivation pathways, compared to the more bulky phenyl groups, resulting in a substantial lowering of the fluorescence quantum yield. The phenyl-containing compounds display consequently higher Φ_f, many of which are close to that of DPA. Same trend of similarities is found regarding fluorescence lifetime (τ_f) for the more emissive compounds (Table 4.1).

Using nanosecond transient absorption no triplet states were detected upon direct excitation of any of the compounds. Instead platinum(II)–octaethylporphyrin (PtOEP) (Figure 4.6) was used as a triplet sensitizer to facilitate the measurement of deaerated samples. The transient absorption kinetic trace was fit to equation (2.17) to yield triplet excited state lifetime (τ_T) which displays the same trend as for the compounds with higher Φ_f; longer triplet lifetimes for the diphenyl- and shorter for the thiophene substituted compounds as indicated in Table 4.1. The solubility in toluene was determined to be above 40 mM for all compounds except for **4** displaying a solubility roughly one order of magnitude less.

Using equation (2.7) the k_{TET} rate constant is determined with PtOEP as the sensitizer for all compounds. The obtained k_{TET} (Table 4.1) is approximately diffusion limited ($\sim 1 \times 10^9$ $M^{-1}s^{-1}$) for all compounds as expected. This suggests that the energy of the

Table 4.1: Determined photophysical properties for 9,10-substituted anthracenes as possible TTA–UC annihilators in toluene.

[a]C.	[b]Sol.	ε ([c]$Abs_{\max}$)	Φ_f	τ_f	τ_T	[d]k_{TET}	[d]k_{TTA}	[d]Φ_{UC}
	(mM)	$\times 10^{-4}$ ($M^{-1}cm^{-1}$) (Wavelength (nm))		(ns)	(ms)	$\times 10^{-9}$ ($M^{-1}s^{-1}$)	$\times 10^{-9}$ ($M^{-1}s^{-1}$)	
1	93	1.21 (395), 1.25 (375), 0.76 (356)[127]	1.0[128]	6.97	8.61	2.15	2.51	0.077
2	115	0.92 (401), 0.955 (380), 0.56 (360)	∼0.7[129]	—	—	3.97	—	—
3	39	1.21 (395), 1.28 (374), 0.79 (356)	0.96 ± 0.020	6.93	7.73	1.93	2.31	0.079
4	8	1.22 (395), 1.29 (374), 0.795 (356)	1.0 ± 0.010	6.84	9.55	1.92	2.25	0.087
5	83	1.24 (395), 1.31 (375), 0.80 (357)	0.99 ± 0.003	5.54	1.73	1.81	1.98	0.069
6	47	1.245 (396), 1.32 (375), 0.815 (357)	0.84 ± 0.065	5.50	18.95	2.25	—	—
7	256	1.255 (397), 1.315 (377), 0.8 (358)	0.09 ± 0.002	—	0.043	2.07	—	—
8	61	1.35 (400), 1.365 (379), 0.815 (360)	0.02 ± 0.000	—	0.005	2.52	—	—
9	76	1.28 (397), 1.32 (376), 0.80 (358)	0.026± 0.006	—	0.043	2.17	—	—
10	107	1.23 (396), 1.30 (375), 0.80 (357)	0.77 ± 0.016	4.69	8.50	1.90	1.77	—

[a] Compound. [b] Solubility. [c] Reported values are the average of two independent measurements. [d] PtOEP as the sensitizer.

first triplet excited state (T_1) of all compounds is lower than that of PtOEP (1.86 eV[40]) as is the case for DPA (1.77 eV[130]).

The functionality of the derivatives as annihilators in TTA–UC was investigated for derivatives **3**, **4**, **5** and **10** as well as for the reference **1** with PtOEP as the sensitizer. Transient absorption kinetics of the TTA–UC process were simulated and fit (see SI of **Paper III** for details about the model and fitting procedure) to the measurements and gives k_{TTA} (Table 4.1). Furthermore the Φ_{UC} was determined for compounds with the highest Φ_f, namely **1**, **3**, **4**, and **5** again with PtOEP as the sensitizer relative to ZnOEP as the reference (Table 4.1).

The characteristic UC excitation intensity dependence produces non-linear dependence for low excitation intensities and linear dependence for high excitation intensities (Chapter 2). In the linear region where the TTA–UC process no longer is limited by the annihilator triplet concentration, the Φ_{UC} (Figure 4.7b) is independent of excitation intensity, which will be discussed further in **Paper VII**.[114,122] The Φ_{UC}'s obtained for the investigated derivatives as annihilators in TTA–UC are very similar to **4** having the highest and **5** having the lowest Φ_{UC} which might be associated to the difference in τ_T which is important in the diffusion controlled TTA–UC process. Overall, derivatives **3**, **4** and **5** together with PtOEP constitute well functioning TTA–UC systems.

In short, modifications done to the DPA phenyl in the *para*-position resulted in minor photophysical changes and the chromophores retained their annihilator functionality in the TTA–UC process with PtOEP as the sensitizer.

4.2.2 Exciton migration in DPA dendrimers

As the second step in the pursuit of supramolecular TTA–UC system and in agreement with the findings in **Paper III**, two generations of DPA dendrimers, G1 and G2 (Figure 4.8) were synthesized and photophysically investigated in **Paper IV** with DPA as the reference. These molecules contain 3 and 9 DPA units respectively and display high solubility despite their relatively large size. This is due to their three-dimensional structure resulting from steric constraints between the anthracene groups with large dihedral angles.[131]

Despite the large difference in size between DPA, G1 and G2 (Figure 4.8) the spectral properties remain very similar. Figure 4.9a shows very similar absorption and emission spectra. The differences found in Figure 4.9a include minor change in the relative ratio of the vibronic peaks and a slight red-shift of the 0-0 transition energies with increasing molecule size (the E_{0-0} are located at 401 nm, 405 nm, and 408 nm for DPA, G1 and G2 respectively). The Φ_f of G1 and G2 in toluene are close to unity similarly to that of DPA while the fluorescence lifetimes of the compounds shorten with increased molecule size suggesting an increase in the radiative rate constant (k_f) (Table 4.2). This in combination with an almost linear increase of the molar absorptivity with the molecule size (Figure 4.9a) suggests that there may only be a weak electronic coupling between the covalently connected DPA constituting the dendrimers. However the increasingly larger radiative rate constants indicate that there may be a non-zero coupling between the individual DPA building blocks which points towards a at least partially delocalized exciton.[132]

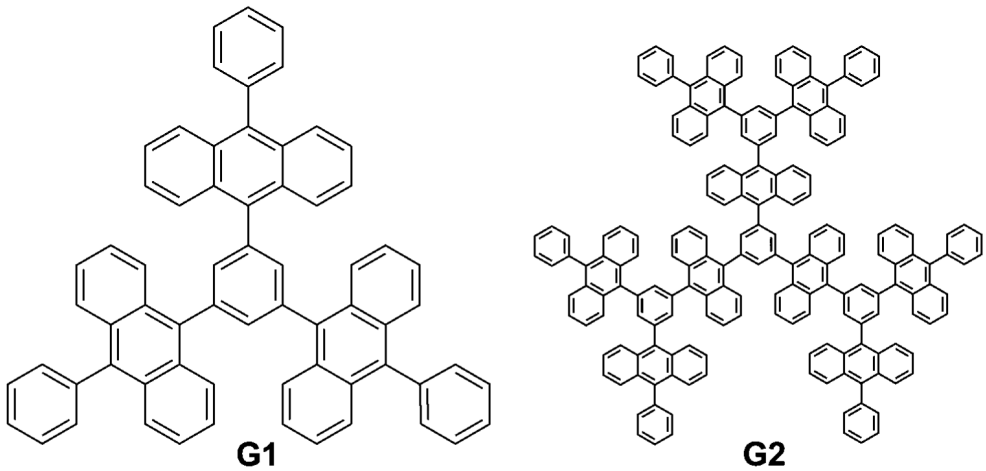

Figure 4.8: Structures of the investigated DPA dendrimers G1 and G2.

Table 4.2: Photophysical properties for the investigated molecules.

Chromophores	Φ_f	τ_f (ns)	k_f (s^{-1})
DPA	[a]1.02	7.0	1.4×10^8
G1	[a]1.03	5.3	1.9×10^8
G2	0.99	4.5	2.2×10^8

[a] Φ_f appear to exceed unity but this is a mare effect of the chromophore and the reference quantum yield (0.97 for DPA in cyclohexane[133]) being close to unity in combination with minor measurement fluctuations.

The investigation of the exciton delocalization in the dendrimers is performed using fluorescence anisotropy measurements. At 100 K DPA displays an increasing anisotropy with increasing excitation wavelength over the lowest absorption band. The anisotropy reaches a maximum value of around 0.4 indicating the existence of almost collinear absorption and emission transition dipoles, as previously reported.[92,134] At the same temperature G1 and G2 display an overall lower anisotropy compared to DPA with interesting oscillatory features of resonance with the vibronic peaks of the absorption, as seen in Figure 4.9b. This result is not characteristic for an exciton localized on a single DPA dendrimer subunit having the emission transition dipole along the phenyl substituents of the anthracene.[131]

In an attempt to explain the observations in Figure 4.9b a fully delocalized exciton model is considered and in the case of G1, individual transition dipoles along the phenyls in each of the DPA elements, as illustrated in Figure 4.10a, are assigned. The transition dipole moment of the dendrimer is given by the linear combination of all the individual DPA transition dipole moments where three unique combinations of them are possible.[135] One of these is forbidden (E', G1 transition dipole moment is zero) and of high energy

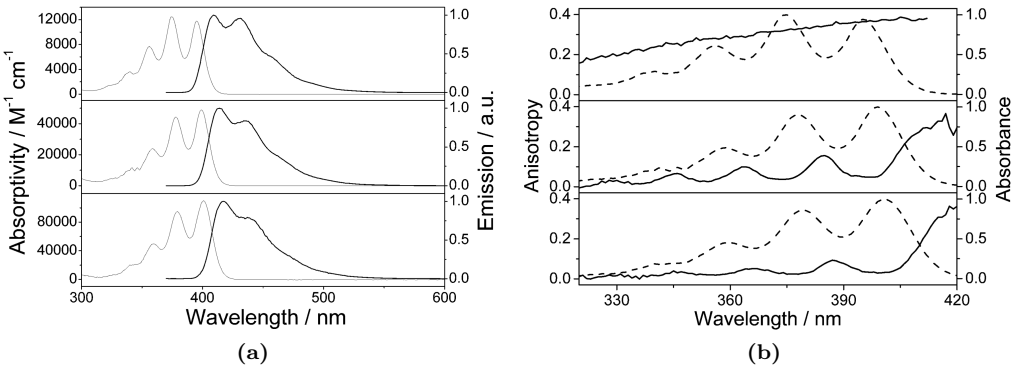

(a) (b)

Figure 4.9: (a) Molar absorptivity (thin line) and emission (thick line) spectra of the chromophores in toluene. (b) Absorption (dashed lines) with steady-state fluorescence excitation anisotropy (solid lines) in 2-MTHF at 100 K with emission monitored at 415 nm for DPA and 430 nm for G1 and G2. In both sub-figures from top to bottom is data for DPA, G1 and G2.

while the other two at lower energy are allowed (E'' and E'''), degenerate and may be pictured as two perpendicular components in a threefold rotation symmetry.

In this model one of the perpendicular transitions is assumed to have the limiting anisotropy of $r_{max} = 0.3$ (the maximum value at the red-edge of the G1 anisotropy) then using equation (3.8) the perpendicular ($\omega = 90°$) transition has an anisotropy equal to -0.15. Since these anisotropy quantities are additive it is possible to resolve the absorption spectra of each of the two allowed degenerate excited states using the anisotropy data of G1.[115] The resulting absorption components are found in Figure 4.10b together with the ground state absorption spectra of G1 at 100 K. Thus the degeneracy is lifted probably due to static and dynamic distortions of the dendrimer geometry and the energy splitting of the two transitions as estimated from Figure 4.10b is about 250 cm^{-1}. This result indicates the presence of two nearly degenerate transitions and explains the presence of the oscillations in the anisotropy of G1 (Figure 4.9b) which arise from the alternating excitation of the two transitions (E'' and E''') upon sweeping of the excitation wavelength over the G1 dendrimer absorption spectra. This explanation is also supported by semi-empirical INDO/S calculations of AM1-optimized structures of the dendrimers. Given the similarities between the absorption and anisotropy spectra of G1 and G2, the same explanation for the anisotropy oscillations may be suggested although for G2 a more complicated delocalized exciton model would be necessary considering the greater number of DPA units involved.

However, this effect of exciton delocalization is only seen at low temperatures and therefore time-resolved fluorescence anisotropy is employed to investigate the kinetics of the phenomenon. This is done as a function of temperature as well as excitation wavelength. In accordance with the results from the G1 steady-state data (Figure 4.10b) the excitation at 385 nm should predominantly excite the lowest (E''', red) transition with high anisotropy and 395 nm should excite mostly (E'', blue) transition with low anisotropy.

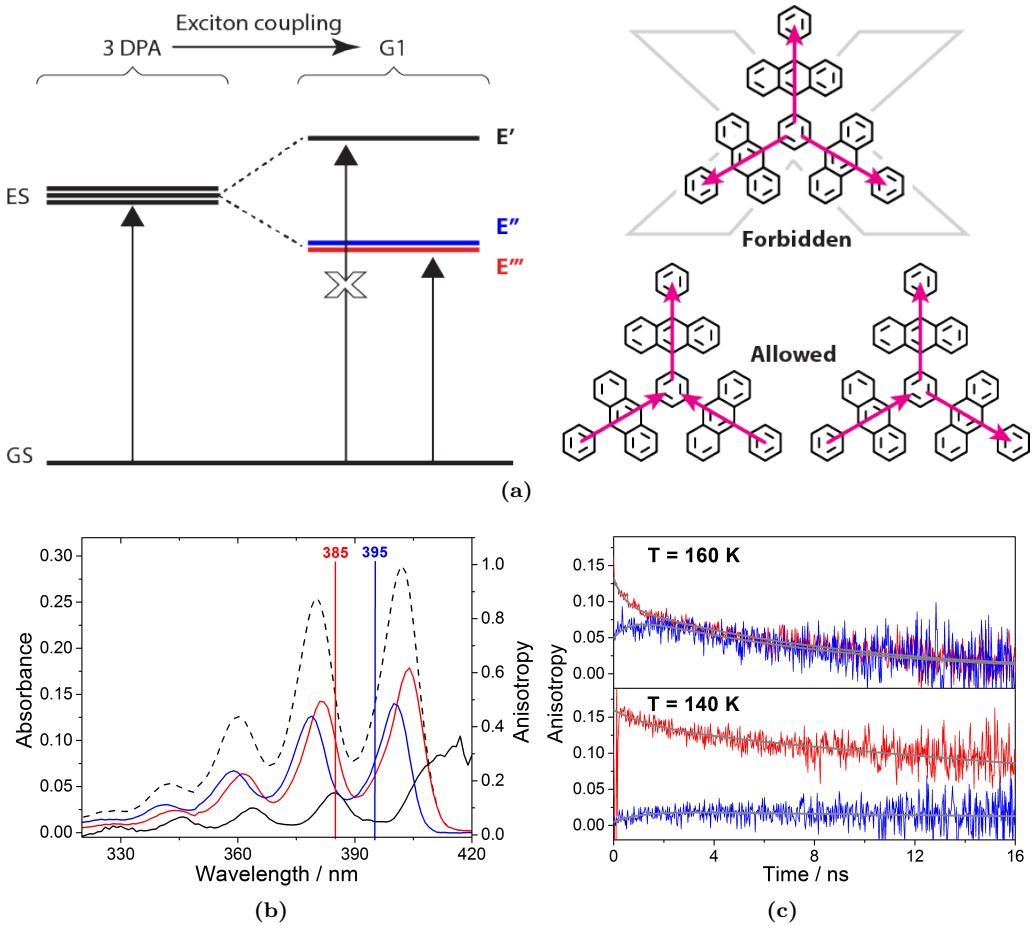

Figure 4.10: Diagram and data for the G1 dendrimer. (a) Exciton coupling band diagram illustrating the case of a fully delocalized exciton model. The notations are GS, ES, and forbidden (E') and allowed (E'',E''') excited states. (b) Absorption (dashed) and the individual resolved absorption components of states E'' (blue) and E''' (red) at 100 K. Solid vertical lines indicate the chosen excitation wavelengths used in the time-resolved anisotropy measurements corresponding approximately to the local max and minimum of the steady state excitation anisotropy (black, from Figure 4.9b) and consequently predominant excitations of E''' and E'', respectively. (c) Time-resolved emission fluorescence anisotropy decays at two different temperatures. Excitation at 385 nm excites predominantly E''' (red) and 395 nm excites predominantly E''(blue). The solid gray line represents the fit of a bi-exponential model with the fitting parameters found in Table 4.3.

Table 4.3: Extracted parameters for the fit of fluorescence anisotropy decay of G1 in 2-methyltetrahydrofuran (2-MTHF) as a function of excitation wavelength and temperature.

T (K)	λ_{exc} (nm)	$^*\theta_{calc}$ (ns)	$r_{0,a}$	θ_a (ns)	$r_{0,b}$	θ_b (ns)	χ^2
160	385	5.8	0.04	0.42	0.09	8.6	1.516
	395	5.8	-0.04	0.66	0.09	8.6	0.879
140	385	32.8	0.02	1.5	0.14	34	1.187
	395	32.8	-0.02	1.04	0.02	34	0.973

* The estimation of the rotational correlation time is $\theta_{calc} = \eta V/k_b T$ where η is the viscosity of 2-MTHF at temperature T, V is the volume of the rotating chromophore[136] and k_b is the Boltzmann constant. The rotating volume of the G1 and G2 was assumed to scale linearly with molecule mass with the mass of DPA as a reference.

At room temperature the anisotropies for all three compounds decay mono-exponentially independently of excitation wavelength while the rotational correlation time (θ) increases with the size of the molecules, as expected. At intermediate temperatures of 160 K and 140 K interesting kinetics are observed. Taking G1 as an example clear difference in kinetics are observed for the two excitation wavelengths and required a bi-exponential fit where the fitting parameters are given in Table 4.3.

Excitation at 385 nm produces initially a fast decay while excitation at 395 nm produces a corresponding rise time until both traces join in a slower decay over longer times as observed in Figure 4.10c. The longer decay times agree well with the estimation of the rotational correlation time (Table 4.3) while the presence of the initial faster component further supports the existence of two non-degenerate states. This short correlation time ($\sim$ 0.5 ns at 160 K) far exceeds the expected times for IC (few ps or less) or *inter*-DPA FRET ($\sim$ 100 fs given the proximity of the DPA units in the dendrimers). Therefore this short correlation time more likely represents a population equilibration between the two emissive E'' and E''' states (Figure 4.10a) rather than actual exciton energy migration. The short time is still quite long for an equilibration between two excited states of such small energetic separation but it may be explained by the low temperature in combination with one of the processes being energetically uphill. With additional temperature decrease to 140 K both the short and the long correlation times increase and the longer time is still well predicted from estimations of the rotational motion, as seen in Table 4.3. Using the temperature change with the change in correlation time an Arrhenius activation barrier energy is estimated to $\sim$ 250 cm^{-1} further supporting the interpretation that the decay times reflect population equilibration between two nearly degenerate states.

At even lower temperatures (100 K and 80 K) the upward equilibration rate is too slow for equilibration to occur within the excited state lifetime of the dendrimers. Therefore with varying excitation wavelength an alternating population of the E'' and E''' states will occur followed by emission from the same states. As the transitions are perpendicular this will manifest as an oscillating anisotropy with varied excitation wavelength, thus explaining the observations in Figure 4.9b at low temperature.

It should be noted though that there is a considerable decrease in r_0 obtained from the fitting in Table 4.3 ($r_{0a} + r_{0b}$) compared to the obtained r_0 from the steady-state

measurements (Figure 4.9b) suggesting that there is a fast depolarization process occurring on an even shorter time scale than monitored here. This process might prove to be the energy migration among the DPA units in the dendrimers but requires shorter time-resolution than the shortest one employed here (∼10 ps).

In short, the dendrimers G1 and G2 display high solubility and size control due to their structure and synthesis method. Despite covalent connections between the DPA building blocks no strong electronic coupling is observed and so the absorption and emission properties are similar to that of the DPA monomer. Based on the photophysical and theoretical investigation it is concluded that the singlet excited state is at least partially delocalized with an extremely fast crosswalk within the dendrimer framework.

4.2.3 Search for *intra*-molecular TTA

In this third part towards a supramolecular TTA–UC system, consisting of research done in **Paper V**, the dendrimers G1 and G2 from **Paper IV** together with a new linear DPA oligomer (Oligo) consisting of on average eight DPA units, as seen in Figure 4.11a, are tested as annihilators with DPA as the reference and PdOEP as the sensitizer. The systems are investigated in toluene and in poly(methyl methacrylate) (PMMA), hereafter referred to as Liquid– and Solid media, respectively, in order to probe the mechanism of *intra*-molecular triplet-triplet annihilation (TTA2) within the large annihilators as opposed to the more common *inter*-molecular triplet-triplet annihilation (TTA1) which dominates in Liquid media and occurs between individual molecules.

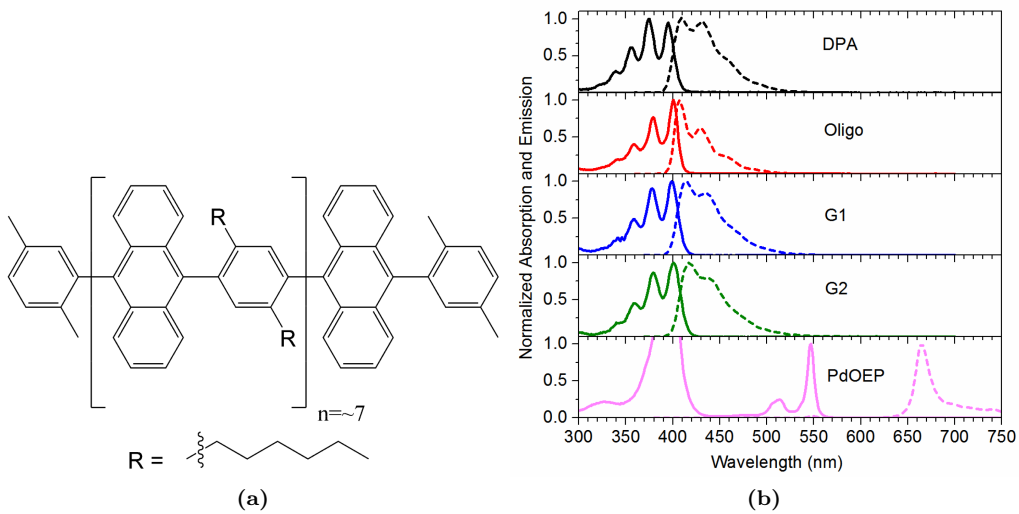

Figure 4.11: (a) Structure of the Oligo employed in this study. The structures of DPA and PdOEP are found in Figure 4.6 as **1** and **MOEP**, respectively. The dendrimer structures are found in Figure 4.8. (b) Absorption (solid lines) emission spectra (dashed lines) in toluene of all the compounds employed in this study.

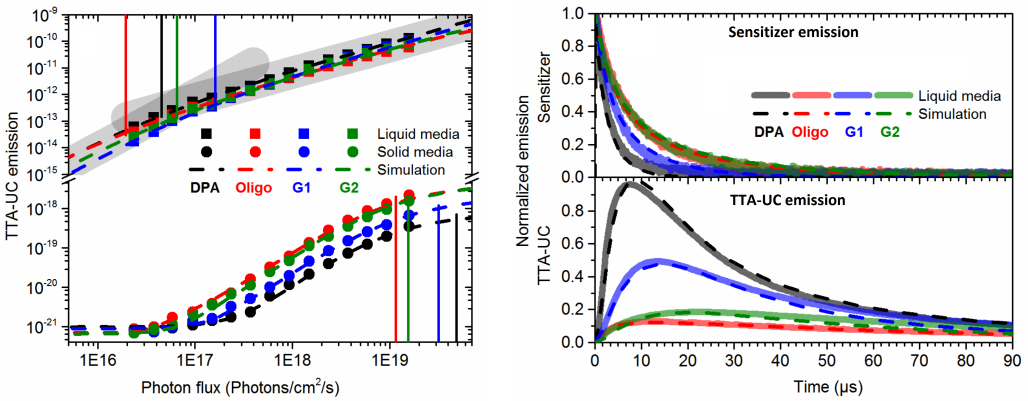

(a) **(b)**

Figure 4.12: (a) Steady-state TTA–UC emission as a function of excitation photon flux with the DPA, Oligo, G1 and G2 as the annihilators in toluene (Liquid media) and in PMMA (Solid media). Gray lines are a guide for the eye highlighting the quadratic and linear slopes in the Liquid media data. Vertical lines indicate the position of the numerically established threshold excitation intensities between the quadratic and the linear region. (b) Time-resolved sensitizer (PdOEP; top) and TTA–UC (bottom) emission captured in Liquid media.

The dendrimers G1 and G2 share many similarities to DPA as discussed in subsection 4.2.2. This is also the case for the new Oligo where the molar absorptivity scales almost linearly with the number of constituting DPA units. The absorption and emission spectra contain very similar features to that of DPA, as seen in Figure 4.11b, with minor distortions in the relative vibronic peak intensities. The fluorescence quantum yield (Φ_f) as well as the fluorescence (τ_f) and triplet (τ_T) lifetimes are similar to that of the DPA and are found in Table 4.4.

In order to facilitate comparison between the different annihilators the molecular annihilator concentrations in all samples and measurements are set to correspond to the same amount of DPA units. The absolute concentrations of the sensitizer and the annihilators are, however, limited by the highest solubility of the PdOEP–Oligo system in PMMA. Thus, for all samples the sensitizer (PdOEP) concentration is 173 μM and the annihilator concentrations are 200 μM (DPA), 25 μM (Oligo), 67 μM (G1) and 22 μM (G2). These concentrations are far from optimal in Liquid media where in the optimal case a large excess of annihilator is used compared to the sensitizer in order to ensure an efficient TET process.

In Liquid media a very similar excitation intensity dependence for TTA–UC is observed (Figure 4.12a) for all annihilators while DPA displays a somewhat higher UC efficiency. This is probably due to the highest annihilator molecule concentration in the DPA TTA–UC-system which ensures the most efficient TET step among all four samples. This effect is also supported by the observation in Figure 4.12b where the sensitizer emission

from the DPA sample is the most quenched one among the four annihilators and the quenching scales well with the absolute annihilator concentrations in accordance with Stern-Volmer kinetics (subsection 2.2.2). The time-resolved TTA–UC data in Liquid media displays a more prompt UC emission generation for the more abundant and faster diffusing DPA and gradually weaker but more long-lived traces for the larger and slower diffusing supramolecular annihilators.

The proposed mechanism for the *intra*-molecular TTA2 demands the presence of a doubly excited triplet annihilator (^{3}A**) carrying two triplet excitons. As the annihilators and the sensitizer are not associated to each other in any way the sensitization process which is required consists of a first sequential *inter*-molecular triplet energy transfer (TET1) and a second sequential *inter*-molecular triplet energy transfer to the same molecule as TET1 (TET2). It is due to the nature of this diffusion controlled two-part sensitization process that TTA2 should not be observable in the Liquid media. In short, once TET1 occurs a ^{3}A* is formed. This excited species is relatively short-lived and in scarce concentration compared to the ^{1}A. Thus, under diffusion conditions it is very unlikely that a TET2 will occur instead of another TET1 to rise another ^{1}A to ^{3}A*. Well before a sufficient ^{3}A* bulk concentration reaches the levels that might be required for TET2 to start occurring, as opposed to TET1, the ^{3}A* species will be readily consumed through the competing *inter*-molecular diffusion controlled TTA1 process. This proposed mechanism explains why the TTA2 channel should be inactive and why the difference between the TTA–UC signal of the different annihilators in Liquid media is so similar.

Considering this kinetics model the PMMA samples were prepared in which diffusion is nearly eliminated. Remarkably, the TTA–UC efficiency in this Solid media is higher for samples containing larger annihilators than the smaller ones, as seen in Figure 4.12a. This is despite the fact that the concentration of annihilator molecules is lower for the larger annihilators thus decreasing the efficiency of the important TET steps. The obvious and dramatic lowering of the overall UC emission intensity for all Solid media samples is expected as there is no affinity between the sensitizer and the annihilators. Therefore the observed UC emission can only originate from the few positions within the solid matrix where one or several sensitizers happen to be close enough to at least one supramolecular or several DPA annihilators, forming a functional TTA–UC cluster. In the case of DPA there is another statistical demand for the formation of such a cluster which is that at least two DPA molecules need to be close enough to each other in order for TTA1 to occur. With these two statistical demands on DPA it is not surprising that the UC intensity produced by DPA is much weaker in solid matrix compared to the Oligo and the dendrimers which lack the latter requirement.

The steady-state TTA–UC in Solid media in Figure 4.12a also displays somewhat abnormal features in the low and high excitation intensity regions. In the low excitation intensity region the rate of excitation of the sensitizer is proportional to first order decay of the triplet sensitizer and annihilator producing an apparent excitation intensity independent region. At high excitation intensities, a bleach of the sensitizer ground state occurs efficiently capping off the TTA–UC emission. The bleach is attributed mainly to the elimination of diffusion but also to the longer sensitizer lifetime and significantly lower active sensitizer concentration (Table 4.4) that is actually contributing to TTA–UC emission.

Table 4.4: Parameters for both steady-state and time-resolved simulations. Arrows indicate global application of variables. Values without footnote are determined from complementary experiments. The final S or A in the parameter subscript denotes sensitizer or annihilator, respectively.

Simulation parameter		Liquid media				Solid media			
	Unit	DPA	Oligo	G1	G2	DPA	Oligo	G1	G2
[S]	(μM)	⟵ 173 ⟶				⟵ **[*]0.031** ⟶			
[A]	(μM)	200	25	67	22	**[*]24×10^{-6}**	**[*]61×10^{-6}**	**[*]32×10^{-6}**	**[*]65×10^{-6}**
Φ_{fA}		[b]0.97	0.89	[b]1.00	[b]0.99	⟵ [c]1.00 ⟶			
k_{TTAS}	(M^{-1}s^{-1})	⟵ **[*]2.6×10^{9}** ⟶				⟵ **[*]2.0×10^{5}** ⟶			
τ_{PS}	(ms)	⟵ 0.32 ⟶				⟵ 1.6 ⟶			
k_{TET1}	(M^{-1}s^{-1})×10^{-9}	1.6	2.5	1.9	2.5	⟵ **[*]7.5** ⟶			
k_{TTA1}	(M^{-1}s^{-1})×10^{-9}	**[*]0.37**	**[*]0.33**	**[*]0.56**	**[*]0.94**	⟵ **[*]220** ⟶			
k_{TET2}	(M^{-1}s^{-1})×10^{-9}	[d]N.A.	**[*]0.25**	**[*]0**	**[*]0**	[d]N.A.	⟵ **[*]0.13** ⟶		
k_{TTA2}	(s^{-1})×10^{-9}	[d]N.A.	⟵ [a]1000 ⟶			[d]N.A.	⟵ [c]1000 ⟶		
τ_{TA}	(ms)	**[*]3.4**	**[*]5.5**	**[*]1.4**	**[*]1.8**	18	24	20	20
τ_{fA}	(ns)	[b] 7.0	4.9	[b] 5.3	[b] 4.5	9.1	6.4	8.2	6.0

[a]Estimated value. [b]**Paper IV** [c]Set value, based on values from Liquid media. [d]Not applicable. [*]**Optimized simulation variables.**

The TTA–UC is known to display quadratic followed by linear dependence on excitation intensity when going from low to high intensity.[114] The transition between these regions is referred to as the I_{th} and is often used as a figure of merit for TTA–UC sensitizer-annihilator pair systems. In this study the I_{th} is derived numerically by finding the intercept between the quadratic and linear components of the steady-state TTA–UC intensity (Figure 4.12a). The components are derived from the differential equations constituting the simulation of the TTA–UC process and implemented using the optimized parameters from Table 4.4. However, the simulation also takes into account the effects such as TTAS and TTA2 which cause the mathematical quadratic and linear components to not be of pure quadratic and linear nature. For more details and derivation refer to **Paper V** and its supporting information. The numerically determined I_{th} does however agree well (within a few percent) with the ideal excitation intensity threshold (I_{th}^{ideal}) prediction in equation (2.15) for the samples in Liquid media. This suggests that even though the samples are not optimally prepared in terms of concentrations the steady-state TTA–UC emission excitation intensity dependence can still be described in terms of quadratic and linear regions for the sake of predicting I_{th}. The same is not true for the samples in Solid media where the difference between the numerically projected (due to sensitizer bleach) I_{th} and the I_{th}^{ideal} value is several orders of magnitude in excitation intensity. The reason for this is that the approximations necessary for deriving the I_{th}^{ideal} expression do not hold and in extension that there are no valid quadratic or linear regions for these Solid media samples. This result illustrates the importance of assuring that the TTA–UC system being characterized is or can be approximated to an ideal system before describing it in terms of the quadratic/linear regions for defining the I_{th}.

The optimization of the TTA–UC simulation for the Liquid media samples was conducted globally on steady-state and time-resolved data. The individual sample variables for this simulation were TTA1 rate constant (k_{TTA1}), TET2 rate constant (k_{TET2}) and τ_T. The TTAS rate constant (k_{TTAS}) was set as a global variable since the sensitizer and its concentration is the same in all samples. The Solid media simulation was optimized only on steady-state data with the *effective* annihilator concentrations as the only sample individual variables. The *effective* sensitizer concentration together with the rate constants k_{TTAS}, TET1 rate constant (k_{TET1}), k_{TTA1} and k_{TET2} were applied globally over the four PMMA samples. The full set of the simulation parameters including the optimized values are given in Table 4.4.

For the Liquid media samples the first and globally fitted parameter, k_{TTAS}, is as expected diffusion limited. The sample individual k_{TTA1} are however all approximately one order of magnitude lower than what is expected of such diffusion controlled rate constant ($\sim 10^9$ $M^{-1}s^{-1}$; Table 4.4). This can be attributed to the fact that this simulation model does not explicitly include spin statistics (subsection 2.2.3). Instead the effect of spin statistics is included in the estimation of the TTA rates so that the k_{TTA} simply reflects the rate of successfully forming a singlet excited annihilator from the fusion of two triplets. This is possible since the data being fitted is entirely emissive and thus only reflects the end-state of the TTA–UC process including whatever effects spin statistics may have had up to the emission of the UC photons. The optimized values for k_{TET2} in the case of G1 and G2 are approximately zero supporting the hypothesis that the TTA2-channel is inactive in Liquid media. The same is not true regarding the value for

Oligo which is puzzling. The optimized values for the τ_T of the annihilators all fall in the same order of magnitude as that of DPA and agree well with previously reported values of 1-5 ms.[128,137]

Since the employed mathematical model is based on a purely diffusive TTA–UC system the fitting to the data of the Solid media samples was made with the sensitizer (global) and the annihilator concentrations as variables as well. This is motivated by the hypothesis that only a few active TTA–UC clusters within the solid PMMA matrix, and consequently only a subset of the S and A molecules, produce the observed UC signal. The obtained k_{TET1} and k_{TET2} are in the orders of magnitude as those for the Liquid media while k_{TTA1} is considerably higher. A possible explanation for the significantly higher k_{TTA1} could be that, while not very likely, if two annihilators in the Solid media are in close proximity the *inter*-molecular triplet-triplet annihilation (TTA1) may occur at similar rates as the *intra*-molecular TTA2. The k_{TTAS} is several orders of magnitude lower than that of the Liquid media which seems reasonable as the recorded UC signal only originates from successful TTA–UC clusters where the sensitizers are efficiently quenched by the annihilators. Overall it stands to reason that if the supposed TTA–UC clusters function they do so well and therefore other competing depletion channels are less efficient.

The sensitizer and annihilator concentrations obtained from the optimization of the Solid media samples are in the pM range (Table 4.4) which further supports the hypothesis that only a subset of the molecules in the bulk are responsible for the observed UC signal. A ratio between the optimized active and the bulk annihilator concentrations will be at least proportional to the probability of forming successful UC clusters. By applying this to a probability density function for the Nearest-Neighbor distances of finite particles with ideal-gas approximation in 3 dimensions, an *inter*-particle distance within these clusters can be obtained.[138] Since the shape or the size of the annihilators are not accounted for in the distribution function the obtained distances are only proportional to the actual *inter*-particle distances. However, if they are normalized to the distance for the Oligo and scaled to 8 (average number of DPA units in Oligo), the relative distance ratios become 1.5, 8, 3.5 and 9 for DPA, Oligo, G1 and G2 respectively. This scales well with the amount of DPA units in each supramolecular annihilator suggesting that the more DPA units there is in the annihilator the larger *inter*-molecular distances are tolerated for a functional TTA–UC cluster in Solid media.

This result, in combination with the correlating stronger UC emission for the fewer and larger annihilators, as illustrated more clearly in Figure 4.13, as well as an increased TTA2 channel contribution in higher viscosity media (Table 4.4) supports the hypothesis that efficient *intra*-molecular triplet-triplet annihilation (TTA2) is occurring within the supramolecular annihilators employed in this study.

In short, supramolecular annihilators G1, G2 and Oligo were tested and compared to DPA for UC through *intra*-molecular triplet-triplet annihilation (TTA2) in PMMA. The fewer but larger supramolecular annihilators give rise to higher TTA–UC efficiency than the many but smaller DPA indicating that there is a positive effect on TTA–UC in diffusion-free environment when the annihilators are covalently attached to form larger structures like G1, G2 and Oligo. This effect is attributed to the supramolecular annihilators ability to carry two triplet excitons and allow for triplet exciton migration

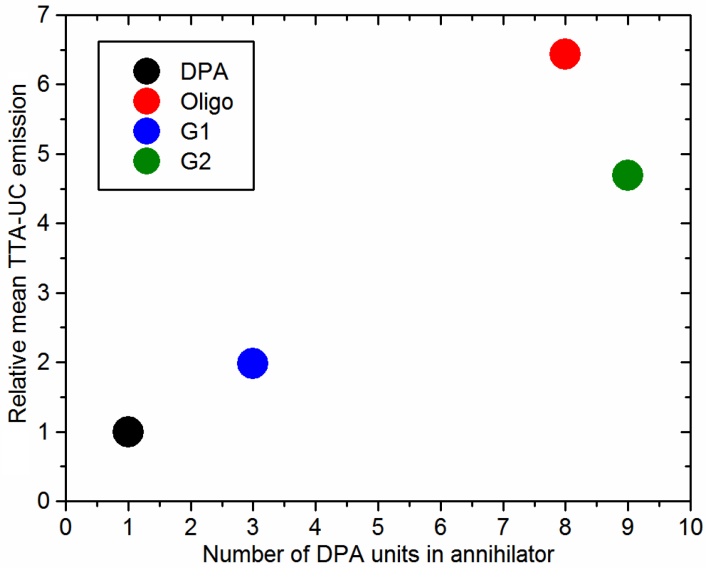

Figure 4.13: Average relative TTA–UC emission from the Solid media samples in Figure 4.12a. Data is used in the excitation intensity range between 3.7×10^{17} – 1.6×10^{18} photons/cm^2/s.

within the molecular framework which is a prerequisite for TTA2. As seen in Figure 4.13 the effect scales near linearly with the supramolecular annihilator size.

4.2.4 Search for *intra*-molecular TET

In this fourth step towards completely *intra*-molecular TTA–UC the possibility for *intra*-molecular triplet energy transfer (*intra*TET) is explored through coordination of pyridine substituted annihilators to ZnOEP as the sensitizer. The study is covered in **Paper VI** where the coordinating annihilators have varied bridge length from the anthracene to the pyridine substituent. Their capability as annihilators is investigated along with their photophysical properties in relation to that of DPA.

In Figure 4.14 the absorption and emission are displayed, along with the molecular structures, for all involved chromophores. In agreement with previous results (**Paper III-V**), modification of the DPA phenyls in the *para*-position or symmetrically in the *meta*-positions yields minimal perturbation of the spectral absorption- and emission characteristics. However, it is evident from Figure 4.14 that the increase of the pyridine-substituted arm length results in a gradual appearance of new absorption bands at the blue-side of the absorption spectra. The emission spectra maintain high similarity to that of the DPA but there is a slight red-shift of the of the 0-0 transitions for the compounds. The fluorescence quantum yield (Φ_f) remains overall high for the Ph_nAnPyr molecules although longer pyridine arms correlate to a minute Φ_f lowering, as seen in Table 4.5.

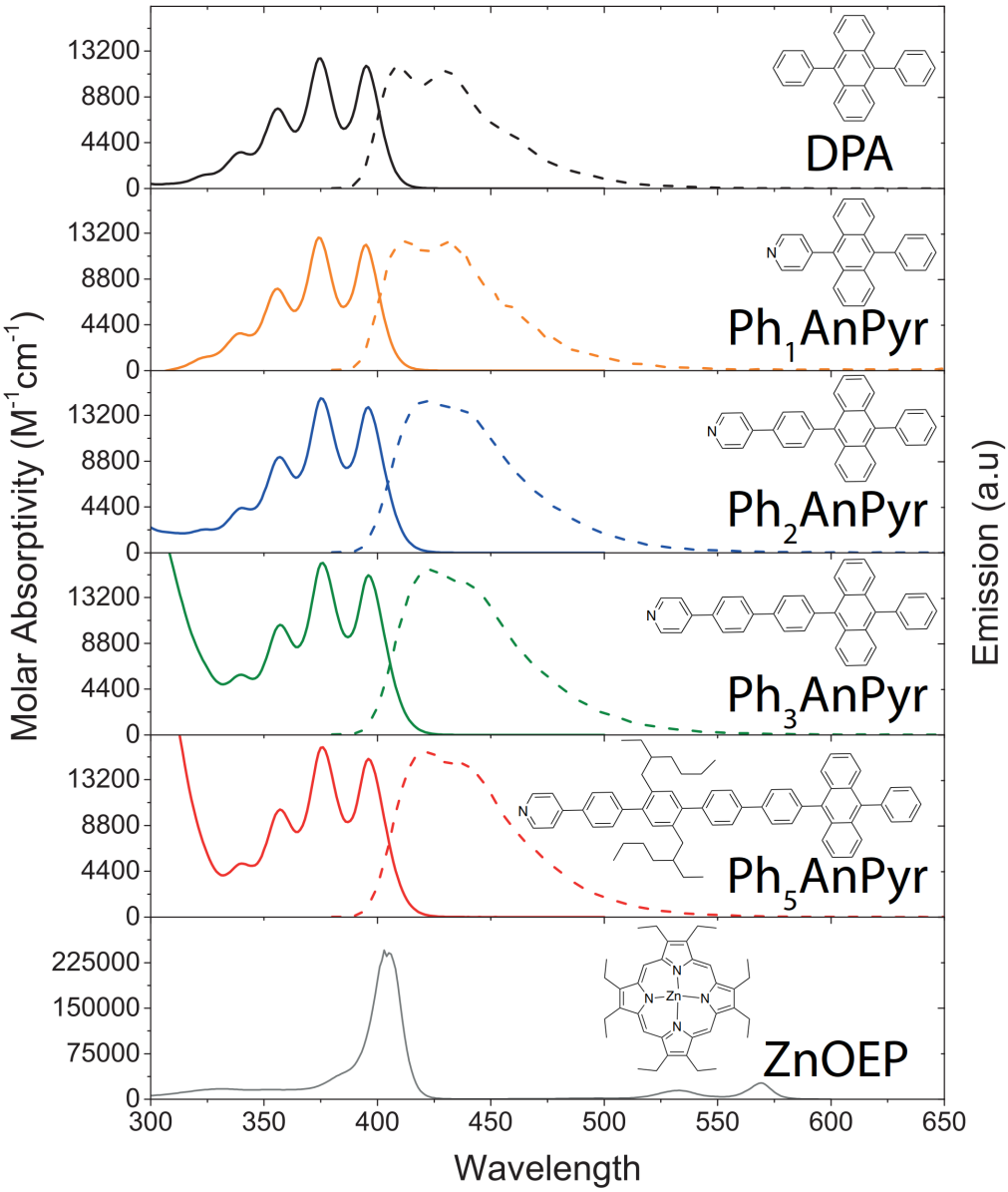

Figure 4.14: Molar absorptivity (solid) and normalized emission (dashed) in toluene for all chromophores used in this study.

Table 4.5: Photophysical properties of the investigated coordinating annihilators in degassed toluene.

Compound	Φ_f	τ_f (ns)	K_B (M^{-1})
DPA	1.0[128]	6.97[a]	0
Ph_1AnPyr	0.96 ± 0.020[a]	5.29 ± 0.01	2300
Ph_2AnPyr	0.85 ± 0.019	3.55 ± 0.01	5900
Ph_3AnPyr	0.85 ± 0.003	3.17 ± 0.01	5800
Ph_5AnPyr	0.86 ± 0.052	3.33 ± 0.01	6000

[a] **Paper III**

The Lewis acid-base coordination between the Ph_nAnPyr coordinators and the ZnOEP metal core is confirmed and investigated by tracking the red-shift and perturbation of the ZnOEP absorption spectra as a function of added coordinator. The binding constant (K_B) for the different coordinators obtained from the fitting of the titration data can be found in Table 4.5. From the binding constants the sensitizer-coordinator complex lifetime can be estimated by assuming a approximately diffusion controlled ($10^8 - 10^9$ $M^{-1}s^{-1}$) association constant. The complex lifetimes obtained are $6 - 60$ μs (for $K_B = 6000$ M^{-1}) which is considerably shorter than the triplet lifetimes of the ZnOEP (~ 200 μs) and Ph_nAnPyr which are assumed to be similar to that of Ph_1AnPyr at 7.7 ms (**Paper III**). It is therefore likely that the TTA and thus UC emission does not originate from coordinated species which could be beneficial if there exists a fast FRET-based quenching of the UC from the coordinated annihilators back to the sensitizer, as this process is strongly distance dependent.

The study of the UC efficiency of the different Ph_nAnPyr with ZnOEP was conducted with $\sim 90\%$ of the sensitizer coordinated except for the Ph_3AnPyr due to solubility issues where $\sim 67\%$ of the sensitizer is coordinated. The Φ_{UC} obtained for the coordinating and non-coordinating annihilators range between 3-20% (Figure 4.15b) despite the close proximity between the annihilator and the sensitizer in the coordinated complexes, further supporting the hypothesis of complex dissociation prior to TTA–UC generation. The smallest coordinator, Ph_1AnPyr, displays a decrease in Φ_{UC} compared to DPA unlike the similar Φ_{UC} of the two with a non-coordinating sensitizer in **Paper III**. This might indicate that at least some part of the TTA events do involve coordinated annihilators and the generated UC photons are subjugated to FRET quenching by the sensitizer, thus lowering the overall efficiency. The $Ph_{2,3,5}$AnPyr display even lower Φ_{UC} despite the longer bridges which should lower the FRET quenching efficiency by increasing the anthracene-ZnOEP distance. This can be attributed to a less efficient TTA step which is supported by the quadratic-linear threshold of the TTA–UC emission found at higher excitation intensities than that for the DPA and Ph_1AnPyr.[114] This in turn could be caused by an increase of unfavorable collision geometries between these bulkier annihilators, thus not yielding excited state singlets as frequently as the smaller DPA and Ph_1AnPyr. Another reason might be the higher binding constant (Table 4.5) for the $Ph_{2,3,5}$AnPyr causing more TTA events to involve coordinated annihilators and thus subjecting the UC excited singlet state to FRET quenching. One important aspect to consider is the

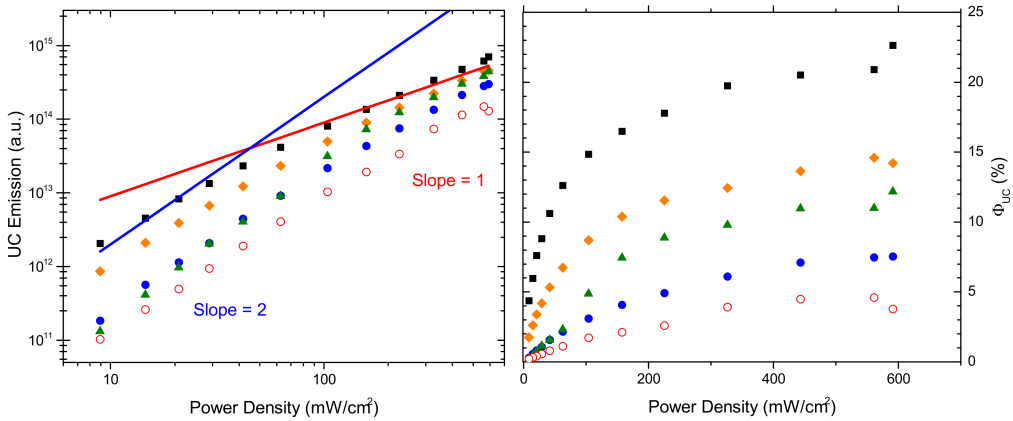

Figure 4.15: (a) UC emission vs. excitation (532 nm) intensity. The solid lines serve as a guide for the eye to identify linear (Slope = 1) and quadratic (Slope = 2) regions in the UC excitation intensity dependence. (b) Φ_{UC} for the DPA and the $Ph_{1\text{-}3,5}$AnPyr with ZnOEP as the sensitizer in toluene. The legend is DPA(■), Ph_1AnPyr(◆), Ph_2AnPyr(●), Ph_3AnPyr(▲), Ph_5AnPyr(○).

efficiency of the TET step. The k_{TET} for the ZnOEP-DPA pair was determined to 7.8×10^8 $M^{-1}s^{-1}$ to compare with the PtOEP-DPA system from **Paper III** where the same rate was 2×10^9 $M^{-1}s^{-1}$. This is explained by the lower excited triplet state energy of the ZnOEP at 1.78 eV.[139] When considering the triplet excited state energies of DPA and Ph_1AnPyr at 1.72 and 1.73 eV (**Paper III**), respectively, it is easily understood that in this case the vital energetic down-hill driving force for the TET step from the sensitizer to the annihilator is very small. Furthermore as the singlet excited state of the ZnOEP is lowered upon coordination (red-shift of the absorption spectra) it is not unlikely that the same might occur for the triplet excited state which would further decrease the TET driving force and thus also the efficiency.

In an attempt to decrease the effects of diffusion samples containing polystyrene, less annihilator and more sensitizer were prepared. However at these low annihilator concentrations relative to the sensitizer, it is estimated that less than 5% of the sensitizer is coordinated with an annihilator provided that the K_B is unaffected by the presence of polystyrene. Under these conditions the overall Φ_{UC} was decreased for all annihilators while the DPA and Ph_1AnPyr performed more similarly and the longer $Ph_{2,3,5}$AnPyr also displayed more similarities to each other.

The assumed FRET quenching of the UC singlet excited state of the coordinators by the adjacent ZnOEP was further investigated where the distance, the relative transition dipole angle and spectral overlap between the two chromophores are key factors. The choice of coordination as the binding between the annihilator and the sensitizer stemmed from an expected average 90° angle between the annihilator singlet excited transition

Table 4.6: Estimation of the geometrical properties of the coordination complexes.

Compound	τ_{DA} (ps)	η_{FRET} (%)	r_d^a (Å)	R_0 (Å)	$< \kappa^2 >$	Binding Angle (°)
Ph_1AnPyr	<20	>99.6	8.0			
Ph_2AnPyr	<20	>99.4	12.2			
Ph_3AnPyr	27 ± 7	99.2 ± 0.2	17.3	38	0.19	75
Ph_5AnPyr	152 ± 10	95.4 ± 0.3	25.0	42	0.29	71

[a] Distance from the ZnOEP metal center to the center of the anthracene in the coordinators was estimated from AM1 optimized structures of the complex.

dipole and the delocalized in-plane singlet transition dipole of the ZnOEP. In such case the FRET quenching efficiency would be minimized, at least to the point where an effect of distance modulation by the variable bridge length in $Ph_{1\text{-}3,5}$AnPyr would have an effect on the energy transfer process.

The FRET efficiency (η_{FRET}) was determined by relating the unquenched fluorescence lifetime of the non-coordinated annihilators (τ_0) to the quenched lifetime of the annihilators coordinated to ZnOEP (τ_{DA}). This in combination with the anthracene–Zn center-to-center distances (r_d) obtained from AM1 optimized structures of the complexes gives the R_0. Further the R_0 in combination with the spectral overlap integral for the coordinating annihilator and ZnOEP is used to give the average orientation factor $< \kappa^2 >$ and in turn the relative binding angle for the coordination complexes. The results are given in Table 4.6 and for more details on the derivation refer to **Paper VI**. It is important to note the coordination complexes in room temperature exhibit a distribution of binding angles and the apparent angle given in Table 4.6 represents how broad this distribution is from 90°. Due to limitations in the time resolution of the fluorescence measurements only angles for $Ph_{3,5}$AnPyr were determined. The projected η_{FRET} for $Ph_{1,2}$AnPyr are however expected to be close to unity as seen in Table 4.6.

It is evident from the results that the parasitic FRET back-transfer from the UC singlet excited annihilator to the ZnOEP sensitizer is efficient in the employed system. This is due to the relatively short distance between the anthracene and ZnOEP in the complexes in combination with large deviation from the expected 90° binding angle. This does not however exclude coordination as a possible path to *intra*TET if a number of optimizations of these systems are considered. Some of these are the use of a sensitizer with higher triplet excited state energy in combination with stronger coordination to the annihilator. While bridging length might be hard to increase further the spectral overlap of the sensitizer-absorption and annihilator-emission may be minimized in order to minimize the TTA–UC quenching through FRET.

In short, a new type of annihilator consisting of a pyridine substituted DPA with intermediate variable bridge length was synthesized. Utilizing the coordination functionality between the pyridine substituent and the ZnOEP as the sensitizer the coordination complex was investigated for *intra*-molecular triplet energy transfer (*intra*TET). The *intra*TET could not be experimentally resolved, probably due to a combination of weak binding between the coordinating species, non-optimal energy level of the sensitizer triplet

excited state, and high parasitic quenching of the annihilator singlet excited state by FRET back to the sensitizer. The coordination binding may still be a promising path in the pursuit for *intra*TET if a more appropriate sensitizer with an energetically higher lying triplet excited state is used. Furthermore, the binding strength should be increased and the spectral overlap between the annihilator emission and sensitizer absorption should be minimized in order to minimize FRET efficiency (η_{FRET}).

4.2.5 Characterizing TTA–UC

Throughout the scientific work presented in this Thesis the characterization of the TTA–UC process has been at a key factor for obtaining and describing the results. Arguably during the later years the field of organic TTA–UC has been more focused on the improvement of the TTA–UC mechanics as well as application optimization of already known TTA–UC systems rather than the development of entirely new sensitizers and annihilators.[140] However in the earlier days of the field many new TTA–UC molecule pairs were presented, along with their system characteristics like Φ_{UC} and upconversion energy shift (UES). However, at times the Φ_{UC} was given for an arbitrary excitation intensity at which the study was performed and the UES was reported often simply between the most prominent features of the annihilator UC emission- and the sensitizer absorption spectra. With time the importance of the excitation intensity threshold (I_{th}) was illustrated and supported by the study of TTA–UC kinetics which gave new perspectives to characterization procedures of the TTA–UC systems.[114]

In **Paper VII**, aside from an overview of the field, some key characterization questions are addressed. The I_{th} is probably one of the more straight forward characteristic to determine for a TTA–UC system but it is still, like many other characteristics, dependent on the relative concentrations of the sensitizer and annihilator. The same is true for the Φ_{UC} but in addition it also, to a degree, depends on the excitation intensity that it is measured at. This is due to the presence of a quadratic and linear UC dependence on excitation intensity.

At low excitation intensities the first and pseudo-first order deactivations of the excited triplet states dominate resulting in the TTA–UC efficiency being below its maximum. Experimentally this manifests as quadratic dependence on excitation intensity for the UC emission. As the excitation intensity increases a threshold point (I_{th}) is reached where a significant part of the excited triplet state consumption starts to occur through the TET and TTA processes. With further increase of the excitation intensity the UC emission displays a linear dependence on excitation intensity.[9,21,44,58,74,114,141] It is due to this system behaviour that Φ_{UC} should always be determined above the I_{th} where Φ_{UC} does not depend on excitation intensity as also illustrated in **Paper III** and **VI**.

Aside from characterizing TTA–UC systems at the correct excitation intensity it is also important to assure that the system composition is optimal in terms of the relative sensitizer-annihilator concentrations. A good estimate for these concentrations in fluid systems includes considering the triplet excited state lifetimes of the two species as well as an estimate of the diffusion distance that may be covered by the species during their triplet excited state lifetimes. It is desirable to maintain efficient quenching of the sensitizer, thus often high concentration of the annihilator is used. This normally also ensures

that triplet-triplet annihilation of the sensitizer (TTAS) does not occur as the sensitizer triplet excited lifetime is significantly shortened thus lowering the chances of colliding with another triplet excited sensitizer. Aside from this the absolute concentration of the sensitizer should be high enough so that good absorption of the excitation light is maintained without significant inner-filter effects that might affect the measurements. The absolute annihilator concentration should be high enough that the inter-annihilator distances can be covered within their triplet excited state lifetimes, thus assuring that TTA process occurs more often than the natural decay of the annihilator triplet excited state. On the other hand it is also important to not set the annihilator concentrations too high as this might lead to TTA–UC occurring too close to the sensitizers and thus being quenched through FRET. Another possible downside is that the homo-TET between triplet excited and ground state annihilators might occur more often than TTA between two triplet excited annihilators which might increase the overall natural decay of the sensitized triplet excited state.

The last and probably most obvious characteristic of a TTA–UC system is the spectral one. This includes the spectral positions of the sensitizer absorption and annihilator emission which usually are the source for naming the system e.g. "red-to-yellow", "yellow-to-green", "green-to-blue". However it can also be of interest to report how far the UC photons are upconverted. This characteristic leaves room for interpretation as the sensitizer absorption and the annihilator emission are often spectrally broad. It boils down to where one chooses to excite the sensitizer and where the emission is captured. Should this be done at the peaks of absorption and emission? The location of the most intense peaks may not represent the majority of the species spectra though, which could be misleading.

Instead a better way may be to report the energy difference between the weighted center points of the sensitizer absorption and the annihilator emission. However, as this is a TTA–UC system characteristic, the upconverted annihilator emission spectra should be used from the optimally prepared TTA–UC sample. Thus any possible effects of inner-filter or re-absorption should be left as is. In accordance with Figure 4.16 first the spectra intensity is corrected as

$$I(\nu) = \lambda^2 I(\lambda) \tag{4.1}$$

and the wavelength (λ) scale is converted to wavenumber (ν) in cm^{-1}. Then the lower ν_L^A (blue side) and upper ν_U^A (red side) integration limits are set for the annihilator (A) and a weighted center ($\bar{\nu}_W^A$) of the UC emission spectra is obtained as

$$\bar{\nu}_W^A = \frac{\int_{\nu_L^A}^{\nu_U^A} E^A(\nu)\nu \; d\nu}{\int_{\nu_L^A}^{\nu_U^A} E^A(\nu) \; d\nu} \tag{4.2}$$

where $E^A(\nu)$ is the emission spectra of the annihilator as a function of wavenumber from Figure 4.16.

The obtained weighted emission spectra center for the UC emission is then used as the lower (blue side) integration limit for the sensitizer (S) absorption ($\bar{\nu}_W^A = \nu_L^S$) and the upper ν_U^S (red side) integration limit is set to where the absorption of the S ends. Thus

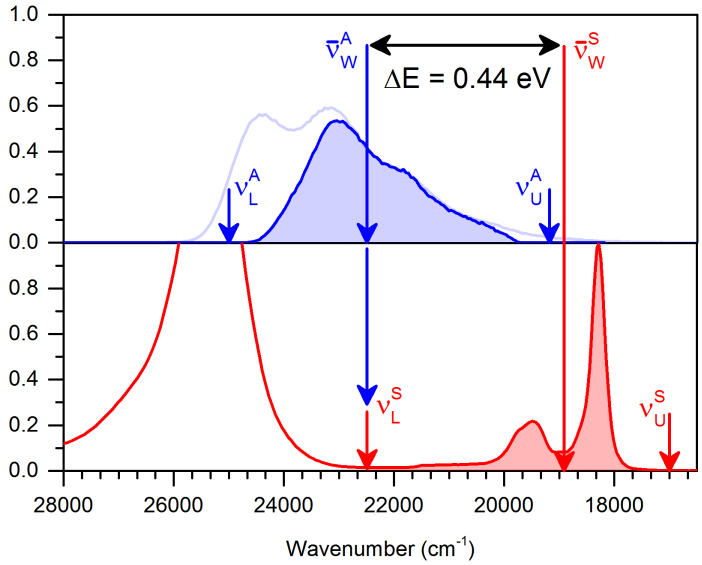

Figure 4.16: Top: The DPA UC emission with perturbing effects of the PdOEP sensitizer absorption. In faded color is the unperturbed directly excited DPA emission spectra for comparison. Bottom: The sensitizer PdOEP absorption (red). The shaded parts of the spectra represent the integrated area and the vertical arrow illustrate the integration limits (ν_L and ν_U) as well as the obtained weighted spectra centers $\bar{\nu}_W^A$ and $\bar{\nu}_W^S$ and the energy difference between them.

the weighted center of the sensitizer absorption is obtained similarly to equation (4.2) as

$$\bar{\nu}_W^S = \frac{\int_{\nu_L^S=\bar{\nu}_W^A}^{\nu_U^S} A^S(\nu)\nu \; d\nu}{\int_{\nu_L^S=\bar{\nu}_W^A}^{\nu_U^S} A^S(\nu) \; d\nu} \tag{4.3}$$

where $A^S(\nu)$ is the sensitizer absorption as a function of wavenumber. The obtained $\bar{\nu}_W^A$ and $\bar{\nu}_W^S$ can now be converted to eV and the difference will give a more standardized and fair estimation of the upconversion energy shift (UES) as illustrated in Figure 4.16.

In short, it is important to perform characterizations of any sort in a consistent way in order to facilitate comparability and repeatability. This is especially important for systems that are more complex, such as the TTA–UC, where the particular experimental conditions may affect the results and hence the reported characteristics. In **Paper VII** a number of good practice guidelines are brought up for characterization of TTA–UC systems and also a method for determining upconversion energy shift (UES) in a more controlled and objective way is suggested.

4.2.6 Discussion and conclusions

The work summarized in Section 4.2 focuses on the pursuit of completely supramolecular TTA–UC and a number of steps towards that goal have been covered including investigation of the effects of different modifications to the known DPA molecules (**Paper III**), photophysical characterization of larger DPA dendrimers (**Paper IV**) and their application with the DPA oligomer (Oligo) system in search of *intra*-molecular triplet-triplet annihilation (TTA2) capability (**Paper V**). On top of this also *intra*-molecular triplet energy transfer (*intra*TET) was investigated in coordinated annihilator-sensitizer complexes (**Paper VI**) followed by an overview of TTA–UC characterization procedures and suggestions to new ones (**Paper VII**).

Modifications of the 9,10-substituents to the known chromophore and TTA–UC annihilator DPA with electron withdrawing and donating groups proved to have minor effect on the absorption spectrum of the compounds. Thiophene modifications resulted in significant decrease of emissivity while less so for phenyl substituents. A common conclusion is that modification at the *para*-position of the phenyls cause least perturbation to the absorption and emission properties. This probably has to do with the phenyl-to-phenyl first singlet excited state transition dipole which remains more or less unperturbed if symmetry is maintained in this manner. The compounds complying with this observation (**3**,**4** and **5** in Figure 4.6) also proved to be well functioning annihilators when applied in TTA–UC with PtOEP as the sensitizer.

In accordance with these findings 1st generation DPA dendrimer (G1) and 2nd generation DPA dendrimer (G2) (Figure 4.8) were constructed and photophysically characterized. The photophysical properties of the constituting DPA subunit was maintained to a large extent in terms of spectral properties and fluorescence quantum yield (Φ_f). The singlet excited state is however at least partially delocalized with an exciton migration within the conjugated structure that is faster than a few ps. This finding illustrates the possibility to covalently connect multiple DPA units to form large structures where the electronic coupling between the subunits is high enough to allow fast exciton migration but low enough that the supramolecular structure maintains many of the individual subunit characteristics.

Using the same G1 and G2 molecules along with a new linear DPA oligomer (Oligo) (Figure 4.11a) capability to perform *intra*-molecular triplet-triplet annihilation (TTA2) was investigated. The prerequisite for this process is the capacity to carry two triplet excitons and allow for triplet exciton migration within the supramolecular structure. In order to facilitate the TTA2 process, the TTA–UC systems consisting of the supramolecular annihilators and PdOEP as the sensitizer were prepared in poly(methyl methacrylate) (PMMA) to eliminate effects of diffusion. The results were compared with that of DPA as the annihilator with the conclusion that increased size of the supramolecular annihilator structures correlate to increased TTA–UC efficiency in PMMA. This result supports the hypothesis of triplet exciton migration and TTA2 within the supramolecular annihilators paving the way for future complete *intra*-molecular TTA–UC systems.

As a natural next step the possibility of *intra*-molecular triplet energy transfer (*intra*TET) was investigated using pyridine substituted anthracenes (Figure 4.14) with the ability to coordinate to the metal center of ZnOEP acting as the sensitizer. The hypothesis

of minimized FRET quenching of UC emission due to a near 90°angle between the singlet excited state transitions of the annihilator and the sensitizer proved inaccurate. Instead large flexibility in this angle was proved through photophysical characterization which in combination with relatively short sensitizer-annihilator distances made FRET quenching efficient. The *intra*TET could not be experimentally resolved but several improvements to the system design are suggested. These include matching the sensitizer triplet excited state energy better to that of the annihilator in order to ensure large enough force for the TET step as well as ensuring less spectral overlap between the sensitizer absorption and the annihilator emission, minimizing the effect of FRET quenching. Furthermore, a 10 times increase of the current binding constant of ~ 6000 M^{-1} would be required to ensure a reasonably high sensitizer-annihilator complex concentration to reliably study the *intra*TET process.

Optimizing the *intra*TET process in accordance with the given suggestions and in combination with the already established supramolecular annihilators capable of TTA2 could indeed yield functional *intra*-molecular TTA–UC system. Such a system would operate with *intra*-molecular energy transfer rates exceeding the diffusion limit thus making it functional in air equilibrated solutions without the requirements of protective layers, solid matrices or rigorous deoxygenation.

Lastly the practices around characterization of the TTA–UC systems are addressed with recommendations regarding the employed experimental procedures. While the TTA–UC characteristics are obtained in a more agreed-upon manner today, it was not entirely so in the younger days of the field. It was not uncommon that for example Φ_{UC} was reported at intensities below I_{th}, i.e. the quadratic excitation intensity dependence region. Nowadays most reports of TTA–UC characteristics like I_{th} and Φ_{UC} often involve a declared excitation intensity ramping making the characterization conclusions much clearer. There is however no obvious correct way of reporting the upconversion of photons in terms of energy. It is common to refer to the energy gap between the most intense peaks of the sensitizer absorption and annihilator UC emission. This can however be misleading as the most intense peaks may not necessarily represent the majority of the spectrum. Instead a suggestion is made to refer to the energy gap between the weighted spectral centers of the two TTA–UC components with emphasis on the red side of the sensitizer absorption as seen in Figure 4.16.

CHAPTER 5

Concluding remarks and outlook

The work presented in this Thesis has been focused on the improvement of the known bimolecular TTA–UC system in fluid environment and the pursuit of a fully supramolecular TTA–UC system capable of *intra*-molecular triplet energy transfer (*intra*TET) and *intra*-molecular triplet-triplet annihilation (TTA2). In some way this falls in line with the current development of the organic TTA–UC field where the focus is being shifted from pure search for new sensitizer-annihilator pairs to more detailed understanding of the mechanics of the known TTA–UC systems which opens up new paths for applications. In my opinion this is a good bottom-up approach in terms of knowledge which may prove more fruitful in time than the more top-down approach which often governs the young days of a developing research field. With this in mind the work presented here can be categorized as being partly basic research but also applied research in terms of using knowledge from inter-molecular TTA–UC to create and characterize systems with new *intra*-molecular capabilities.

The first part of the results presented in this Thesis concerns TTA–UC in fluid environment. The central topic of deoxygenating the TTA–UC samples is addressed in a simple way through the addition of a third species acting as a sacrificial agent, a scavenger, for capturing dissolved singlet excited O_2 ($^1O_2$*) in the sample (**Paper I**). The idea of using oxygen scavengers is appealing as it assures reproducibility of oxygen removal through the dependence on the sensitizer and annihilator concentrations (as they both act as sensitizers for O_2), the concentration of the scavenger and the excitation light. With the knowledge of these parameters any user should be able to reproduce the determined characteristics of a TTA–UC system.

The application of TTA–UC for increasing the conversion efficiency of the $FvRu_2$ solar thermal fuel was also demonstrated (**Paper II**). The energetically useful photoisomerization reaction of $FvRu_2$ from its low-energy to high-energy form requires photons that are scarce in the solar spectrum. The application of TTA–UC fits therefore very well in this concept and signifies its potential importance for future solar energy conversion. In this particular application the TTA–UC system was in fluid form and was being deployed in a microfluidic chip. Naturally this puts certain demands on the sealing quality in order to prevent air from dissolving in the fluid and the fluid from leaking out, especially in a supposed real life long-term application. Suffice to say, the same application would have been simpler if the TTA–UC system could be applied as a solid.

The second part of the results in this Thesis concerns the pursuit of supramolecular TTA–UC system capable of *intra*-molecular triplet energy transfer (*intra*TET) and *intra*-molecular triplet-triplet annihilation (TTA2) with the end-goal to have a highly efficient TTA–UC system in solid state. To this end, the possibility of structural modification of the known annihilator DPA was explored (**Paper III**) with the goal of obtaining better annihilators or at least maintaining properties similar to that of DPA. Modifications at the *para*-positions of the DPA's 9,10-substituents show great promise as annihilators, probably due to maintained symmetry along the phenyl-to-phenyl plane. In accordance with these findings two generations of DPA dendrimers (G1 and G2) were synthesized and photophysically characterized in search of singlet exciton delocalization (**Paper IV**). The results revealed an excited state splitting and most probably an extremely fast singlet exciton delocalization. The same dendrimers and a new linear DPA oligomer (Oligo) were used as annihilators in diffusion-free environment to resolve possible TTA2

within their supramolecular structures (**Paper V**). An increasing TTA–UC efficiency was observed in diffusion-free environment correlating with increasing size of the annihilator which can be explained with the TTA2 mechanism. As a natural next step the idea of *intra*TET was considered for investigation. To aid in this endeavour a new pyridine substituted DPA annihilator was synthesized with the ability to coordinate axially to the metal core of the ZnOEP sensitizer (**Paper VI**). In this coordination complex the relative average sensitizer-annihilator transition moment angle was expected to be near 90°, thus minimizing the expected FRET quenching of the singlet excited annihilator back to the sensitizer. The expected *intra*TET could not be experimentally resolved, instead a number of optimization measures were suggested that might enable the resolution of the *intra*TET in future studies.

With this fundamental background the next logical step would be to construct large supramolecular annihilators like the G1, G2 or Oligo (**Paper V**) but with pyridine substituted ends serving as docking stations for coordinating sensitizers. In accordance with the optimization suggestions from **Paper VI** the coordinated sensitizer would need to have a triplet excited state energy higher than that of the supramolecular annihilator to assure efficient *intra*TET. The binding constant would need to be high in order to maintain the complete supramolecular TTA–UC system even in a fluid or semi-fluid like paint. However, considering the findings in **Paper IV** the UC singlet exciton might be highly delocalized and therefore might travel around the supramolecular annihilator several times before relaxing and the UC photon is emitted. This implies that the singlet exciton would at times be very close to the coordinated sensitizers increasing the possibility for FRET quenching to occur back to the sensitizer. It would therefore be crucial to have a sufficient spectral mismatch between the annihilator UC emission and the sensitizer absorption spectra in order to minimize FRET back transfer of the UC generated excited singlet state. A further improvement of such fully supramolecular TTA–UC system in terms of application for solar energy would be the coordination of different kinds of sensitizers to the same annihilator, thus upconverting a wider portion of the visible spectrum per supramolecular TTA–UC molecule.

A natural benchmark for a supramolecular TTA–UC system is that it should function well in diffusion-free environment. This is used in this Thesis to experimentally resolve the *intra*-molecular processes (**Papers V-VI**). However, a supramolecular TTA–UC may just as well be applied in fluid systems as the diffusion allows for a more even excitation as opposed to a diffusion restrictive environment where some molecules can be excited all the time while others not at all. This can lead to local photodegradation of the material and in extension the loss of TTA–UC functionality in the application.

Additionally, the question of TTA–UC characterization is addressed (**Paper VII**). It is highly recommended to perform system characterizations in the linear region above excitation intensity threshold (I_{th}) in order to facilitate comparability and reproducibility. Additionally, a more objective way of reporting upconversion energy shift (UES) for different TTA–UC sensitizer-annihilator pairs is suggested.

As a final note, the major goal of constructing a functional supramolecular TTA–UC system was not realized within the work presented in this Thesis. However, the knowledge gained in this pursuit will be useful in its future realization.

CHAPTER 6

Acknowledgments

I would like to thank the following people:

My supervisor **Bo Albinsson** for giving me the opportunity to work as a PhD student in your group. Thank you for your patience, your guidance and for trusting me with my own ideas.

My co-supervisor **Kasper Moth-Poulsen** for being a great coach throughout this journey, for always being positive and providing creative solutions to problems.

My co-authors for their contribution to the papers.

Maria Abrahamsson for being a great friend and for always taking the time to talk regardless of subject. Thank you for your help and guidance throughout this journey and also for reading my thesis.

Magnus Bälter for being a fantastic friend. Your honesty and humor is greatly valued. Thank you for the awesome time sharing the office. In dire times, always remember the *Quantum indian*!

Joachim Wallenstein for your friendship. Don't underestimate the social aspects of *störningsjouren* and always keep smiling, it rubs off! :-)

Valeria Saavedra for all the talks and laughs. Thank you for inviting me to see Mexico City, *Jefa!*

Victor Gray for keeping an open mind and putting up with my office raids (often during Fridays around *fika-o'clock*). Also, thank you for reading my Thesis.

Rita and Pegah for brightening the days with your humor. We should really consider getting the *gang* back together, it's been a while... Rita: Thank you for reading my Thesis.

Nikola Marković for fruitful discussions and for taking the time to answer questions that usually never take as little time as I initially claim.

Marcus Wilhelmsson for allowing me to do my diploma work in your group and introducing me to the world of Physical chemistry.

Past and present roomies for awesome times with lots of laughs.

Past and present colleagues and Balb-group members for making the time at the division rewarding and fun. Special thanks to Mélina, Jens and Laura for a fantastic atmosphere.

My family and friends that have supported me throughout this time.

A very special thanks to

My fantastic wife **Maria** for making me laugh every day and being by my side through good and bad. Thank you for your unconditional love and support, especially throughout the writing of this Thesis. Thank you for taking care of everything around me so that I could focus on writing and for the invaluable feedback and discussions.
Indeed, *together we are strong!* I love you!

My wonderful son **Adrian** to whom this Thesis is dedicated. You have contributed more to this thesis than you might think. One smile from you can keep me going at the most difficult times. I love you!

CHAPTER 7

References

[1] N. S. Lewis and D. G. Nocera. Powering the planet: Chemical challenges in solar energy utilization. *Proceedings of the National Academy of Sciences* **103**.43 (2006), 15729–15735.
[2] N. S. Lewis. Powering the planet. *MRS Bull.* **32**.10 (2007), 808–820.
[3] W. E. Council. *World Energy Scenarios: Composing energy futures to 2050*. Stretegic report. World Energy Council, 2013.
[4] I. E. Agiency. *Energy and Air Pollution - World Energy Outlook Special Report*. Report. Organisation for Economic Co-operation and Development/International Energy Agiency, 2015.
[5] W. E. Council. *World Energy Resources - 2013 Survey: Summary*. Report. World Energy Council, 2013.
[6] W. E. Council. *World Energy Resources - E-storage: Shifting from cost to value - Wind and solar applications*. Report. World Energy Cuncil, 2016.
[7] H. B. Gray. Powering the planet with solar fuel. *Nat. Chem.* **1**.1 (2009), 7–7.
[8] T. J. Kucharski, Y. Tian, S. Akbulatov, and R. Boulatov. Chemical solutions for the closed-cycle storage of solar energy. *Energy & Environmental Science* **4**.11 (2011), 4449.
[9] T. N. Singh-Rachford and F. N. Castellano. Low power visible-to-UV upconversion. *J. Phys. Chem. A* **113**.20 (2009), 5912–7.
[10] T. N. Singh-Rachford and F. N. Castellano. Photon upconversion based on sensitized triplet-triplet annihilation. *Coord. Chem. Rev.* **254**.21-22 (2010), 2560–2573.
[11] W. Shockley and H. J. Queisser. Detailed Balance Limit of Efficiency of p-n Junction Solar Cells. *J. Appl. Phys.* **32**.3 (1961), 510.
[12] M. J. Tayebjee, D. R. McCamey, and T. W. Schmidt. Beyond Shockley-Queisser: Molecular Approaches to High-Efficiency Photovoltaics. *J. Phys. Chem. Lett.* **6**.12 (2015), 2367–78.
[13] R. S. Khnayzer, J. Blumhoff, J. A. Harrington, A. Haefele, F. Deng, and F. N. Castellano. Upconversion-powered photoelectrochemistry. *Chem Commun (Camb)* **48**.2 (2012), 209–11.
[14] Y. Y. Cheng, B. Fückel, R. W. MacQueen, T. Khoury, R. G.C. R. Clady, T. F. Schulze, N. J. Ekins-Daukes, M. J. Crossley, B. Stannowski, K. Lips, and T. W. Schmidt. Improving the light-harvesting of amorphous silicon solar cells with photochemical upconversion. *Energy & Environmental Science* **5**.5 (2012), 6953.
[15] X. Cao, B. Hu, and P. Zhang. High Upconversion Efficiency from Hetero Triplet–Triplet Annihilation in Multiacceptor Systems. *J. Phys. Chem. Lett.* **4**.14 (2013), 2334–2338.
[16] A. Turshatov, D. Busko, Y. Avlasevich, T. Miteva, K. Landfester, and S. Baluschev. Synergetic effect in triplet-triplet annihilation upconversion: highly efficient multichromophore emitter. *ChemPhysChem* **13**.13 (2012), 3112–5.
[17] C. A. Parker and C. G. Hatchard. Delayed Fluorescence from Solutions of Anthracene and Phenanthrene. *Proceedings of the Royal Society A: Mathematical, Physical and Engineering Sciences* **269**.1339 (1962), 574–584.
[18] C. A. Parker. Sensitized P-Type Delayed Fluorescence. *Proc. R. Soc. London, Ser. A* **276**.1364 (1963), 125–135.

[19] C. A. Parker. Phosphorescence and Delayed Fluorescence from Solutions. *Advances in Photochemistry* **2** (1964), 305–383.

[20] C. A. Parker, C. G. Hatchard, and T. A. Joyce. P-type delayed fluorescence from ionic species and aromatic hydrocarbons. *J. Mol. Spectrosc.* **14**.1-4 (1964), 311–319.

[21] R. R. Islangulov, D. V. Kozlov, and F. N. Castellano. Low power upconversion using MLCT sensitizers. *Chem Commun (Camb)* 30 (2005), 3776–8.

[22] D. V. Kozlov and F. N. Castellano. Anti-Stokes delayed fluorescence from metal-organic bichromophores. *Chem Commun (Camb)* 24 (2004), 2860–1.

[23] P. E. Keivanidis, S. Baluschev, T. Miteva, G. Nelles, U. Scherf, A. Yasuda, and G. Wegner. Up-Conversion Photoluminescence in Polyfluorene Doped with Metal(II)–Octaethyl Porphyrins. *Adv. Mater.* **15**.24 (2003), 2095–2098.

[24] A. Monguzzi, R. Tubino, and F. Meinardi. Diffusion Enhanced Upconversion in Organic Systems. *Int. J. Photoenergy* **2008** (2008), 1–5.

[25] A. Monguzzi, J. Mezyk, F. Scotognella, R. Tubino, and F. Meinardi. Upconversion-induced fluorescence in multicomponent systems: Steady-state excitation power threshold. *Phys. Rev. B* **78**.19 (2008).

[26] R. R. Islangulov and F. N. Castellano. Photochemical upconversion: anthracene dimerization sensitized to visible light by a RuII chromophore. *Angew. Chem. Int. Ed. Engl.* **45**.36 (2006), 5957–9.

[27] T. N. Singh-Rachford, R. R. Islangulov, and F. N. Castellano. Photochemical upconversion approach to broad-band visible light generation. *J. Phys. Chem. A* **112**.17 (2008), 3906–10.

[28] S. Baluschev, V. Yakutkin, T. Miteva, Y. Avlasevich, S. Chernov, S. Aleshchenkov, G. Nelles, A. Cheprakov, A. Yasuda, K. Mullen, and G. Wegner. Blue-green up-conversion: noncoherent excitation by NIR light. *Angew. Chem. Int. Ed. Engl.* **46**.40 (2007), 7693–6.

[29] V. Yakutkin, S. Aleshchenkov, S. Chernov, T. Miteva, G. Nelles, A. Cheprakov, and S. Baluschev. Towards the IR limit of the triplet-triplet annihilation-supported up-conversion: tetraanthraporphyrin. *Chemistry* **14**.32 (2008), 9846–50.

[30] M. Filatov, I. Z. Ilieva, K. Landfester, and S. Baluschev. Exploring the IR-Limit of the Triplet- Triplet Annihilation Upconversion: Tetraaryltetraanthra [2, 3] porphyrin-Family. *Nanotechnology* (2013), 531–534.

[31] F. Deng, W. Sun, and F. N. Castellano. Texaphyrin sensitized near-IR-to-visible photon upconversion. *Photochem. Photobiol. Sci.* (2014).

[32] F. Deng, J. R. Sommer, M. Myahkostupov, K. S. Schanze, and F. N. Castellano. Near-IR phosphorescent metalloporphyrin as a photochemical upconversion sensitizer. *Chem Commun (Camb)* **49**.67 (2013), 7406–8.

[33] Y. Y. Cheng, T. Khoury, R. G. Clady, M. J. Tayebjee, N. J. Ekins-Daukes, M. J. Crossley, and T. W. Schmidt. On the efficiency limit of triplet-triplet annihilation for photochemical upconversion. *Phys. Chem. Chem. Phys.* **12**.1 (2010), 66–71.

[34] T. N. Singh-Rachford and F. N. Castellano. Triplet Sensitized Red-to-Blue Photon Upconversion. *J. Phys. Chem. Lett.* **1**.1 (2010), 195–200.

[35] T. N. Singh-Rachford and F. N. Castellano. Supra-nanosecond dynamics of a red-to-blue photon upconversion system. *Inorg. Chem.* **48**.6 (2009), 2541–8.

[36] T. N. Singh-Rachford, A. Nayak, M. L. Muro-Small, S. Goeb, M. J. Therien, and F. N. Castellano. Supermolecular-chromophore-sensitized near-infrared-to-visible photon upconversion. *J. Am. Chem. Soc.* **132**.40 (2010), 14203–11.

[37] Y. Y. Cheng, B. Fuckel, T. Khoury, R. G. Clady, N. J. Ekins-Daukes, M. J. Crossley, and T. W. Schmidt. Entropically driven photochemical upconversion. *J. Phys. Chem. A* **115**.6 (2011), 1047–53.

[38] V. Gray, D. Dzebo, A. Lundin, J. Alborzpour, M. Abrahamsson, B. Albinsson, and K. Moth-Poulsen. Photophysical characterization of the 9,10-disubstituted anthracene chromophore and its applications in triplet–triplet annihilation photon upconversion. *J. Mater. Chem. C* **3**.42 (2015), 11111–11121.

[39] Z. Q. Liang, B. Sun, C. Q. Ye, X. M. Wang, X. T. Tao, Q. H. Wang, P. Ding, B. Wang, and J. J. Wang. New anthracene derivatives as triplet acceptors for efficient green-to-blue low-power upconversion. *ChemPhysChem* **14**.15 (2013), 3517–22.

[40] M. Penconi, F. Ortica, F. Elisei, and P. L. Gentili. New molecular pairs for low power non-coherent triplet–triplet annihilation based upconversion: dependence on the triplet energies of sensitizer and emitter. *J. Lumin.* **135** (2013), 265–270.

[41] T. N. Singh-Rachford, A. Haefele, R. Ziessel, and F. N. Castellano. Boron dipyrromethene chromophores: next generation triplet acceptors/annihilators for low power upconversion schemes. *J. Am. Chem. Soc.* **130**.48 (2008), 16164–5.

[42] F. Deng, A. J. Francis, W. W. Weare, and F. N. Castellano. Photochemical upconversion and triplet annihilation limit from a boron dipyrromethene emitter. *Photochem. Photobiol. Sci.* **14**.7 (2015), 1265–70.

[43] K. Moor, J. H. Kim, S. Snow, and J. H. Kim. [C70] fullerene-sensitized triplet-triplet annihilation upconversion. *Chem Commun (Camb)* **49**.92 (2013), 10829–31.

[44] W. Wu, J. Zhao, J. Sun, and S. Guo. Light-harvesting fullerene dyads as organic triplet photosensitizers for triplet-triplet annihilation upconversions. *J. Org. Chem.* **77**.12 (2012), 5305–12.

[45] S. K. Sugunan, C. Greenwald, M. F. Paige, and R. P. Steer. Efficiency of Noncoherent Photon Upconversion by Triplet-Triplet Annihilation: The C60 Plus Anthanthrene System and the Importance of Tuning the Triplet Energies. *J. Phys. Chem. A* (2013).

[46] W. Yang, J. Zhao, C. Sonn, D. Escudero, A. Karatay, H. G. Yaglioglu, B. Küçüköz, M. Hayvali, C. Li, and D. Jacquemin. Efficient Intersystem Crossing in Heavy-Atom-Free Perylenebisimide Derivatives. *J. Phys. Chem. C* **120**.19 (2016), 10162–10175.

[47] X. Cui, J. Zhao, P. Yang, and J. Sun. Zinc(ii) tetraphenyltetrabenzoporphyrin complex as triplet photosensitizer for triplet-triplet annihilation upconversion. *Chem Commun (Camb)* **49**.87 (2013), 10221–3.

[48] Y. Ma, J. Peng, X. Jiang, X. Guo, and D. Zhao. Sensitizer design for efficient triplet-triplet annihilation upconversion: annihilator-appended tris-cyclometalated Ir(III) complexes. *Chem. Commun.* (2014).

[49] Y. Y. Cheng, B. Fuckel, T. Khoury, R. G.C. R. Clady, M. J. Y. Tayebjee, N. J. Ekins-Daukes, M. J. Crossley, and T. W. Schmidt. Kinetic Analysis of Photochemical Upconversion by Triplet-Triplet Annihilation: Beyond Any Spin Statistical Limit. *J. Phys. Chem. Lett.* **1**.12 (2010), 1795–1799.

[50] S. Hoseinkhani, R. Tubino, F. Meinardi, and A. Monguzzi. Achieving the photon up-conversion thermodynamic yield upper limit by sensitized triplet-triplet annihilation. *Phys. Chem. Chem. Phys.* **17**.6 (2015), 4020–4.

[51] N. Yanai, M. Kozue, S. Amemori, R. Kabe, C. Adachi, and N. Kimizuka. Increased vis-to-UV upconversion performance by energy level matching between a TADF donor and high triplet energy acceptors. *J. Mater. Chem. C* (2016).

[52] L. Tsakalakos, S. Baluschev, G. Nelles, K. Landfester, and T. Miteva. Sun-light upconversion in multi-component organic systems: development towards application for solar cells outcome enhancement. **8471** (2012), 84710E–84710E–8.

[53] S. Baluschev, V. Yakutkin, G. Wegner, T. Miteva, G. Nelles, A. Yasuda, S. Chernov, S. Aleshchenkov, and A. Cheprakov. Upconversion with ultrabroad excitation band: Simultaneous use of two sensitizers. *Appl. Phys. Lett.* **90**.18 (2007), 181103.

[54] Y. Murakami. Photochemical photon upconverters with ionic liquids. *Chem. Phys. Lett.* **516**.1-3 (2011), 56–61.

[55] Y. Murakami, H. Kikuchi, and A. Kawai. Kinetics of photon upconversion in ionic liquids: energy transfer between sensitizer and emitter molecules. *J. Phys. Chem. B* **117**.8 (2013), 2487–94.

[56] Y. Murakami, H. Kikuchi, and A. Kawai. Kinetics of photon upconversion in ionic liquids: time-resolved analysis of delayed fluorescence. *J. Phys. Chem. B* **117**.17 (2013), 5180–7.

[57] S. Hisamitsu, N. Yanai, and N. Kimizuka. Photon-Upconverting Ionic Liquids: Effective Triplet Energy Migration in Contiguous Ionic Chromophore Arrays. *Angew. Chem. Int. Ed. Engl.* (2015).

[58] P. Duan, N. Yanai, and N. Kimizuka. Photon upconverting liquids: matrix-free molecular upconversion systems functioning in air. *J. Am. Chem. Soc.* **135**.51 (2013), 19056–9.

[59] M. Poznik, U. Faltermeier, B. Dick, and B. König. Light upconverting soft particles: triplet–triplet annihilation in the phospholipid bilayer of self-assembled vesicles. *RSC Adv.* **6**.48 (2016), 41947–41950.

[60] T. Ogawa, N. Yanai, A. Monguzzi, and N. Kimizuka. Highly Efficient Photon Upconversion in Self-Assembled Light-Harvesting Molecular Systems. *Sci. Rep.* **5** (2015), 10882.

[61] H. Kouno, T. Ogawa, S. Amemori, P. Mahato, N. Yanai, and N. Kimizuka. Triplet energy migration-based photon upconversion by amphiphilic molecular assemblies in aerated water. *Chem. Sci.* **7**.8 (2016), 5224–5229.

[62] S. Mutsamwira, E. W. Ainscough, A. C. Partridge, P. J. Derrick, and V. V. Filichev. DNA-Based Assemblies for Photochemical Upconversion. *J. Phys. Chem. B* **119**.44 (2015), 14045–52.

[63] J. H. Kim and J. H. Kim. Encapsulated triplet-triplet annihilation-based upconversion in the aqueous phase for sub-band-gap semiconductor photocatalysis. *J. Am. Chem. Soc.* **134**.42 (2012), 17478–81.

[64] A. Turshatov, D. Busko, S. Baluschev, T. Miteva, and K. Landfester. Micellar carrier for triplet–triplet annihilation-assisted photon energy upconversion in a water environment. *New J. Phys.* **13**.8 (2011), 083035.

[65] M. Shirakawa, N. Fujita, T. Tani, K. Kaneko, and S. Shinkai. Organogel of an 8-quinolinol platinum(II) chelate derivative and its efficient phosphorescence emission effected by inhibition of dioxygen quenching. *Chem Commun (Camb)* 33 (2005), 4149–51.

[66] M. Shirakawa, N. Fujita, T. Tani, K. Kaneko, M. Ojima, A. Fujii, M. Ozaki, and S. Shinkai. Organogels of 8-quinolinol/metal(II)-chelate derivatives that show electron- and light-emitting properties. *Chemistry* **13**.15 (2007), 4155–62.

[67] P. Duan, N. Yanai, H. Nagatomi, and N. Kimizuka. Photon upconversion in supramolecular gel matrixes: spontaneous accumulation of light-harvesting donor-acceptor arrays in nanofibers and acquired air stability. *J. Am. Chem. Soc.* **137**.5 (2015), 1887–94.

[68] M. Haring, R. Perez-Ruiz, A. Jacobi von Wangelin, and D. D. Diaz. Intragel photoreduction of aryl halides by green-to-blue upconversion under aerobic conditions. *Chem Commun (Camb)* (2015).

[69] K. Sripathy, R. W. MacQueen, J. R. Peterson, Y. Y. Cheng, M. Dvořák, D. R. McCamey, N. D. Treat, N. Stingelin, and T. W. Schmidt. Highly efficient photochemical upconversion in a quasi-solid organogel. *J. Mater. Chem. C* **3**.3 (2015), 616–622.

[70] R. Vadrucci, C. Weder, and Y. C. Simon. Organogels for low-power light upconversion. *Mater. Horiz.* **2**.1 (2015), 120–124.

[71] X. Liu, J. Fei, P. Zhu, and J. Li. Facile Co-assembly of Dipeptide-based Organogel toward Efficient Triplet-Triplet Annihilation Photonic Upconversion. *Chem. Asian J.* (2016).

[72] Y. Murakami, Y. Himuro, T. Ito, R. Morita, K. Niimi, and N. Kiyoyanagi. Transparent and Nonflammable Ionogel Photon Upconverters and Their Solute Transport Properties. *J. Phys. Chem. B* **120**.4 (2016), 748–55.

[73] X. Tong, J. Xiang, F. Shi, and Y. Zhao. Near-Infrared Light-Sensitive Supramolecular Gel with Enhanced Visible Light Upconversion. *Adv. Opt. Mater.* (2016).

[74] J. H. Kim, F. Deng, F. N. Castellano, and J. H. Kim. High Efficiency Low-Power Upconverting Soft Materials. *Chem. Mater.* **24**.12 (2012), 2250–2252.

[75] A. Monguzzi, F. Bianchi, A. Bianchi, M. Mauri, R. Simonutti, R. Ruffo, R. Tubino, and F. Meinardi. High Efficiency Up-Converting Single Phase Elastomers for Photon Managing Applications. *Adv. Energy Mater.* **3**.5 (2013), 680–686.

[76] P. B. Merkel and J. P. Dinnocenzo. Low-power green-to-blue and blue-to-UV upconversion in rigid polymer films. *J. Lumin.* **129**.3 (2009), 303–306.

[77] A. Monguzzi. On the effects of a solid environment on sensitized up-conversion. *Proc. of SPIE* **8435** (2012), 843511.

[78] Y. C. Simon and C. Weder. Low-power photon upconversion through triplet–triplet annihilation in polymers. *J. Mater. Chem.* **22**.39 (2012), 20817.

[79] P. C. Boutin, K. P. Ghiggino, T. L. Kelly, and R. P. Steer. Photon Upconversion by Triplet–Triplet Annihilation in Ru(bpy)3- and DPA-Functionalized Polymers. *J. Phys. Chem. Lett.* **4**.23 (2013), 4113–4118.

[80] S. H. Lee, J. R. Lott, Y. C. Simon, and C. Weder. Melt-processed polymer glasses for low-power upconversion via sensitized triplet-triplet annihilation. *J. Mater. Chem. C* **1**.33 (2013), 5142–5148.

[81] S. H. Lee, D. C. Thevenaz, C. Weder, and Y. C. Simon. Glassy poly(methacrylate) terpolymers with covalently attached emitters and sensitizers for low-power light upconversion. *Journal of Polymer Science Part a-Polymer Chemistry* **53**.14 (2015), 1629–1639.

[82] S. Raisys, K. Kazlauskas, S. Jursenas, and Y. C. Simon. The Role of Triplet Exciton Diffusion in Light-Upconverting Polymer Glasses. *ACS Appl. Mater. Interfaces* (2016).

[83] A. Monguzzi, M. Frigoli, C. Larpent, R. Tubino, and F. Meinardi. Low-Power-Photon Up-Conversion in Dual-Dye-Loaded Polymer Nanoparticles. *Adv. Funct. Mater.* **22**.1 (2012), 139–143.

[84] J. S. Lissau, J. M. Gardner, and A. Morandeira. Photon Upconversion on Dye-Sensitized Nanostructured ZrO2Films. *J. Phys. Chem. C* **115**.46 (2011), 23226–23232.

[85] J. S. Lissau, D. Nauroozi, M.-P. Santoni, S. Ott, J. M. Gardner, and A. Morandeira. Anchoring Energy Acceptors to Nanostructured ZrO2Enhances Photon Upconversion by Sensitized Triplet–Triplet Annihilation Under Simulated Solar Flux. *J. Phys. Chem. C* **117**.28 (2013), 14493–14501.

[86] J. S. Lissau, D. Nauroozi, M.-P. Santoni, T. Edvinsson, S. Ott, J. M. Gardner, and A. Morandeira. What Limits Photon Upconversion on Mesoporous Thin Films Sensitized by Solution-Phase Absorbers? *J. Phys. Chem. C* **119**.9 (2015), 4550–4564.

[87] J. S. Lissau, D. Nauroozi, M.-P. Santoni, S. Ott, J. M. Gardner, and A. Morandeira. Photon Upconversion from Chemically Bound Triplet Sensitizers and Emitters on Mesoporous ZrO2: Implications for Solar Energy Conversion. *J. Phys. Chem. C* **119**.46 (2015), 25792–25806.

[88] P. Mahato, A. Monguzzi, N. Yanai, T. Yamada, and N. Kimizuka. Fast and long-range triplet exciton diffusion in metal-organic frameworks for photon upconversion at ultralow excitation power. *Nat. Mater.* **14**.9 (2015), 924–30.

[89] P. Mahato, N. Yanai, M. Sindoro, S. Granick, and N. Kimizuka. Preorganized Chromophores Facilitate Triplet Energy Migration, Annihilation and Upconverted Singlet Energy Collection. *J. Am. Chem. Soc.* **138**.20 (2016), 6541–9.

[90] G. Bergamini, P. Ceroni, P. Fabbrizzi, and S. Cicchi. A multichromophoric dendrimer: from synthesis to energy up-conversion in a rigid matrix. *Chem Commun (Camb)* **47**.48 (2011), 12780–2.

[91] A. J. Tilley, B. E. Robotham, R. P. Steer, and K. P. Ghiggino. Sensitized non-coherent photon upconversion by intramolecular triplet–triplet annihilation in a diphenylanthracene pendant polymer. *Chem. Phys. Lett.* (2014).

[92] J. R. Lakowicz. *Principles of Fluorescence Spectroscopy*. 3rd ed. 233 Spring Street; New York; NY 10013; USA: Springer Science+Business Media, LLC, 2006.

[93] J. M. Hollas. *Modern spectroscopy*. 3rd ed. John Wiley & Sons, 2004.

[94] N. J. Turro, V. Ramamurthy, and J. C. Scaiano. *Modern molecular photochemistry of organic molecules*. University Bcience Books, 2010.

[95] B. Valeur. *Molecular Fluorescence: Principles and Applications*. Wiley-VCH Verlag, GmbH, 2001.

[96] M. Kasha. Characterization of electronic transitions in complex molecules. *Discuss. Faraday Soc.* **9** (1950), 14.

[97] T. W. Schmidt and F. N. Castellano. Photochemical Upconversion: The Primacy of Kinetics. *J. Phys. Chem. Lett.* **5**.22 (2014), 4062–72.

[98] M. A. Filatov, S. Baluschev, and K. Landfester. Protection of densely populated excited triplet state ensembles against deactivation by molecular oxygen. *Chem. Soc. Rev.* (2016).

[99] J. Zhou, Q. Liu, W. Feng, Y. Sun, and F. Li. Upconversion luminescent materials: advances and applications. *Chem. Rev.* **115**.1 (2015), 395–465.

[100] F. N. Castellano and C. E. McCusker. MLCT sensitizers in photochemical upconversion: past, present, and potential future directions. *Dalton Trans.* **44**.41 (2015), 17906–17910.

[101] R. C. Evans, P. Douglas, and H. D. Burrow. *Applied photochemistry*. Springer, 2013.

[102] D. L. Dexter. A Theory of Sensitized Luminescence in Solids. *J. Chem. Phys.* **21**.5 (1953), 836.

[103] T. F. Schulze and T. W. Schmidt. Photochemical upconversion: Present status and prospects for its application to solar energy conversion. *Energy Environ. Sci.* (2014).

[104] J. Saltiel and B. W. Atwater. Spin-Statistical Factors in Diffusion-Controlled Reactions. *Advances in Photochemistry* **14** (1988), 1–90.

[105] J. B. Birks. The quintet state of the pyrene excimer. *Phys. Lett. A* **24**.9 (1967), 479–480.

[106] D. Y. Kondakov, T. D. Pawlik, T. K. Hatwar, and J. P. Spindler. Triplet annihilation exceeding spin statistical limit in highly efficient fluorescent organic light-emitting diodes. *J. Appl. Phys.* **106**.12 (2009), 124510.

[107] B. Dick and B. Nickel. Accessibility of the lowest quintet state of organic molecules through triplet-triplet annihilation; an indo ci study. *Chem. Phys.* **78**.1 (1983), 1–16.

[108] S. M. Bachilo and R. B. Weisman. Determination of Triplet Quantum Yields from Triplet–Triplet Annihilation Fluorescence. *J. Phys. Chem. A* **104**.33 (2000), 7711–7714.

[109] O. L. J. Gijzeman, F. Kaufman, and G. Porter. Oxygen quenching of aromatic triplet states in solution. Part 1. *Journal of the Chemical Society, Faraday Transactions 2* **69** (1973), 708.

[110] A. Monguzzi, R. Tubino, M. M. Salamone, and F. Meinardi. Energy transfer enhancement by oxygen perturbation of spin-forbidden electronic transitions in aromatic systems. *Phys. Rev. B* **82**.12 (2010).

[111] G. J. Hoijtink. The influence of paramagnetic molecules on singlet-triplet transitions. *Mol. Phys.* **3**.1 (1960), 67–70.

[112] Y.-N. Chiu. On Singlet-Triplet Transitions Induced by Exchange with Paramagnetic Molecules and the Intermolecular Coupling of Spin Angular Momenta. *J. Chem. Phys.* **56**.10 (1972), 4882.

[113] J. E. Auckett, Y. Y. Chen, T. Khoury, R. G.C. R. Clady, N. J. Ekins-Daukes, M. J. Crossley, and T. W. Schmidt. Efficient up-conversion by triplet-triplet annihilation. *J. Phys. Conf. Ser.* **185** (2009), 012002.

[114] A. Haefele, J. Blumhoff, R. S. Khnayzer, and F. N. Castellano. Getting to the (Square) Root of the Problem: How to Make Noncoherent Pumped Upconversion Linear. *J. Phys. Chem. Lett.* **3**.3 (2012), 299–303.

[115] B. Valeur and G. Weber. Resolution of the fluorescence excitation spectrum of indole into the 1La and 1Lb excitation bands. *Photochem. Photobiol.* **25**.5 (1977), 441–444.

[116] W. R. Ware. Oxygen Quenching of Fluorescence in Solution: An Experimental Study of the Diffusion Process. *J. Phys. Chem.* **66**.3 (1962), 455–458.

[117] M. A. Filatov, E. Heinrich, D. Busko, I. Z. Ilieva, K. Landfester, and S. Baluschev. Reversible oxygen addition on a triplet sensitizer molecule: protection from excited state depopulation. *Phys. Chem. Chem. Phys.* **17**.9 (2015), 6501–10.

[118] D. Dzebo, K. Börjesson, V. Gray, K. Moth-Poulsen, and B. Albinsson. Intramolecular Triplet-Triplet Annihilation in 9,10-diphenyl anthracene oligomers and dendrimers (2016). (Manuscript, submitted).

[119] K. Moth-Poulsen, D. Ćoso, K. Börjesson, N. Vinokurov, S. K. Meier, A. Majumdar, K. P. C. Vollhardt, and R. A. Segalman. Molecular solar thermal (MOST) energy storage and release system. *Energy & Environmental Science* **5**.9 (2012), 8534.

[120] Y. Kanai, V. Srinivasan, S. K. Meier, K. P. Vollhardt, and J. C. Grossman. Mechanism of thermal reversal of the (fulvalene)tetracarbonyldiruthenium photoisomerization: toward molecular solar-thermal energy storage. *Angew. Chem. Int. Ed. Engl.* **49**.47 (2010), 8926–9.

[121] M. R. Harpham, S. C. Nguyen, Z. Hou, J. C. Grossman, C. B. Harris, M. W. Mara, A. B. Stickrath, Y. Kanai, A. M. Kolpak, D. Lee, D.-J. Liu, J. P. Lomont, K. Moth-Poulsen, N. Vinokurov, L. X. Chen, and K. P. C. Vollhardt. X-ray Transient Absorption and Picosecond IR Spectroscopy of Fulvalene(tetracarbonyl)diruthenium on Photoexcitation. *Angew. Chem. Int. Ed.* **51**.31 (2012), 7692–7696.

[122] V. Gray, D. Dzebo, M. Abrahamsson, B. Albinsson, and K. Moth-Poulsen. Triplet-triplet annihilation photon-upconversion: towards solar energy applications. *Phys. Chem. Chem. Phys.* **16**.22 (2014), 10345–10352.

[123] C. Ye, B. Wang, R. Hao, X. Wang, P. Ding, X. Tao, Z. Chen, Z. Liang, and Y. Zhou. Oil-in-water microemulsion: an effective medium for triplet–triplet annihilated upconversion with efficient triplet acceptors. *J. Mater. Chem. C* 2 (2014).

[124] C. Wohnhaas, A. Turshatov, V. Mailander, S. Lorenz, S. Baluschev, T. Miteva, and K. Landfester. Annihilation upconversion in cells by embedding the dye system in polymeric nanocapsules. *Macromol. Biosci.* **11**.6 (2011), 772–8.

[125] A. J. Svagan, D. Busko, Y. Avlasevich, G. Glasser, S. Baluschev, and K. Landfester. Photon energy upconverting nanopaper: a bioinspired oxygen protection strategy. *ACS Nano* **8**.8 (2014), 8198–207.

[126] J.-H. Ho, Y.-H. Chen, L.-T. Chou, P.-W. Lai, and P.-S. Chen. The improvement of π-conjugation by the lateral benzene of anthracene and naphthalene. *Tetrahedron Lett.* **55**.42 (2014), 5727–5731.

[127] E. Gazis. *UV Atlas of organic compounds.* Vol. 3. Butterworths, London, 1967.

[128] G. Heinrich, S. Schoof, and H. Gusten. 9,10-diphenylanthracene as a fluorescence quantum yield standard. *Journal of Photochemistry* **3**.2 (1974), 315–320.

[129] R. L. Barnes and J. B. Birks. 'Excimer' Fluorescence. X. Spectral Studies of 9-Methyl and 9, 10-Dimethyl Anthracene. *Proceedings of the Royal Society A: Mathematical, Physical and Engineering Sciences* **291**.1427 (1966), 570–582.

[130] S. K. Chattopadhyay, C. V. Kumar, and P. K. Das. Triplet-related photophysics of 9,10-diphenylanthracene. A kinetic study of reversible energy transfer from anthracene triplet by nanosecond laser flas. *Chem. Phys. Lett.* **98**.3 (1983), 250–254.

[131] S. Watanabe, Y. Shimodo, and K. Morihashi. Theoretical investigation of hole mobility in 9,10-diphenylanthracene by density functional calculations. *Theor. Chem. Acc.* **130**.4-6 (2011), 807–813.

[132] J. Hernando, J. P. Hoogenboom, E. M. van Dijk, J. J. Garcia-Lopez, M. Crego-Calama, D. N. Reinhoudt, N. F. van Hulst, and M. F. Garcia-Parajo. Single molecule photobleaching probes the exciton wave function in a multichromophoric system. *Phys. Rev. Lett.* **93**.23 (2004), 236404.

[133] K. Suzuki, A. Kobayashi, S. Kaneko, K. Takehira, T. Yoshihara, H. Ishida, Y. Shiina, S. Oishi, and S. Tobita. Reevaluation of absolute luminescence quantum yields of standard solutions using a spectrometer with an integrating sphere and a back-thinned CCD detector. *Phys. Chem. Chem. Phys.* **11**.42 (2009), 9850–60.

[134] F. V. Bright and L. B. McGown. Three-component determinations using fluorescence anisotropy measurements and wavelength selectivity. *Anal. Chem.* **58**.7 (1986), 1424–1427.

[135] M. Kasha, H. R. Rawls, and M. Ashraf El-Bayoumi. The exciton model in molecular spectroscopy. *Pure Appl. Chem.* **11**.3-4 (1965).

[136] B. S. Johnson, M. D. Ediger, Y. Yamaguchi, Y. Matsushita, and I. Noda. Concentration and temperature dependence of molecular motions in polystyrene/tetrahydrofuran solutions. *Polymer* **33**.18 (1992), 3916–3924.

[137] A. P. Darmanyan. Generation of 1O2 and the mechanism of internal conversion in 9,10-diphenylanthracene. *Chem. Phys. Lett.* **91**.5 (1982), 396–400.

[138] S. Chandrasekhar. Stochastic problems in physics and astronomy. *Rev. Mod. Phys.* **15**.1 (1943). As reprinted from: P. Hertz, *Math. Ann.* **67**.387 (1909), 0001–0089.

[139] G.-Z. Wu, W.-X. Gan, and H.-K. Leung. Photophysical properties of meso-substituted octaethylporphines and their zinc complexes. *J. Chem. Soc., Faraday Trans.* **87**.18 (1991), 2933.

[140] C. E. McCusker and F. N. Castellano. Materials Integrating Photochemical Upconversion. *Top. Curr. Chem.* **374**.2 (2016).

[141] F. Deng, J. Blumhoff, and F. N. Castellano. Annihilation limit of a visible-to-UV photon upconversion composition ascertained from transient absorption kinetics. *J. Phys. Chem. A* **117**.21 (2013), 4412–9.

[142] D. Dzebo, K. Moth-Poulsen, and B. Albinsson. Robust Triplet-Triplet Annihilation Upconversion by Efficient Oxygen Scavenging (2016). (Manuscript in progress).

[143] K. Börjesson, D. Dzebo, B. Albinsson, and K. Moth-Poulsen. Photon upconversion facilitated molecular solar energy storage. *J. Mater. Chem.A* **1**.30 (2013), 8521–8524.

[144] K. Börjesson, M. Gilbert, D. Dzebo, B. Albinsson, and K. Moth-Poulsen. Conjugated anthracene dendrimers with monomer-like fluorescence. *RSC Adv.* **4**.38 (2014), 19846–19850.

[145] V. Gray, K. Börjesson, D. Dzebo, M. Abrahamsson, B. Albinsson, and K. Moth-Poulsen. Porphyrin–Anthracene Complexes: Potential in Triplet–Triplet Annihilation Upconversion. *J. Phys. Chem. C* (2016).